UNIVERSITY OF KWAZULU-NATAL

SLURRY-PHASE DESULPHURIZATION OF TYRE DERIVED OIL USING UNSUPPORTED AND SUPPORTED ALKALINE EARTH METAL OXIDES

by

Sagar Ramdeo

216007834

A dissertation submitted in fulfilment of the requirements for the degree of

Master of Science in Chemical Engineering

School of Chemical Engineering

Faculty of Engineering

Supervisor: Prof. David Lokhat

Co-Supervisor: Prof. Milan Carsky

2021

Declaration

I Sagar Ramdeo declare that

(i)   The research reported in this dissertation/thesis, except where otherwise indicated, is my original research.

(ii) This dissertation/thesis has not been submitted for any degree or examination at any other university.

(iii) This dissertation/thesis does not contain other persons' data, pictures, graphs or other information, unless specifically acknowledged as being sourced from other persons.

(iv) This dissertation/thesis does not contain other persons' writing, unless specifically acknowledged as being sourced from other researchers. Where other written sources have been quoted, then:
a) their words have been re-written, but the general information attributed to them has been referenced;
b) where their exact words have been used, their writing has been placed inside quotation marks, and referenced.

(v)   Where I have reproduced a publication of which I am author, co-author or editor, I have indicated in detail which part of the publication was actually written by myself alone and have fully referenced such publications.

(vi) This dissertation/thesis does not contain text, graphics or tables copied and pasted from the Internet, unless specifically acknowledged, and the source being detailed in the dissertation/thesis and in the References sections.

Signed: …………………..

Acknowledgements

I would like to express my gratitude to the following people for their contribution to this work:

- My supervisors, Prof. David Lokhat and Prof. Milan Carsky for their expertise, guidance and support.
- Miss N. Hadebe, Mrs. T. Mofokeng and Mrs. P. Ntombela for their assistance and guidance in the laboratory.
- My family and friends for their motivation, support, and encouragement during the toughest of times especially during the peak of the pandemic.

Abstract

The global consumption of tyres continues to increase to meet industrial, commercial, and personal transportation needs, which means that more tyres reach end-of-life. There are various methods of dealing with waste tyres, such as shredding, incineration, landfill, pyrolysis, and rethreading. The pyrolysis of waste tyres can be used to produce alternative fuels. The main waste tyre pyrolysis products are tyre pyrolysis oil, non-condensable gases and char. Due to the composition of tyres, some unwanted components end up in tyre derived oil. These unwanted components are sulphur-containing compounds, metal and metalloid impurities, and polycyclic aromatic hydrocarbons. Significant sulphur emissions such as sulphur oxides, sulphate particulate matter, and sulphur-containing compounds are released during the direct combustion of tyre derived oil. The sulphur emissions cause acid rain and environmental pollution that is harmful to human and animal health. As a result, many countries have enforced policies to minimize sulphur emissions. The study served the following purposes: (1) to identify and characterize high-value compounds within tyre derived oil to supplement existing literature for tyre derived oil as a potential replacement to conventional liquid fuels, (2) to synthesize and characterize supported alkaline earth metal oxides for desulphurization, (3) to desulphurize tyre derived oil using unsupported and supported alkaline earth metal oxides, and (4) to develop a mathematical model to describe the desulphurization results. The tyre derived oil was obtained from Mandini, a tyre pyrolysis company based in Alberton, Johannesburg. The GC-MS results showed that the tyre derived oil consists of a complex mixture of organic compounds, within the C_5-C_{36} range. The main aromatic compounds found in the tyre derived oil were toluene (0.71 %), styrene (0.15 %), xylene (1.39 %), limonene (6.55 %), cymene (2.56 %) and benzothiazole (0.80 %). The high percentage of aromatics and naphthenic components make the tyre derived oil suitable as an alternative to conventional liquid fuels. The alkaline earth metal oxides of calcium, magnesium, and barium were chosen to desulphurize tyre derived oil. The silica-supported alkaline earth metal oxides were synthesized using the wet impregnation technique. The SEM-EDX analysis confirmed the presence of alkaline earth metal oxides on the surface of the silica particles. The untreated and treated tyre derived oil was analysed using a GC-PFDP to determine the performance of the alkaline earth metal oxides in terms of the total sulphur adsorbed. A 56.76 wt.% desulphurization was optimally achieved at a temperature of 240 °C for 30 min with a 0.0375 g/ml sorbent-to-oil ratio, using supported calcium oxide. The following sizes of silica gel were used for the invention: (1) silica gel with a 30 Å pore size and a 100-200 mesh particle size, (2) silica gel with a 60 Å pore size and a 35-60 mesh particle size, and (3) silica gel with a 150 Å pore size and a 35-60 mesh particle size. The desulphurization results, using supported alkaline earth metal oxides, suggested that pore diameter and mesh particle size do not significantly impact desulphurization for the operating conditions studied. Combining the supported alkaline earth metal oxides did not improve the desulphurization of the tyre derived oil at a temperature of 240 °C for 30 min with a 0.0125 g/ml sorbent-to-oil ratio. The balance between temperature, reaction time and sorbent-to-oil ratio provides the impetus for continued research into the combined effect of alkaline earth metal oxides for desulphurization.

List of Contents

List of Figures

List of Tables

CHAPTER 1

1. Introduction

1.1. Background and Problem Statement

With the increasing population size, the global consumption of tyres continues to increase to meet industrial, commercial, and personal transportation needs. Thus, resulting in more tyres reaching end-of-life. In 2014, the Recycling and Economic Development Initiative of South Africa (REDISA) reported that approximately 11 million tyres were sold locally per year. All these tyres (except tyres exported) will become waste. The estimated mass of the tyres sold (which will become waste) is 275 000 tonnes (REDISA, 2014). Sending waste tyres to landfill sites represents a lost opportunity in terms of economic and environmental sustainability. At the same time, due to the rising concerns of crude oil prices and the environment, governments are paying particular attention to the research and development of alternative fuels.

Hartley et al. (2017) reported on the processing of end-of-life tyres in South Africa; that being, rethreading of tyres (25 wt.%), incineration (16 wt.%), shredding (23 wt.%), pyrolysis (18 wt.%) and landfill (18 wt.%). The pyrolysis of waste tyres presents an alternative to using fossil fuels. By definition, pyrolysis is a hydrocarbon thermal cracking process in an oxygen-free environment. During pyrolysis, the long chain organic hydrocarbons in the waste tyres are transformed into low molecular weight products. Simultaneously, the inorganic constituents, mainly from carbon black and steel, are retained as a solid residue. The main waste tyre pyrolysis products are tyre pyrolysis oil, also called tyre derived oil (TDO), the non-condensable gases and char.

Tyres are composed of rubber/elastomers (45 to 47 wt.%), carbon black (21.5 to 22 wt.%), metal (12 to 25 wt.%), zinc oxide (1 to 2 wt.%), textile (0 to 10 wt.%), sulphur (1 to 2 wt.%) and additives (5 to 7.5 wt.%) (Evans and Evans, 2006; Nkosi and Muzenda, 2014; Kushida and Mihara, 2016). Due to the composition of tyres, some unwanted components end up in tyre derived oils. These unwanted components are (1) sulphur-containing compounds, (2) metal and metalloid impurities, and (3) polycyclic aromatic hydrocarbons (Pilusa et al., 2013). During the direct combustion of tyre derived oil, significant sulphur emissions such as sulphur oxides, sulphate particulate matter and sulphur-containing compounds are released into the atmosphere. The sulphur emissions cause acid rain and environmental pollution that is harmful to human and animal health (Grennfelt et al., 2019). As a result, many countries have enforced policies to minimize the emissions of these compounds.

There are stringent restrictions to limit the amount of sulphur emissions from power plants and on the amounts of sulphur allowable in fuels used in transportation. In 2006, the South African government promulgated the Petroleum Products Act. The regulations include, amongst others, the reduction of the permitted sulphur concentration from 3000 ppm to 500 ppm; the production of a niche diesel grade with

a maximum sulphur content of 50 ppm and permitting several blends of bio-diesel up to a level of 100 % bio-diesel (Department of Minerals and Energy, 2006).

There is a great need to create alternative methods to desulphurize oils, at minimal cost, without compromising safety. Babich and Moulijn (2003) reported the progress achieved in desulphurization technologies, such as catalysis-based hydrodesulphurization (HDS) technologies and in 'non-HDS' processes of sulphur removal (alkylation, extraction, precipitation, oxidation and adsorption). HDS processes are viewed as mature technology; however, it may not be feasible for small scale industries due to elevated process temperatures and pressures (Ahmad et al., 2016). Therefore, slurry-phase desulphurization can be an alternative for small scale industries due to low operating temperatures and pressures.

1.2.   Research Aims and Objectives

The project involves the slurry-phase desulphurization of tyre derived oil (TDO) by employing various unsupported and supported alkaline earth metal oxides. The wet impregnation method will be applied to synthesize the supported alkaline earth metal oxides using silica gel as the support. The alkaline earth metal oxides will be characterized using a Scanning Electron Microscope (SEM) equipped with an Energy Dispersive X-Ray (EDX) probe for semi-quantitative elemental analysis. The alkaline earth metals which were suited for the invention include the oxides of calcium, magnesium and barium. The alkaline earth metal oxides were chosen based on feasibility and chemical stability.

To compare the performance of the various reactive adsorbents in terms of the total sulphur adsorbed, the untreated and treated TDO will be analysed using a gas chromatograph equipped with a pulsed flame photometric detector (PFPD). The composition and functional groups of the untreated TDO will be determined by gas chromatography-mass spectrometry (GC-MS) and Fourier Transform Infrared Spectroscopy (FTIR), respectively. The characterization of the untreated TDO aims to supplement existing literature for TDO as a potential replacement to conventional liquid fuels and to identify the high-value compounds within the TDO.

A 2^3 factorial design and response surface methodology will be applied to investigate the interaction of the desulphurization parameters, i.e., reaction temperature, reaction time and amount of reactive adsorbent. According to Das and Dewanjee (2018), the 2^3 factorial design and response surface methodology is a useful tool that offers some general advantages: (1) a reduction in the number of experiments thus reducing costs, (2) the possibility of determining the mathematical correlations between experimental variables, for a better understanding of the process and (3) the determination of suitable operating conditions for process scale-up.

1.3.   Novel Contribution to Knowledge and Research Benefits

There is limited published information for the desulphurization of liquid fuels using alkaline earth metal oxides. This report is the first to present the desulphurization of tyre derived oil using alkaline earth metal oxides. Further investigation was carried out using a combination of the alkaline earth metal oxides for desulphurization.

The waste tyre pyrolysis process is a well-studied concept in South Africa; however, it has not yielded significant commercial success. Several pyrolysis plants have been shut down in South Africa due to non-compliance with environmental regulations as well as limited and unregulated markets (Nkosi et al., 2020). Major tyre companies, such as Goodyear and Firestone, have invested in the pyrolysis of waste tyres but could not attract local markets for the pyrolysis products and they failed to incorporate the project into their core business model (Vestel, 2010). The research presents a solution for improving tyre derived oil for the South African market, potentially local and offshore investors.

1.4.   Thesis Outline

- Chapter 1 provides motivation for the proposed research, the scope of the project and the unique contributions to knowledge.
- Chapter 2 provides a review of the literature required to understand the rules and regulations of sulphur emissions, the existing desulphurization technologies, and the synthesis of reactive adsorbents.
- Chapter 3 contains a comparative study of the composition of tyre derived oil.
- Chapter 4 dives into the desulphurization of tyre derived oil.
- Chapter 5 communicates the purpose and findings of the study.
- The appendices contain images of the apparatus and sample calculations.

1.5. References

- Ahmad, S., Ahmad, M., Naeem, K., Humayun, M., Sebt-E-Zaeem, S. and Faheem, F. (2016). Oxidative desulfurization of tire pyrolysis oil. *Chemical Industry and Chemical Engineering Quarterly*, 22(3), pp.249-254.

- Babich, I.V. and Moulijn, J.A. (2003). Science and technology of novel processes for deep desulfurization of oil refinery streams: a review⋆. *Fuel*, 82(6), pp.607-631.

- Das, A. and Dewanjee, S. (2018). Optimization of Extraction Using Mathematical Models and Computation. *Computational Phytochemistry*, pp.75-106.

- Department of Minerals and Energy (2006). Petroleum Products Act (120/1977): Regulations: Petroleum Products Specifications And Standards. Pretoria: The Government Printing Works.

- Evans, A. and Evans, R. (2006). The Composition Of A Tyre: Typical Components. Banbury: The Waste & Resources Action Programme.

- Grennfelt, P., Engleryd, A., Forsius, M., Hov, Ø., Rodhe, H. and Cowling, E. (2019). Acid rain and air pollution: 50 years of progress in environmental science and policy. *Ambio*, 49(4), pp.849-864.

- Hartley, F., Caetano, T. and Daniels, R. (2017). Economic Benefits Of Extended Producer Responsibility Initiatives In South Africa The Case Of Waste Tyres. Johannesburg: Trade & Industrial Policy Strategies, p.6.

- Kushida, N. and Mihara, S. (2016). Rubber Composition For Tires And Pneumatic Tire. US9309387B2.

- Nkosi, N. and Muzenda, E. (2014). A Review and Discussion of Waste Tyre Pyrolysis and Derived Products. *Proceedings of the World Congress on Engineering*, vol. 2.

- Nkosi, N., Muzenda, E., Mamvura, T., Belaid, M. and Patel, B. (2020). The Development of a Waste Tyre Pyrolysis Production Plant Business Model for the Gauteng Region, South Africa. *Processes*, 8(7), p.766.

- Pilusa, T.J., Shukla, M. and Muzenda, E. (2013). Pyrolytic Tyre Derived Fuel: A Review. Johannesburg: International Conference on Chemical, Mining and Metallurgical Engineering.

- Recycling and Economic Development Initiative of South Africa (2014). REDISA Integrated Industry Waste Tyre Management Plan. *Taylor EnviroWaste Consulting*, p.12.

- Vestel, L. (2010). *For Tire Recyclers, a Holy Grail*. [online] The New York Times. Available at: <https://green.blogs.nytimes.com/2010/05/03/for-tire-recyclers-a-holy-grail/> [Accessed 14 March 2021].

CHAPTER 2

2. Literature Review

2.1. Sulphur Content in Tyre Derived Oil

Tyres are made from a range of materials, which include rubber/elastomers (45 to 47 wt.%), carbon black (21.5 to 22 wt.%), metal (12 to 25 wt.%), zinc oxide (1 to 2 wt.%), textile (0 to 10 wt.%), sulphur (1 to 2 wt.%) and additives (5 to 7.5 wt.%) (Evans and Evans, 2006; Nkosi and Muzenda, 2014; Kushida and Mihara, 2016). Each material has a purpose that ensures the tyre's proper functioning, either to provide durability, tractability or strength. The average sulphur content, 1.62 wt.%, was deduced from the ultimate analysis of tyres reported by various researchers (refer to Table 2.1). The sulphur comes from the rubber vulcanization stage during the tyre manufacturing process. The vulcanization stage involves the cross-linking of rubber monomers using a sulphur cross-linking agent (Miguel Martín-Martínez, 2002).

Table 2.1. Ultimate analysis of tyre samples.

Ultimate Analysis (wt.%)	(Juma et al., 2007)	(Lee et al., 1995)	(Ozcan et al., 2016)	(Frigo et al., 2014)	(Cunliffe and Williams, 1998)	(Murillo et al., 2006)
C	81.24	83.8	80.04	83.2	86.4	88.6
H	7.36	7.6	8.7	8.9	8	8.3
N	0.49	0.4	0.3	0.3	0.5	0.4
S	1.99	1.4	1.6	1.6	1.7	1.4
O	~8.92	3.1	9	6	3.4	1.2

Pyrolysis is an important area of research. Several studies have investigated the pyrolysis of waste tyres both on a laboratory and an industrial scale. The pyrolysis process involves the thermal cracking of heavy hydrocarbons to low molecular weight hydrocarbons under an inert or partial oxidizing atmosphere. The waste tyre pyrolysis process yields a gaseous fraction of non-condensable gases, an oily fraction containing organic substances, and a solid fraction comprised of carbon, metal, and other inert material. Due to the sulphur content in tyres, unwanted sulphur-containing compounds form during pyrolysis and end up in tyre derived oil. The sulphur-containing compounds found in the oil can be grouped into five categories: thiophenes, benzothiophenes, dibenzothiophenes, benzothiazoles and isothiocyanates (Trongyong and Jitkarnka, 2015). Table 2.2 shows the sulphur content of tyre derived oil at various pyrolysis operating conditions. Researchers mainly vary the pyrolysis operating conditions to optimize for a low sulphur content and a high liquid yield.

Table 2.2. Sulphur content of tyre derived oil obtained at various pyrolysis operating conditions.

Reference	Reactor	Heating Rate (ºC/min)	Residence Time (h)	Temperature (ºC)	Sulphur Content (wt.%)
(Banar et al., 2012)	Stainless steel fixed bed reactor	5	1	400	1.07
		35			0.11
(Aydın and İlkılıç, 2012)	Fixed bed reactor	12	4	500	0.906
(Cunliffe and Williams, 1998)	Nitrogen purged static-bed batch reactor	5	1.5	450	1.4
				500	1.4
				600	1.3
(Alvarez et al., 2017)	Conical spouted bed reactor	10^3-10^4 ºC/s	30-500 ms	425	1.15
				475	1.17
				575	1.27
(Jantaraksa et al., 2015)	Stainless steel tubular fixed bed reactor	25	-	400	1.15
(Yazdani et al., 2019)	Rotary kiln (heated with electric coil)	-	-	550	0.85
(Taleb et al., 2020)	Fixed bed reactor	15	1	500	1.27

2.2.   Environmental Effects and Regulations of Sulphur Emissions

Sulphur is inherent in petrol, diesel, jet fuel and lubricating oil, because sulphur is naturally found in crude oil from which these oils and fuels are derived. Sulphur is also present in tyre derived oil (refer to Table 2.2). During the direct combustion of tyre derived oil, significant sulphur emissions such as sulphur oxides, sulphate particulate matter (PM) and organic sulphur compounds are released into the atmosphere. These sulphur emissions are highly toxic and of environmental concern; as such, the reduction of sulphur emissions into the atmosphere is a high global priority (Welz et al., 2009).

2.2.1.   Effects of Sulphur Emissions on Human Health and the Environment

Atmospheric reactions involving sulphur oxides (SO_x) create tiny particles known as particulate matter (PM). The emission of particulate matter, carbon monoxide (CO), nitrogen oxides (NO_x), non-methane hydrocarbons, airborne toxins, and sulphur oxides (SO_x) are usually produced at high temperatures with incomplete combustion of fuel (Brijesh and Sreedhara, 2013). A higher sulphur content will result in more particulate matter being produced during the combustion of fuel. Particulate matter, less than 2.5 microns in diameter, ($PM_{2.5}$) can enter the bloodstream via the lungs (Burtraw and Goulder, 2013). The International Agency for Research on Cancer has confirmed that $PM_{2.5}$ is a

recognized carcinogen (Cohen et al., 2013). According to Lee et al. (2014) and Wei et al. (2019), exposure to high concentrations of $PM_{2.5}$ is linked to an increase in hospital admissions that are related to infections of the respiratory organs, nonfatal heart attacks and other acute outcomes. There are also negative effects on reproduction as a result of long-term exposure to $PM_{2.5}$. Some of the problems identified were pre-term delivery, stillbirth, low birth weight and congenital heart defects (Harris et al., 2014; Saha et al., 2018). The international implementation of vehicle emission standards equivalent to Euro 6 (refer to Figure 2.1) would reduce the amount of premature mortality between 120 000 and 280 000 in 2030 (McClellan et al., 2012).

Everything in an ecosystem is connected and susceptible to acid rain as a result of sulphur emissions. The biological effects of acid rain are most clearly seen in aquatic environments, such as lakes, streams, rivers banks and marshes where it can be harmful to living matter. As acid flows through the soil, acidic rainwater can leach nutrients and minerals from the soil that trees require for growth. At high altitudes, acidic fog and clouds could remove nutrients from tree foliage, resulting in brown or dead leaves (USGS, 2020). Therefore, the trees would be unable to photosynthesize, which makes them fragile and less able to survive during freezing temperatures.

Sometimes dust particles, as well as sulphur emissions, can become acidic. The acidic particles can land on statues, buildings, and other human-made structures and damage their surfaces (US EPA, 2020). The acidic particles causes the deterioration of paint, stone and metal, which decreases the aesthetics of monuments, buildings and other structures. Thus, resulting in high maintenance costs for the public and private sector. The use of low sulphur fuels would be economically valuable since it will prevent hospital admissions, loss of working days, low-quality crops, and damage to commercial plantations (Sadare et al., 2017).

2.2.2. Regulations for Sulphur Emissions in South Africa

In 2006, the South African government promulgated the Petroleum Products Act: Regulations regarding Petroleum Products Specification and Standards (henceforth referred to as the 2006 regulations) in Notice R. 627 of Government Gazette No. 28958. The regulations included amongst others, the reduction of the permitted sulphur concentration from 3000 ppm to 500 ppm; the production of a niche diesel grade with a maximum sulphur content of 50 ppm; as well as permitting various blends of biodiesel up to a level of 100 %. Prior to the 2006 regulations, the oil industry was based on voluntary specifications that were stipulated by the South African National Standards (SANS) under the auspices of the South African Bureau of Standards (SABS). The self-regulation of fuel quality was referred to as Cleaner Fuels One (CF1), which was aligned to meeting Euro 2 emission standards (i.e. a maximum sulphur content of 500 ppm). In South Africa, the initially envisaged path towards cleaner fuels was to attain Euro 2 standards from 2006; Euro 3 from 2008; Euro 4 from 2010 and Euro 5 from 2017. Cleaner

Fuels Two (CF2) specifications and standards were proposed to be largely compliant with the Euro 5 emission standards (Pilusa et al., 2013). According to Mahotas (2019), to comply with the CF2 Regulations, oil companies must invest in refinery upgrades because the current configurations of their refineries do not allow them to produce cleaner fuels as specified by the CF2 regulations. The oil refining companies have expressed their reluctance to invest in refinery upgrades because of the significant investments required, coupled with the absence of the guarantee of investment recovery (Mahotas, 2019). The CF2 regulations remain a priority to the South African government. The next step involves finalizing the implementation date in order to provide policy certainty.

1993	• Euro 1 Standards • Specification: maximum of 2000 ppm of sulphur in diesel fuel for highway vehicles
1996	• Euro 2 Standards • Achieved the biggest reduction in emissions of all the standards. • Specification: maximum sulphur content in diesel fuel of 500 ppm
2000	• Euro 3 Standards • Specification: maximum of 350 ppm of sulphur in diesel fuel for highway vehicles
2005	• Euro 4 Standards • Significant emissions reduction moving from Euro 2 to Euro 4 • Specification: maximum of 50 ppm of sulphur in diesel fuel and availability of diesel fuel with less than 10 ppm sulphur
2008/9	• Euro 5 Standards • Specification: maximum sulphur content of 10 ppm in diesel fuel for highway vehicles
2014	• Euro 6 Standards • Soot-free vehicle emission standards, most progressively limiting the sulphur content in diesel fuel to 10 ppm or less.

Figure 2.1. European union sulphur emissions' regulations timeline (Dieselnet, 2020).

2.3. Existing Desulphurization Technologies and their Challenges

During desulphurization, sulphur-containing compounds are decomposed or separated without decomposition or both separated and then decomposed. When sulphur-containing compounds are decomposed, gaseous or sulphur products are formed, and the hydrocarbon contents are recovered. In separating sulphur-containing compounds without decomposition, the sulphur-containing compounds are separated or transformed into other compounds that are more separable. The simultaneous separation and decomposition of sulphur-containing compounds have shown promising results for producing ultra-low sulphur fuels.

Babich and Moulijn (2003) illustrated the progress achieved in desulphurization technologies, such as catalysis-based hydrodesulphurization (HDS) technologies (synthesis of improved catalysts, combination of distillation and HDS advanced reactor design) and in 'non-HDS' processes of sulphur removal (precipitation, alkylation, oxidation, extraction, and adsorption). HDS processes are perceived as mature technology; however, HDS may not be feasible for small scale industries due to elevated process temperatures and pressures (Ahmad et al., 2016). Table 2.3 shows the classification of desulphurization processes based on the nature of the chemical process used for sulphur removal.

Table 2.3. Desulphurization technologies classified by nature of a key process to remove sulphur (Babich and Moulijn, 2003).

Catalytic Transformation with Sulphur Elimination	Physico-chemical Separation/Transformation of Sulphur Compounds
HDS by Advanced Reactor Design	Catalytic Distillation
HDS by Advanced Catalyst	Alkylation
Conventional HDS	Extraction
HDS with Fuel Specification Recovery	Oxidation
	Precipitation
	Adsorption

2.3.1. Hydrodesulphurization (HDS)

Many industries use of the HDS process for the removal of sulphur from waste-derived oils and petroleum distillates. The HDS technology has been used since 1933 and is based on the addition of hydrogen gas (H_2) at elevated pressures and temperatures using catalysts mainly composed of nickel molybdenum sulphide or cobalt molybdenum sulphide (Infantes-Molina et al., 2012; Bae, 2017). In this process, the sulphur-containing compounds in oils and refinery streams are converted to hydrogen disulphide gas (H_2S). H_2S gas is harmful; therefore, it is usually transformed to elemental sulphur via the Claus process (a catalytic oxidation process with air) (Kohl and Nielsen, 1997).

The typical reaction conditions of the HDS process are at elevated pressures, between 10 and 300 bar, and at elevated temperatures, between 300 and 450 °C (Kumar and Banerjee, 2009; Soriano et al., 2010). High temperatures increase coke formation in the refining process, consequently increasing the deactivation rate of the catalyst. High pressures, on the other hand, cause increased side reactions, i.e., saturation of olefins, which lowers octane numbers for petrol and cetane numbers for diesel fuel.

The molecular structure of sulphur-containing compounds also influences sulphur removal for the HDS process. The reactivity of sulphur-containing compounds in HDS follows the following order (from most to least reactive): thiophene > alkylated thiophene > benzothiophene > alkylated benzothiophene > dibenzothiophene and alkylated dibenzothiophene without substituents at the 4 and 6 positions > alkylated dibenzothiophene with one substituent at either the 4 or 6 positions > alkylated dibenzothiophene with alkyl substituents at the 4 and 6 positions (Gates and Topsøe, 1997; Shafi and Hutchings, 2000).

Tyre Derived Oil (TDO) contains dibenzothiophenes, resulting in the limited effectiveness of HDS because of the steric hindrance on the sulphur atom in dibenzothiophene and its derivatives (Egorova and Prins, 2004). The removal of unreactive and refractory aromatic S-compounds is the most challenging to the HDS processes as they require high quantities of H_2, elevated temperatures, and high catalyst selectivity and reactivity (Chu et al., 2008). These severe operating conditions elevate process costs, thus rendering the HDS process uneconomical for the desulphurization of TDO.

2.3.2. Solvent Extractive Desulphurization (SEDS)

SEDS is due to sulphur-containing compounds being more soluble than other hydrocarbons in an appropriate solvent. SEDS has several advantages over conventional HDS technology. The process does not require severe operating conditions; there is no H_2 consumption, no need for expensive catalysts and operates at ambient pressure and temperature (Babich and Moulijn, 2003; Abro et al., 2014). In addition, SEDS does not modify the chemical structure of the compounds within the fuel; as a result, the equipment required is relatively conventional and does not require special requirements. Therefore, SEDS can be easily integrated into an existing refinery.

However, the efficiency of SEDS is limited by the solubility of sulphur-containing compounds in the solvent. Solvents of various properties have been investigated by researchers. According to Babich and Moulijn (2003), polyethylene glycols, ethanol, acetone, and nitrogen-containing solvents show a reasonable level of 50 to 90 wt.% desulphurization. The solubility can be improved by preparing a solvent mix; however, this is intrinsically inefficient because its composition depends significantly on the spectrum of sulphur compounds in liquid fuels (Babich and Moulijn, 2003; Sharma et al., 2013).

The selected solvent controls the quality of the hydrogen-rich phase and solvent-rich phase, and greatly influences the economics of the SEDS process. The selection of solvent depends on the

properties of the solvent and feedstock, such as density, boiling point/boiling range, miscibility, viscosity, melting point, selectivity, corrosiveness and toxicity. In addition, the chosen solvent is assessed based on its high affinity and capacity for solutes to reduce the required solvent-to-feed ratio (Kumar and Banerjee, 2009). Furthermore, the selected solvent is evaluated to ensure high selectivity to reduce the extractor height, improving the quality of extract, and to increase the yield of the sulphur-rich phase (Kumar and Banerjee, 2009).

2.3.3. Oxidative Desulphurization (ODS)

According to Aida et al. (2000), desulphurization by selective oxidation includes two key steps: oxidation of sulphur compounds and subsequent purification. An oxidant is reacted with sulphur-containing compounds found in fuels at low temperatures (< 93 °C) and low pressures (< 6.9 bar) with/without a catalyst to form sulphoxides and sulphones, which can be removed by either solvent extraction or adsorption (Gatan et al., 2004; Rajendran et al., 2020). This is contrary to the hydrodesulphurization process, where the sulphur-containing compounds are reduced to form H_2S. The oxidation reactivity increases when the electron density of the sulphur compounds are higher, dibenzothiophene > 4.6-dimethyldibenzothiophene > benzothiophene > thiophene, which is the reverse order of HDS (Otsuki et al., 2000; Campos-Martin et al., 2010; Jiang et al. 2011). Thus, the ODS technology can remove organic sulphur compounds that are least reactive to the HDS process, i.e., the derivatives of alkylated thiophenes. The sulphur compounds, i.e., thiols, thioethers and disulphides that are reactive for HDS, are not easy to remove by the ODS process as they oxidize slowly. Therefore, the ODS technology is usually used to supplement the HDS process.

Through the years, various oxidants were reported in literature, such as hydrogen peroxide (H_2O_2), organic peracids, molecular O_2, cyclohexanone hydroperoxide, ozone, tert-butylhydroperoxide, cumene hydroperoxide, nitrogen oxides and air (Rajendran et al., 2020). Even though there are many oxidants, H_2O_2 is constantly emphasized as the superior oxidant because it has more active oxygen (47% by mass unit) and leaves only H_2O (Campos-Martin et al., 2010; Mjalli et al., 2014).

Al-Lal et al. (2015) used two ODS methods: (a) desulphurization by oxidation and methanol extraction and (b) oxidation using Fenton catalysts, ultrasound irradiation and adsorption to improve the purity of the fuel product. For the first method, tyre derived oil, formic acid and H_2O_2 were mixed while simultaneously being heated in a 200W ultrasound bath at 70 ºC for 30 min with stirring. This was followed by three successive extractions using methanol. A 53 wt.% desulphurization was achieved. In the second method, pyrolysis oil, H_2O_2 and solid catalyst were mixed and heated to 90 ºC with stirring and 200 W ultrasound irradiation. The solid catalyst was then filtered, and the liquid was decanted. The best desulphurization rates were recorded for iron (II) and iron (III) chloride as catalysts with 57.1 wt.% and 64.0 wt.% desulphurization, respectively.

Doğan et al. (2012) used the ODS method to remove sulphur-containing compounds from TDO as part of a five-stage purification process: (1) hydro-sulphuric acid treatment, (2) activated bentonite-calcium oxide, (3) vacuum distillation, (4) oxidative desulphurization and (5) washing and drying. For the oxidative desulphurization process, TDO was treated with a mixture containing formic acid and H_2O_2. The TDO mixture was stirred and heated at 60 ^{o}C for 2 hours. The five-stage process achieved 62 wt.% desulphurization.

The main disadvantage of the ODS procedure is the high operating costs, which are due to the sulphone separation unit of this process (Gatan et al., 2004). According to Betiha et al., (2018), the ODS procedure requires significant amounts of oxidizing agent. In addition, the oxidation reaction requires extended reaction times due to low selectivity and reactivity. Catalysts may be used to accelerate the oxidation reaction; however, this presents an added cost for catalyst and catalyst recovery.

2.3.4. Biodesulphurization (BDS)

In the BDS process, bacteria removes organic sulphur compounds from oil fractions without modifying the core carbon chain of the compounds (Mohebali and Ball, 2016). This process uses biological enzymes as a catalyst. The enzymes are produced by bacteria and other microorganisms. According to Deshpande et al. (2005), some microorganisms require sulphur to grow and sustain their biological activity as a result the sulphur content decreases in the oil fractions.

The BDS technology has been found to generate far less greenhouse gas emissions than the HDS process. This technology can only be applied as a complementary process since it cannot do some of the things done by HDS, i.e., induce saturation of some carbon-carbon double bonds and also improve the cracking characteristics of the material. The BDS process requires mild operating conditions (i.e., ambient temperature and pressure) and does not require hydrogen (as compared to HDS), thus saving on energy costs (Mohebali and Ball, 2016). The BDS process is also highly selective due to the involvement of biological enzymes (Soleimani et al., 2007). In addition, there are no undesirable by-products due to the organic nature of biodesulphurization.

Several microorganisms and enzymes can be used for the biodesulphurization of oil fractions, such as Sulpholobus acido-caldarius, Rhodococcus rhodochrous, Pseudomonas or the catalytic system Dsz protein-flavin reductase (Gray et al., 1996; Ohshiro and Izumi, 1999; Luo et al., 2003). The main challenge is to find microorganisms that have a high activity towards sulphur compounds, high sulphur removal ability at high temperatures, longer stability, and high hydrocarbon phase tolerance. Intensive research is continuing in biotechnology to improve the microorganism strains to increase their desulphurization activity; however, this is insufficient to fulfil industrial requirements.

2.3.5. Adsorptive Desulphurization (ADS)

Adsorption is a process that involves separation where gas or liquid molecules are adsorbed on the surface of an adsorbent. This process can be used for the desulphurization of oils and fuels based on an adsorbent's selective ability to adsorb sulphur-containing compounds. The effectiveness of ADS is dependent on the adsorbent properties, which include, adsorbent regeneration, selectivity for sulphur compounds, durability, and adsorption capacity (Babich and Moulijn, 2003; Moosavi et al., 2012). The greatest challenge with this technology is finding or developing suitable adsorbents. ADS can be separated into two groups: physical adsorptive desulphurization and reactive adsorptive desulphurization.

2.3.5.1. Physical Adsorptive Desulphurization

Physical adsorptive desulphurization involves the transfer of sulphur-containing compounds from the liquid phase to the surface of the adsorbent. In this method, the chemical characteristics of the sulphur-containing compounds are preserved, i.e., molecules are adsorbed intact (Gawande and Kaware, 2014). The adsorbent is usually regenerated by flushing the spent adsorbent with a desorbent. The main advantage of this process is the operating conditions (i.e., ambient temperature and pressure) and easy regeneration of the spent adsorbent (Betiha et al., 2018). Activated carbon and Ni-Al_2O_3 have been analysed to be suitable adsorbents for the removal of mercaptans, thiophenes and sulphides (Babich and Moulijn, 2003). However, the major complication of the physical adsorption method is competitive adsorption by olefins and aromatics, which reduces the sulphur uptake by the adsorbent (Yang et al., 2003; Moosavi et al., 2012; Liu et al., 2016).

2.3.5.2. Reactive Adsorptive Desulphurization

In reactive adsorptive desulphurization, the organic sulphur compounds react with chemical species on the surface of the adsorbent. Sulphur is fixed on the adsorbent, usually as sulphide, and the sulphur-free hydrocarbon is released into the purified fuel stream. The adsorptive selectivity and capability are high; however, regenerating the adsorbents for reuse is difficult (Babich and Moulijn, 2003; Dasgupta et al., 2013).

Metal oxides have been found to show tremendous potential due to their high reactivity towards sulphur compounds (Adeyi and Aberuagba, 2012). Aydın and İlkılıç (2012) have reported that by adding calcium oxide (CaO), sodium hydroxide (NaOH) and calcium hydroxide (Ca(OH)$_2$) in different quantities to waste tyres and pyrolyzing at 500 ˚C, decreases sulphur content. The maximum desulphurization was 34.25 wt.% by using 5 % Ca(OH)$_2$ in mass, to waste tyre. The sulphur content in the pyrolysis liquids were considerably reduced with the use of Ca(OH)$_2$ and CaO sorbent, while the

use of NaOH was not as effective. When the amount of Ca(OH)$_2$ and CaO increased, the amount of sulphur in the liquid products decreased. Aydın and İlkılıç (2012) concluded that the pyrolysis reaction was suitable with the usage of 5 % Ca(OH)$_2$ or CaO to reduce sulphur content.

Similarly, Arpa, Yumrutas and Demirbas (2010) have used zeolite, sodium carbonate (NaCO$_3$) and CaO for converting used waste lubricating engine oils into diesel-like fuels by pyrolytic distillation. The effects of the sorbents were assessed based on flash point, sulphur content, density, viscosity, distillation temperature and heating value. The sorbents were used in different ratios, and it was found that by adding 2 wt.% of CaO, the sulphur content decreased from 5710 to 3450 mg/Kg.

Baird and Beardon (1978) presented the simultaneous desulphurization and hydroconversion of heavy hydrocarbon constituents by contacting with alkaline earth metal oxides and alkaline earth metal hydrides, particularly barium oxide, barium hydride, calcium hydride and calcium oxide. According to Baird and Beardon (1978), the hydrides and oxides of calcium and barium are preferred due to their commercial availability and simplicity with which they can be regenerated and recycled.

Table 2.4 provides a summary of the advantages and disadvantages of the various desulphurization technologies reviewed in this chapter.

Table 2.4. Summary of the advantages and disadvantages of various desulphurization technologies.

	Advantages	Disadvantages
Hydrodesulphurization (HDS)	• Industries are experienced with HDS technologies because it has been used since 1933.	• The typical reaction conditions are at elevated temperatures (300 - 450 °C) and pressures (10 - 300 bar). • High temperatures increase coke formation and leads to an increase in the deactivation rate of the catalyst. • High pressures cause increased side reactions which lowers octane numbers for petrol and cetane numbers for diesel fuel. • Requires high quantities of H_2
Solvent Extractive Desulphurization (SEDS)	• The process can operate at ambient temperatures and pressures. • The chemical structure of the fuel does not change; therefore, the equipment required is rather conventional without special requirements, • as a result, the process can be easily integrated into an existing refinery.	• SEDS is limited by the solubility of sulphur-containing compounds in the solvent. • The solubility can be enhanced by preparing a solvent mix; however, this can be expensive.
Oxidative Desulphurization (ODS)	• The oxidation of sulphur-containing compounds occurs at low temperatures (< 93 °C) and low pressures (< 6.9 bar) with/without a catalyst.	• The sulphur compounds that are reactive for HDS are not easy to remove by the ODS process as they oxidize slowly. • There are high process costs, which are due to the sulphone separation unit of this process • The oxidation reaction suffers from low selectivity and activity; therefore, an extended reaction time is required. • A catalyst can be used to accelerate the oxidation reaction; however, this presents an added cost for catalyst and catalyst recovery.
Biodesulphurization (BDS)	• Bacteria removes organic sulphur compounds from oil fractions without degrading the carbon skeleton of the compounds. • The BDS technology has been found to generate far less greenhouse gas emissions than the HDS process. • Requires mild operating conditions (i.e., ambient temperature and pressure) • The BDS process is highly selective due to the involvement of biological catalysts and also does not produce any undesirable products.	• The main challenge is to find microorganisms that have a high activity towards sulphur removal, hydrocarbon phase tolerance, removal ability at high temperatures, and longer stability.
Physical Adsorptive Desulphurization (ADS)	• The operating conditions are at ambient temperatures and pressures. • Easy regeneration of the spent adsorbent.	• The greatest challenge with this technology is finding or developing suitable adsorbents. • There is competitive adsorption by olefins and aromatics, which results in a decrease in sulphur uptake by the adsorbent.
Reactive Adsorptive Desulphurization (ADS)	• The adsorptive selectivity and capability towards sulphur-containing compounds are high. Metal oxides have been found to show tremendous potential.	• Regenerating adsorbents for reuse is difficult when compared to physical ADS. • Finding or developing suitable adsorbents.

2.4. Preparation of Supported Alkaline Earth Metal Oxides

There are several important properties that influence the efficiency of supported alkaline earth metal oxides. The efficiency refers to the desulphurization capability of supported alkaline earth metal oxides at low operating temperatures and pressures. The properties that can lead to efficiency are listed starting with the most significant factor (Del Bianco et al., 1994; Song, 2003):

1. <u>High Surface Area:</u> helps optimize desulphurization when a high surface area of the supported alkaline earth metal oxides are exposed to the sulphur-containing compounds.

2. <u>Sorbent Lifetime:</u> sorbent lifetime is an essential factor, due to the cost of sorbent regeneration, disposal and replacement. All supported alkaline earth metal oxides lose their regenerating ability with time due to several reasons that include poisoning, attrition and sintering (Vogelaar et al., 2007).

3. <u>Strength:</u> this factor plays a role in preventing attrition of the supported alkaline earth metal oxides and, in turn, increases its lifespan.

4. <u>Correct Shape:</u> the morphology and shape of the support can reduce the attrition of the supported alkaline earth metal oxides.

5. <u>Environmental Effects:</u> this step has become crucial in recent years. The supported alkaline earth metal oxides should be recyclable or disposable without causing harm to the environment.

6. <u>Cost:</u> after all the previously mentioned factors, it is essential to pay attention to manufacturing costs. From an economic point of view, the longevity of supported alkaline earth metal oxides cannot be overlooked.

There are several procedures to load an active component onto a support, such as impregnation, coprecipitation, slurry precipitation, fusion, physical mixing, wash coating, etc. (Campanati et al., 2003). This study will concentrate on the use of the impregnation method. This method is attractive because of its methodical simplicity, low costs and limited waste generation (Sietsma et al., 2006).

According to Campanati et al. (2003), impregnation involves the contacting of a solution containing the precursor of an active phase with a solid support. There are two types of impregnation methods: wet impregnation and incipient wet impregnation. The volume of the solution distinguishes the two methods. For incipient wet impregnation, the volume of the solution (with an appropriate concentration) is equal to or slightly less than the pore volume of the support (Campanati et al., 2003). In contrast, wet impregnation uses an excess volume of solution.

In both methods, the solid is separated by drying off the excess solvent. The maximum amount of precursor in solution is limited by the solubility of the precursor. For both methods, the operating variable is temperature, which influences the solution viscosity and, consequently, the wetting time (Campanati et al., 2003).

2.4.1. Synthesis of Magnesium Oxide using Magnesium Salts

Hanif et al. (2009) synthesized MgO-Silica nanocomposites by using the wet impregnation method. Calcined silica was added to deionized water containing dissolved magnesium acetate $(Mg(CH_3COO)_2)$. The material was magnetically stirred for 2 hours at room temperature and then evaporated at 70 °C until a thick slurry was formed. The slurry was then calcined in a muffle furnace at 400 °C in static air for 12 h. The final calcination temperature was attained using a heating rate of 1 °C/min. Hanif et al. (2009) used the silica-supported magnesium oxide as an adsorbent for precombustion CO_2 capture.

Purwajanti et al. (2016) prepared mesoporous metal oxide hollow spheres (MgO-HS) using the wet impregnation method while using microporous carbon hollow spheres (MCHS) as templates. For the synthesis of MgO-HS, magnesium nitrate hexahydrate $(Mg(NO_3)_2.6H_2O)$ was dissolved in deionized water with MCHS. The mixture was sonicated for 1 h and stirred for 24 h at room temperature. The MCHS-$Mg(NO_3)_2$ samples were then separated by centrifugation and dried overnight at 50 °C, followed by calcination at 500 °C in air for 3 h to obtain MgO-HS. Purwajanti et al. (2016) applied the MgO-HS as a high performance arsenite (As(III)) adsorbent.

Isa and Nogawa (1984) studied the dehydration of magnesium acetate tetrahydrate by simultaneous thermogravimetry (TG), derivative thermogravimetry (DTG) and differential thermal analysis (DTA). The experiments were conducted under various atmospheres (open, quasi-sealed, and completely sealed). The conditions of open, quasi-sealed, and completely sealed were reported by *Isa and Okuno (1982)*. According to Isa and Nogawa (1984), the range of temperatures covered was usually from room temperature to 420 °C using a heating rate of 1 °C/min, in most cases. Figure 2.2 shows the thermogravimetric analysis involving the thermal decomposition of magnesium acetate tetrahydrate to magnesium oxide.

(a) Open system

(b) Quasi-sealed system

(c) Completely sealed
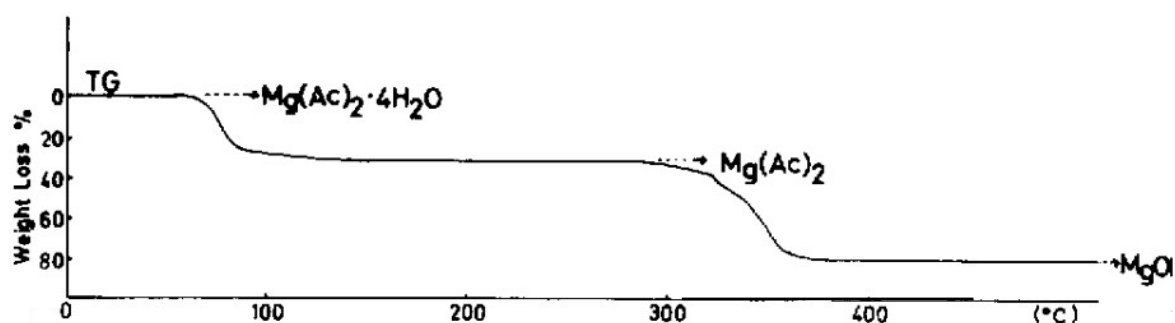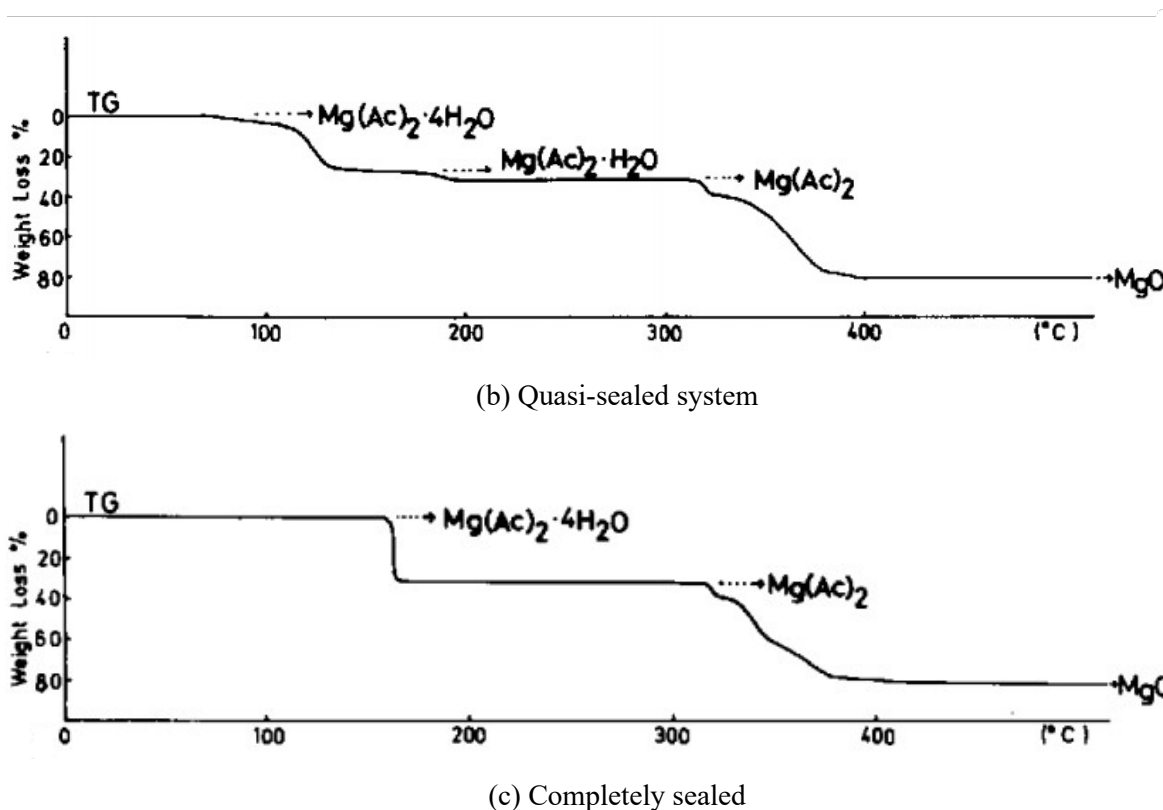
Figure 2.2. Thermogravimetric analysis of magnesium acetate tetrahydrate (Isa and Nogawa, 1984).

2.4.2. Synthesis of Calcium Oxide using Calcium Salts

Witoon et al. (2014) used the incipient wet impregnation method to prepare silica-supported calcium oxide. The unimodal and bimodal porous silica supports were impregnated with the desired amount of calcium nitrate tetrahydrate ($Ca(NO_3)_2.4H_2O$) in an aqueous solution. The slurry mixture was stirred at 60 °C for 1 h and thereafter dried at 120 °C for 12 h. The mixture was calcined at 800 °C for 4 h at a heating rate of 2 °C/min. Witoon et al. (2014) used the silica-supported calcium oxide as a catalyst for biodiesel production by transesterification of palm oil with methanol.

Cho et al. (2009) prepared calcium oxide catalysts using various precursors of calcium oxide, i.e., calcium acetate (CA) monohydrate, calcium carbonate (CC), calcium hydroxide (CH), calcium nitrate (CN) tetrahydrate and calcium oxalate (CO) monohydrate. The precursors were calcined for 2 hours in an electric furnace with a steady flow of nitrogen gas. The calcination temperature was varied from 500 °C to 900 °C with a heating rate of 1.5 °C/min. *Cho et al. (2009)* used the calcined catalysts for the transesterification of tributyrin with methanol. Figure 2.3 shows the thermogravimetric curves of all the precursors. The thermogravimetric curves of calcium nitrate tetrahydrate were recorded after removing the excessive water at 300 °C for 1 h. The conversion of calcium nitrate to calcium oxide was observed at 600 °C.

18
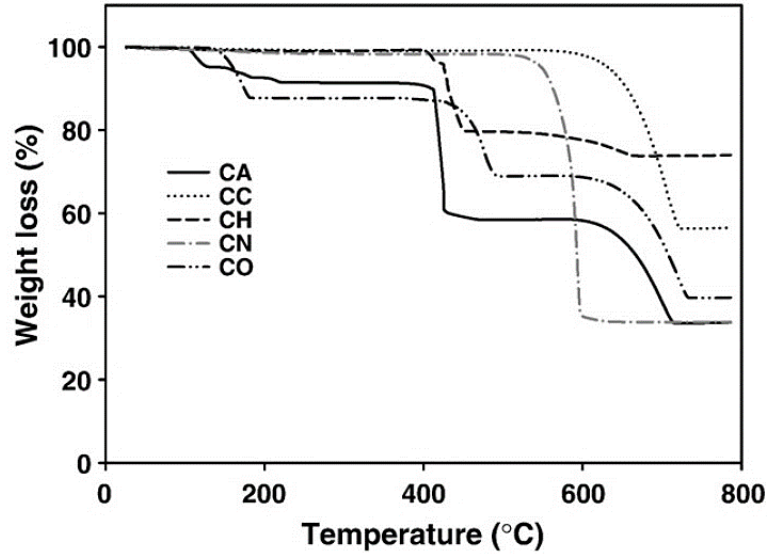
Figure 2.3. Thermogravimetric analysis of various calcium oxide precursors (Cho et al. 2009).

2.4.3. Synthesis of Barium Oxide using Barium Salts

Mallikarjuna et al. (2019) synthesized barium oxide nanocrystals by the microwave oven assisted solution combustion method. For which eucalyptus gum was collected. The eucalyptus gum was dried and crushed to get a fine powder. A known amount of the fine powder was weighed and mixed with distilled water to get gum solutions. Barium nitrate ($Ba(NO_3)_2$) was weighed and mixed with appropriate gum solutions of different concentrations. The mixture was then placed in a microwave oven and heated for 5 minutes at 400 °C. According to Mallikarjuna et al. (2019), a lot of nitrous gas was released during the process resulting in the solution being crystallized. The sample was then taken out and gently crushed and calcined to remove volatile impurities by means of a muffle furnace operated at 700 °C for 3 hours.

The research by Bazeera and Amrin (2017) focused on the preparation and characterization of barium oxide nanoparticles synthesized by a thermochemical method. To synthesize barium oxide nanoparticles, 20 ml ammonia was gradually added to 2 g anhydrous $BaCl_2$ powder under vigorous stirring (550-700 rpm) to produce a solution containing Ba^{+2} ions. The ammonia was gradually added to the anhydrous $BaCl_2$ powder because of the exothermic reaction of $BaCl_2$ with ammonia. The solution temperature was set at 33 °C, 55 °C and 75 °C and the pH was set in the range of 10. Distilled water was subsequently added as a precipitating agent while vigorous stirring of the solution continued until a white precipitate formed. The resulting precipitate was filtered and washed with deionized water. The white precipitate was then dried at 100 °C for 1.5 hours in an oven. To produce BaO nanoparticles, the dried precipitate was calcined at 500 °C for 2 h in a furnace.

2.5. Summary

The literature review has highlighted that sulphur emissions severely impact human life and the environment. Countries worldwide are setting strict standards and specifications for fuels to reduce sulphur emissions. At the same time, due to the rising concerns of crude oil prices and the environment, countries are paying attention to the development of alternative fuels and the use of waste feedstocks, such as tyre derived oil (TDO). However, there is a need to desulphurize TDO, considering that the sulphur content of TDO is within the range of 0.11 wt.% to 1.27 wt.% as presented in Table 2.2. The various desulphurization techniques were reviewed, including the advantages and disadvantages of each desulphurization technique. The focus is on reactive adsorptive desulphurization due to feasibility for small scale implementation as the process requires moderate process temperatures and pressures. For reactive adsorptive desulphurization, metal oxides show tremendous potential; however, there is limited published information on the use of alkaline earth metal oxides. The wet and incipient wet impregnation methods were reviewed for the synthesis of silica-supported alkaline earth metal oxides because of their methodical simplicity, low costs and limited waste generation. Based on the aforementioned issues, the remaining chapters of this report will demonstrate the promising potentials of TDO as an alternative fuel and the desulphurization capability of alkaline earth metal oxides.

2.6. References

- Abro, R., Abdeltawab, A., Al-Deyab, S., Yu, G., Qazi, A., Gao, S. and Chen, X. (2014). A review of extractive desulfurization of fuel oils using ionic liquids. *RSC Adv.*, 4(67), pp.35302-35317.

- Adeyi, A.A. and Aberuagba, F. (2012). Comparative analysis of adsorptive desulphurization of crude oil by manganese dioxide and zinc oxide. *Research Journal of Chemical Sciences*

- Ahmad, S., Ahmad, M., Naeem, K., Humayun, M., Sebt-E-Zaeem, S. and Faheem, F. (2016). Oxidative desulfurization of tire pyrolysis oil. *Chemical Industry and Chemical Engineering Quarterly*, 22(3), pp.249-254.

- Aida T., Yamamoto D., Iwata M., Sakata K., *Rev.* (2000). Development of oxidative desulfurization process for diesel fuel. *Heteroatom Chem,* 22, pp.241-256.

- Al-Lal, A., Bolonio, D., Llamas, A., Lapuerta, M. and Canoira, L. (2015). Desulfurization of pyrolysis fuels obtained from waste: Lube oils, tires and plastics. *Fuel*, 150, pp.208-216.

- Alvarez, J., Lopez, G., Amutio, M., Mkhize, N., Danon, B., van der Gryp, P., Görgens, J., Bilbao, J. and Olazar, M. (2017). Evaluation of the properties of tyre pyrolysis oils obtained in a conical spouted bed reactor. *Energy*, 128, pp.463-474.

- Arpa, O., Yumrutas, R. and Demirbas, A. (2010). Production of diesel-like fuel from waste engine oil by pyrolitic distillation. *Applied Energy*, 87(1), pp.122-127.

- Aydın, H. and İlkılıç, C. (2012). Optimization of fuel production from waste vehicle tires by pyrolysis and resembling to diesel fuel by various desulfurization methods. Fuel, 102, pp.605-612.

- Babich, I.V. and Moulijn, J.A. (2003). Science and technology of novel processes for deep desulfurization of oil refinery streams: a review⋆. *Fuel*, 82(6), pp.607-631.

- Bae, J. (2017). Fuel Processor Lifetime and Reliability in Solid Oxide Fuel Cells. *Solid Oxide Fuel Cell Lifetime and Reliability*, pp.145-171.

- Baird, W.C. Jr. and Bearden, R. Jr. (1978). Desulfurization and Hydroconversion of Residua with Alkaline Earth Metal Compunds and Hydrogen. 4 087 348.

- Banar, M., Akyıldız, V., Özkan, A., Çokaygil, Z. and Onay, Ö. (2012). Characterization of pyrolytic oil obtained from pyrolysis of TDF (Tire Derived Fuel). *Energy Conversion and Management*, 62, pp.22-30.

- Bazeera, A. and Amrin, M. (2017). Synthesis and Characterization of Barium Oxide Nanoparticles. *IOSR Journal of Applied Physics*, 03(01), pp.69-72.

- Betiha, M., Rabie, A., Ahmed, H., Abdelrahman, A. and El-Shahat, M. (2018). Oxidative desulfurization using graphene and its composites for fuel containing thiophene and its derivatives: An update review. *Egyptian Journal of Petroleum*, 27(4), pp.715-730.

- Bond, G. (1987). *Heterogeneous Catalysis: Principles and Applications*. 2nd ed. Oxford: Oxford University Press.

- Bowker, M. (1998). *The Basis and Application of Heterogenous Catalysis*. 1st ed. Oxford: Oxford University Press.

- Brijesh, P. and Sreedhara, S. (2013). Exhaust emissions and its control methods in compression ignition engines: A review. *International Journal of Automotive Technology*, 14(2), pp.195-206.

- Burtraw, D. and Goulder, M. (2013). SO2 Program. *Encyclopedia of Energy, Natural Resource, and Environmental Economics*, pp.212-216.

- Campanati, M., Fornasari, G. and Vaccari, A. (2003). Fundamentals in the preparation of heterogeneous catalysts. *Catalysis Today*, 77(4), pp.299-314.

- Campos-Martin, J., Capel-Sanchez, M., Perez-Presas, P. and Fierro, J. (2010). Oxidative processes of desulfurization of liquid fuels. *Journal of Chemical Technology & Biotechnology*, 85(7), pp.879-890.

- Cho, Y., Seo, G. and Chang, D. (2009). Transesterification of tributyrin with methanol over calcium oxide catalysts prepared from various precursors. *Fuel Processing Technology*, 90(10), pp.1252-1258.

- Chu, X., Hu, Y., Li, J., Liang, Q., Lou, Y., Zhang, X., Peng, X. and Yue, W. (2008). Desulfurization of Diesel Fuel by Extraction with [BF4] −based Ionic Liquids. *Chinese Journal of Chemical Engineering*, 16(6), pp.881-884.

- Cohen, A., Samet, J. and Straif, K. (2013). *Air Pollution and Cancer*. Lyon: International Agency for Research on Cancer.

- Cunliffe, A. and Williams, P. (1998). Composition of oils derived from the batch pyrolysis of tyres. *Journal of Analytical and Applied Pyrolysis*, 44(2), pp.131-152.

- Dasgupta, S., Gupta, P., Aarti, Nanoti, A., Goswami, A., Garg, M., Tangstad, E., Vistad, Ø., Karlsson, A. and Stöcker, M. (2013). Adsorptive desulfurization of diesel by regenerable nickel based adsorbents. *Fuel*, 108, pp.184-189.

- Del Bianco, A., Panariti, N., Di Carlo, S., Beltrame, P. and Carniti, P. (1994). New Developments in Deep Hydroconversion of Heavy Oil Residues with Dispersed Catalysts. 2. Kinetic Aspects of Reaction. *Energy & Fuels*, 8(3), pp.593-597.

- Department of Minerals and Energy. (2006). *Petroleum Products Act 120: Regulations: Specifications and standards*. [online] Available at: http://www.energy.gov.za/files/policies/regulations_petroleumproducts_standards_2006 [Accessed 21 March 2020].

- Deshpande, A., Bassi, A. and Prakash, A. (2005). Ultrasound-Assisted, Base-Catalyzed Oxidation of 4,6-Dimethyldibenzothiophene in a Biphasic Diesel−Acetonitrile System. *Energy & Fuels*, 19(1), pp.28-34.

- Dieselnet. (2020). *Emission Standards: Europe: Cars and Light Trucks*. [online] Available at: https://dieselnet.com/standards/eu/ld.php [Accessed 22 March 2020].

- Doğan, O., Çelik, M. and Özdalyan, B. (2012). The effect of tire derived fuel/diesel fuel blends utilization on diesel engine performance and emissions. *Fuel*, 95, pp.340-346.

- Egorova, M. and Prins, R. (2004). Hydrodesulfurization of dibenzothiophene and 4,6-dimethyldibenzothiophene over sulfided NiMo/γ-Al2O3, CoMo/γ-Al2O3, and Mo/γ-Al2O3 catalysts. *Journal of Catalysis*, 225(2), pp.417-427.

- Evans, A. and Evans, R. (2006). The Composition of a Tyre: Typical Components. *Banbury: The Waste & Resources Action Programme*.

- Frigo, S., Seggiani, M., Puccini, M. and Vitolo, S. (2014). Liquid fuel production from waste tyre pyrolysis and its utilisation in a Diesel engine. *Fuel*, 116, pp.399-408.

- Gatan, R., Barger, P., Gembicki, V. (2004). Oxidative desulfurization: a new technology for ULSD. *ACS Division of Fuel Chemistry*, 49(2), pp.577-579.

- Gates, B. and Topsøe, H. (1997). Reactivities in deep catalytic hydrodesulfurization: challenges, opportunities, and the importance of 4-methyldibenzothiophene and 4,6-dimethyldibenzothiophene. *Polyhedron*, 16(18), pp.3213-3217.

- Gawande, P. R and Kaware J. P. (2018). Isotherm and Kinetics of Desulphurization of Diesel by Batch Adsorption Studies. *International Journal of Chemical Engineering Research*, 10 (1), p.116.

- Gawande, P.R. and Kaware, J.P. (2014). A review on desulphurization of liquid fuel by adsorption. *Int. J. Sci. Res*, *7*, pp.2255-2259.

- Gray, K., Pogrebinsky, O., Mrachko, G., Xi, L., Monticello, D. and Squires, C. (1996). Molecular mechanisms of biocatalytic desulfurization of fossil fuels. *Nature Biotechnology*, 14(13), pp.1705-1709.

- Hanif, A., Sun, M., Tao, Z., Liu, L., Tsang, D., Gu, Q. and Shang, J. (2019). Silica Supported MgO as An Adsorbent for Precombustion CO2 Capture. *ACS Applied Nano Materials*, 2(10), pp.6565-6574.

- Harris, G., Thompson, W., Fitzgerald, E. and Wartenberg, D. (2014). The association of PM2.5 with full term low birth weight at different spatial scales. *Environmental Research*, 134, pp.427-434.

- Infantes-Molina, A., Romero-Perez, A., Eliche-Quesada, D., Merida-Robles, J., Jimenez-Lopez, A. and Rodriguez-, E. (2012). Transition Metal Sulfide Catalysts for Petroleum Upgrading – Hydrodesulfurization Reactions. *Hydrogenation*.

- Isa, K. and Nogawa, M. (1984). Thermal decomposition of magnesium acetate tetrahydrate under self-generated atmosphere. *Thermochimica Acta*, 75(1-2), pp.197-206.

- Isa, K. and Okuno, H. (1982). Thermal Decomposition of Calcium Sulfate Dihydrate under Self-generated Atmosphere. *Bulletin of the Chemical Society of Japan*, 55(12), pp.3733-3737.

- Jantaraksa, N., Prasassarakich, P., Reubroycharoen, P. and Hinchiranan, N. (2015). Cleaner alternative liquid fuels derived from the hydrodesulfurization of waste tire pyrolysis oil. *Energy Conversion and Management*, 95, pp.424-434.

- Jiang, Z., Lu, H., Zhang, Y. and Li, C. (2011). Oxidative Desulfurization of Fuel Oils. *Chinese Journal of Catalysis*, 32(5), pp.707-715.

- Juma, M., Koreňová, Z., Markoš, J., Jelemensky, L. and Bafrnec, M. (2007). Experimental study of pyrolysis and combustion of scrap tire. *Polymers for Advanced Technologies*, 18(2), pp.144-148.

- Kim, J., Ma, X., Zhou, A. and Song, C. (2006). Ultra-deep desulfurization and denitrogenation of diesel fuel by selective adsorption over three different adsorbents: A study on adsorptive selectivity and mechanism. *Catalysis Today*, 111(1-2), pp.74-83.

- Kohl, A. and Nielsen, R. (1997). Sulfur Recovery Processes. *Gas Purification*, pp.670-730.

- Kumar, A. and Banerjee, T. (2009). Thiophene separation with ionic liquids for desulphurization: A quantum chemical approach. *Fluid Phase Equilibria*, 278(1-2), pp.1-8.

- Kushida, N. and Mihara, S. (2016). Rubber Composition for Tires and Pneumatic Tire. US9309387B2.

- Lee, B., Kim, B. and Lee, K. (2014). Air Pollution Exposure and Cardiovascular Disease. *Toxicological Research*, 30(2), pp.71-75.

- Lee, J., Lee, J., Kim, J. and Kim, S. (1995). Pyrolysis of waste tires with partial oxidation in a fluidized-bed reactor. *Energy*, 20(10), pp.969-976.

- Lee, K. and Valla, J. (2019). Adsorptive desulfurization of liquid hydrocarbons using zeolite-based sorbents: a comprehensive review. *Reaction Chemistry & Engineering*, 4(8), pp.1357-1386.

- Liu, B., Peng, Y. and Chen, Q. (2016). Adsorption of N/S-Heteroaromatic Compounds from Fuels by Functionalized MIL-101(Cr) Metal–Organic Frameworks: The Impact of Surface Functional Groups. *Energy & Fuels*, 30(7), pp.5593-5600.

- Luo, M., Xing, J., Gou, Z., Li, S., Liu, H. and Chen, J. (2003). Desulfurization of dibenzothiophene by lyophilized cells of Pseudomonas delafieldii R-8 in the presence of dodecane. *Biochemical Engineering Journal*, 13(1), pp.1-6.

- Mahotas, V. (2019). South African National Workshop on Implementation of Marpol VI on 0.50 % Sulphur Limit. *Petroleum Regulation Hydrocarbons Policy*. Cape Town: Cleaner Fuels Strategy.

- Mallikarjuna, I., Triveni, M. K. and Shivalingaswamy, T. (2019). Microwave oven Aided Synthesis and Characterization of Barium oxide Nanoparticles. *Journal of Applicable Chemistry*, 08(4), pp.1665-1674.

- McClellan, R., Hesterberg, T. and Wall, J. (2012). Evaluation of carcinogenic hazard of diesel engine exhaust needs to consider revolutionary changes in diesel technology. *Regulatory Toxicology and Pharmacology*, 63(2), pp.225-258.

- Miguel Martín-Martínez, J. (2002). Rubber base adhesives. *Adhesion Science and Engineering*, pp.573-675.

- Mjalli, F., Ahmed, O., Al-Wahaibi, T., Al-Wahaibi, Y. and AlNashef, I. (2014). Deep oxidative desulfurization of liquid fuels. *Reviews in Chemical Engineering*, 30(4).

- Mohebali, G. and Ball, A. (2016). Biodesulfurization of diesel fuels – Past, present and future perspectives. *International Biodeterioration & Biodegradation*, 110, pp.163-180.

- Moosavi, E., Dastgheib, S. and Karimzadeh, R. (2012). Adsorption of Thiophenic Compounds from Model Diesel Fuel Using Copper and Nickel Impregnated Activated Carbons. *Energies*, 5(10), pp.4233-4250.

- Murillo, R., Aylón, E., Navarro, M., Callén, M., Aranda, A. and Mastral, A. (2006). The application of thermal processes to valorise waste tyre. *Fuel Processing Technology*, 87(2), pp.143-147.

- Muzenda, E. (2014). A Comparative Review of Waste Tyre Pyrolysis, Gasification and Liquefaction (PGL) Processes. *Int'l Conf. on Chemical Engineering & Advanced Computational Technologies (ICCEACT'2014) Nov. 24-25, 2014 Pretoria (South Africa)*.

- Nkosi, N. and Muzenda, E. (2014). A Review and Discussion of Waste Tyre Pyrolysis and Derived Products. *Proceedings of the World Congress on Engineering*, vol. 2.

- Ohshiro, T. and Izumi, Y. (1999). Microbial Desulfurization of Organic Sulfur Compounds in Petroleum. *Bioscience, Biotechnology, and Biochemistry*, 63(1), pp.1-9.

- Otsuki, S., Nonaka, T., Takashima, N., Qian, W., Ishihara, A., Imai, T. and Kabe, T. (2000). Oxidative Desulfurization of Light Gas Oil and Vacuum Gas Oil by Oxidation and Solvent Extraction. *Energy & Fuels*, 14(6), pp.1232-1239.

- Ozcan, H., Ongen, A. and Pangaliyev, Y. (2016). An Experimental Study of Recoverable Products from Waste Tire Pyrolysis. *Issue 3*, 18(3), pp.582-590.

- Pilusa, T.J., Shukla, M. and Muzenda, E. (2013). Pyrolytic Tyre Derived Fuel: A Review. Johannesburg: International Conference on Chemical, Mining and Metallurgical Engineering.

- Prat, D., Hayler, J. and Wells, A. (2014). A survey of solvent selection guides. *Green Chem.*, 16(10), pp.4546-4551.

- Purwajanti, S., Zhang, H., Huang, X., Song, H., Yang, Y., Zhang, J., Niu, Y., Meka, A., Noonan, O. and Yu, C. (2016). Mesoporous Magnesium Oxide Hollow Spheres as Superior Arsenite Adsorbent: Synthesis and Adsorption Behavior. *ACS Applied Materials & Interfaces*, 8(38), pp.25306-25312.

- Rajendran, A., Cui, T., Fan, H., Yang, Z., Feng, J. and Li, W. (2020). A comprehensive review on oxidative desulfurization catalysts targeting clean energy and environment. *Journal of Materials Chemistry A*, 8(5), pp.2246-2285.

- Ryzhikov, A., Bezverkhyy, I. and Bellat, J. (2008). Reactive adsorption of thiophene on Ni/ZnO: Role of hydrogen pretreatment and nature of the rate determining step. *Applied Catalysis B: Environmental*, 84(3-4), pp.766-772.

- Sadare, O., Obazu, F. and Daramola, M. (2017). Biodesulfurization of Petroleum Distillates— Current Status, Opportunities and Future Challenges. *Environments*, 4(4), p.85.

- Saha, P., Johny, E., Dangi, A., Shinde, S., Brake, S., Eapen, M., Sohal, S., Naidu, V. and Sharma, P. (2018). Impact of Maternal Air Pollution Exposure on Children's Lung Health: An Indian Perspective. *Toxics*, 6(4), p.68.

- Shafi, R. and Hutchings, G. (2000). Hydrodesulfurization of hindered dibenzothiophenes: an overview. *Catalysis Today*, 59(3-4), pp.423-442.

- Sharma, M., Sharma, P. and Kim, J. (2013). Solvent extraction of aromatic components from petroleum derived fuels: a perspective review. *RSC Advances*, 3(26), p.10103.

- Sietsma, J., Jos van Dillen, A., de Jongh, P. and de Jong, K. (2006). Application of ordered mesoporous materials as model supports to study catalyst preparation by impregnation and drying. *Studies in Surface Science and Catalysis*, pp.95-102.

- Soleimani, M., Bassi, A. and Margaritis, A. (2007). Biodesulfurization of refractory organic sulfur compounds in fossil fuels. *Biotechnology Advances*, 25(6), pp.570-596.

- Song, C. (2003). An overview of new approaches to deep desulfurization for ultra-clean gasoline, diesel fuel and jet fuel. *Catalysis Today*, 86(1-4), pp.211-263.

- Soriano, A., Roquero, P. and Klimova, T. (2010). Behavior of NiMo(W)/Zr-SBA-15 deep hydrodesulfurization catalysts in presence of aromatic and nitrogen-containing compounds. *Scientific Bases for the Preparation of Heterogeneous Catalysts - Proceedings of the 10th International Symposium, Louvain-la-Neuve, Belgium, July 11-15, 2010*, pp.525-528.

- Taleb, D., Hamid, H., Deris, R., Zulkifli, M., Khalil, N. and Ahmad Yahaya, A. (2020). Insights into pyrolysis of waste tire in fixed bed reactor: Thermal behavior. *Materials Today: Proceedings*, 31, pp.178-186.

- Trongyong, S. and Jitkarnka, S. (2015). Enhanced Sulphur Removal from Tyre-Derived Oil Using Aluminosilicate MCM-48 with Pyrolysis of Waste Tyres. *Chemical Engineering Transactions*, 45, pp. 679-684.

- Unapumnuk, K., Keener, T., Lu, M. and Liang, F. (2008). Investigation into the removal of sulfur from tire derived fuel by pyrolysis. *Fuel*, 87(6), pp.951-956.

- US EPA. (2020). *Effects of Acid Rain | US EPA*. [online] Available at: https://www.epa.gov/acidrain/effects-acid-rain [Accessed 20 March 2020].

- USGS. (2020). *Forest Affected by Acid Rain*. [online] Available at: https://www.usgs.gov/media/images/forest-affected-acid-rain [Accessed 20 March 2020].

- Vogelaar, B., Steiner, P., van der Zijden, T., van Langeveld, A., Eijsbouts, S. and Moulijn, J. (2007). Catalyst deactivation during thiophene HDS: The role of structural sulfur. *Applied Catalysis A: General*, 318, pp.28-36.

- Wei, Y., Wang, Y., Di, Q., Choirat, C., Wang, Y., Koutrakis, P., Zanobetti, A., Dominici, F. and Schwartz, J. (2019). Short term exposure to fine particulate matter and hospital admission risks and costs in the Medicare population: time stratified, case crossover study. *BMJ*, p.l6258.

- Welz, B., Lepri, F., Araujo, R., Ferreira, S., Huang, M., Okruss, M. and Becker-Ross, H. (2009). Determination of phosphorus, sulfur and the halogens using high-temperature molecular absorption spectrometry in flames and furnaces—A review. *Analytica Chimica Acta*, 647(2), pp.137-148.

- Witoon, T., Bumrungsalee, S., Vathavanichkul, P., Palitsakun, S., Saisriyoot, M. and Faungnawakij, K. (2014). Biodiesel production from transesterification of palm oil with methanol over CaO supported on bimodal meso-macroporous silica catalyst. *Bioresource Technology*, 156, pp.329-334.

- Woodruff, T., Darrow, L. and Parker, J. (2008). Air Pollution and Postneonatal Infant Mortality in the United States, 1999–2002. *Environmental Health Perspectives*, 116(1), pp.110-115.

- Yang, R., Hernandez-Maldonado, A. and Yang, F. (2003). Desulfurization of Transportation Fuels with Zeolites under Ambient Conditions. *ChemInform*, 34(40).

- Yazdani, E., Hashemabadi, S. and Taghizadeh, A. (2019). Study of waste tire pyrolysis in a rotary kiln reactor in a wide range of pyrolysis temperature. *Waste Management*, 85, pp.195-201.

- Zhang, G., Yu, F. and Wang, R. (2009). Research advances in oxidative desulfurization technologies for the production of low sulfur fuel oils. *Petroleum & Coal*, 51(3), pp.196-207.

CHAPTER 3

3. Composition of Tyre Derived Oil: A Comparative Study

3.1. Experimental Work

3.1.1. Gas Chromatography-Mass Spectrometry (GC-MS) Method

The tyre derived oil (TDO) was obtained from Mandini, a tyre pyrolysis plant based in Alberton, Johannesburg. The tyre derived oil was analysed using a Shimadzu GC-MS – QP2010 SE equipped with an AOC-20i auto injector. An SH-Rxi^{TM}-5MS column (0.25 mm internal diameter, 0.25 μm film thickness, 30 m length) was used with a low-polarity phase crossbonded 5% diphenyl / 95% dimethyl polysiloxane. A TDO sample was drawn with a 10 ml syringe. A 0.45 μm PTFE syringe filter was attached to the outlet of the syringe. The TDO was passed into a 2 ml GC vial. An aliquot of 0.5 μl was injected using the auto injector. The oven temperature was initially set at 40 ^{o}C, then increased at 3 ^{o}C/min to 320 ^{o}C and then held isothermally for 10 min to remove all the products from the column. The details of the GC-MS method are presented in Table 3.1.

Table 3.1. Details of the GC-MS method for the TDO analysis.

Specification	Details
Column configuration	SH-Rxi^{TM}-5MS column (0.25 mm Internal Diameter, 0.25 μm Film Thickness, 30 m Length) - Crossbonded 5% diphenyl / 95% dimethyl polysiloxane.
Oven/column temperature	The oven temperature was initially set at 40 ^{o}C, then increased at 3 ^{o}C/min to 320 ^{o}C and then held isothermally for 10 min.
Carrier gas/flowrate	Helium (> 99.999 % Purity), 1.15 ml/min
Total flow	61.8 ml/min
Head column pressure	60.5 kPa
Transfer line temperature	250 ^{o}C
Split ratio	50:1
Injection volume	0.5 μl
Scan mode	33-500 m/z
Ion source temperature	200 ^{o}C
Interface temperature	300 ^{o}C

3.1.2. Fourier-Transform Infrared Spectroscopy (FTIR) Method

A TDO sample was drawn with a 10 ml syringe. A 0.45 μm PTFE syringe filter was attached to the outlet of the syringe. A drop of TDO was placed on the ATR crystal and the sample presser was lowered into position. The FTIR spectrum of the TDO was captured on a Shimadzu IRSpirit equipped with a

single reflection integration-type attenuated total reflection (ATR) attachment. The TDO sample was scanned at room temperature with a resolution of 8 cm^{-1} over a wave number range of 4000–400 cm^{-1}. The details of the FTIR method are presented in Table 3.2.

Table 3.2. Details of the FTIR method for the TDO analysis.

Specification	Details
Instrument	IRSpirit QATR-S (diamond prism)
Resolution	8 cm^{-1}
Wave range	4000–400 cm^{-1}
Apodization function	Happ-Genzel
Detector	DLATGS

3.2. Results and Discussion

3.2.1. Fourier-Transform Infrared Spectroscopy (FTIR) Analysis

The FTIR transmittance spectrum of the tyre derived oil is shown in Figure 3.1. A spectrum analysis allowed for the determination of the functional groups present in the tyre derived oil. The transmittance peaks of the spectrum were identified, as shown in Table 3.3.
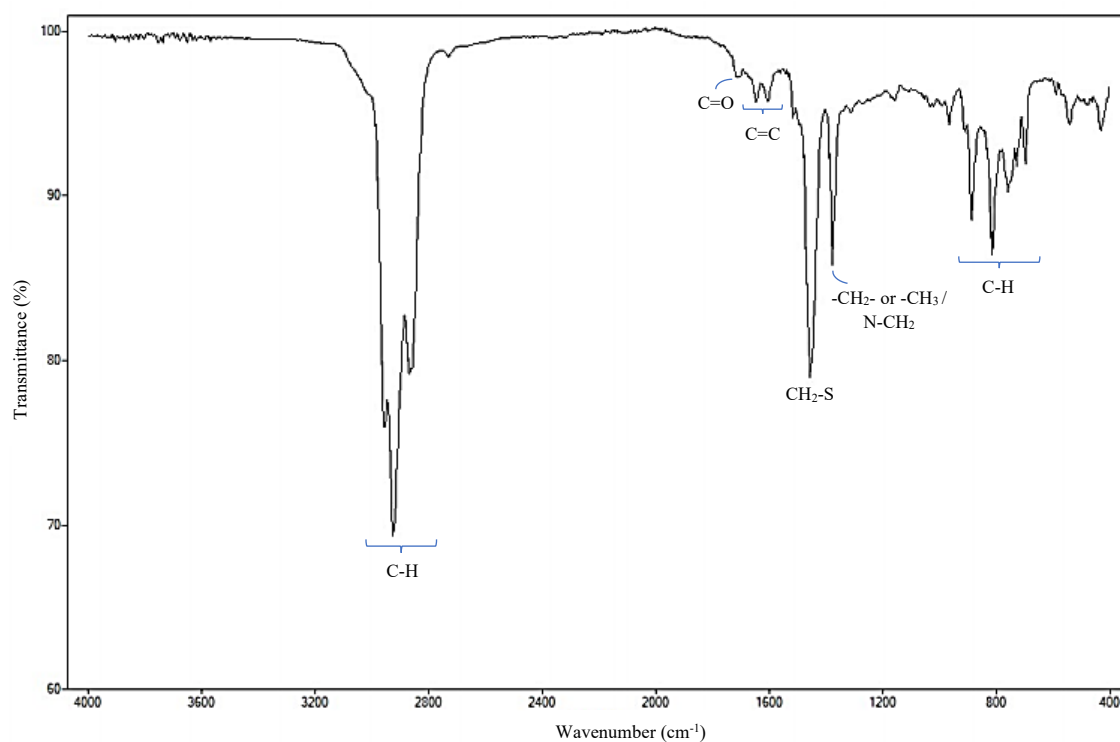
Figure 3.1. FTIR spectrum of the tyre derived oil.

The C=C stretching deformation vibrations between 3110 and 3005 cm^{-1} and the C=C stretching vibrations between 1690 and 1560 cm^{-1} indicates the presence of alkenes (Rofiqul Islam et al., 2008; Islam et al., 2010, Alvarez et al., 2017). Whereas, the C-H stretching vibrations between 3000 and 2770 cm^{-1} are related to alkanes (Rofiqul Islam et al., 2008; Islam et al., 2010; Alvarez et al., 2017; Taleb et al., 2020). The peaks between 1750 and 1690 cm^{-1} correspond to C=O stretching relating to carbonyl/carboxyl functional groups (such as aldehydes, ketones and carboxylic acids) (Alvarez et al., 2017; Taleb et al., 2020). The sharp peak at 1455 cm^{-1} is associated with sulphur containing compounds (Alvarez et al., 2017). Whereas, the sharp peak at 1375 cm^{-1} is assigned to -CH$_2$-/-CH$_3$ groups or the contribution of nitrogen-containing compounds (Alvarez et al., 2017). Finally, the region between 930 and 680 cm^{-1} corresponds to C-H out-of-plane bending resulting from aromatic compounds (Rofiqul Islam et al., 2008; Islam et al., 2010; Alvarez et al., 2017; Taleb et al., 2020).

Table 3.3. FTIR functional groups present in tyre derived oil.

Transmittance Bands (cm^{-1})					Band Assignment	Class of Compounds
(Alvarez et al., 2017)	(Taleb et al., 2020)	(Rofiqul Islam et al., 2008)	(Islam et al., 2010)	Present Work		
3500-3200	3500–3200	-	-	-	O-H stretching	Phenols, alcohols, or carboxylic acids
-	-	3100-3005	3095-3005	3110-3005	C=C stretching	Alkenes
3050	-	-	-	-	C-H stretching	Aromatic compounds
-	3018	-	-	-	C=H stretching	Alkenes
3000-2700	3100-2700	3000-2800	3000-2800	3000-2770	C-H stretching	Alkanes
1750-1675	1750-1675	-	-	1750-1690	C=O stretching	Carbonyl (such as aldehydes and ketones) /Carboxyl
-		1675-1605	1680-1620	1690-1625	C=C stretching	Alkenes
1650-1605	1650-1605	-	-	-	C=C stretching	Aromatic compounds
1600-1550	-	-	-	1625-1560	C=C stretching	Alkenes
-	-	1600-1545	1600-1525	-	C=C stretching	Aromatic compounds
-	1520-1115	1520-1115	1520-1220	-	C-H bending	Alkanes
1450	-	-	-	1455	CH$_2$-S	Sulphur containing compounds
1370	-	-	-	1375	-CH$_2$- or -CH$_3$	Alkanes
					N-CH$_2$ and/or N-B-N; B – benzoid moieties	Nitrogen containing compounds
-	1150-1000	-	-	-	C-H in-plane bending	Aromatic compounds
-	1020-845	1020-845	1035-830	-	C=C stretching	Alkenes
900-700	810-693	810-660	825-650	930-680	C-H out-of-plane blending	Aromatic compounds

3.2.2. Gas Chromatography-Mass Spectrometry (GC-MS) Analysis
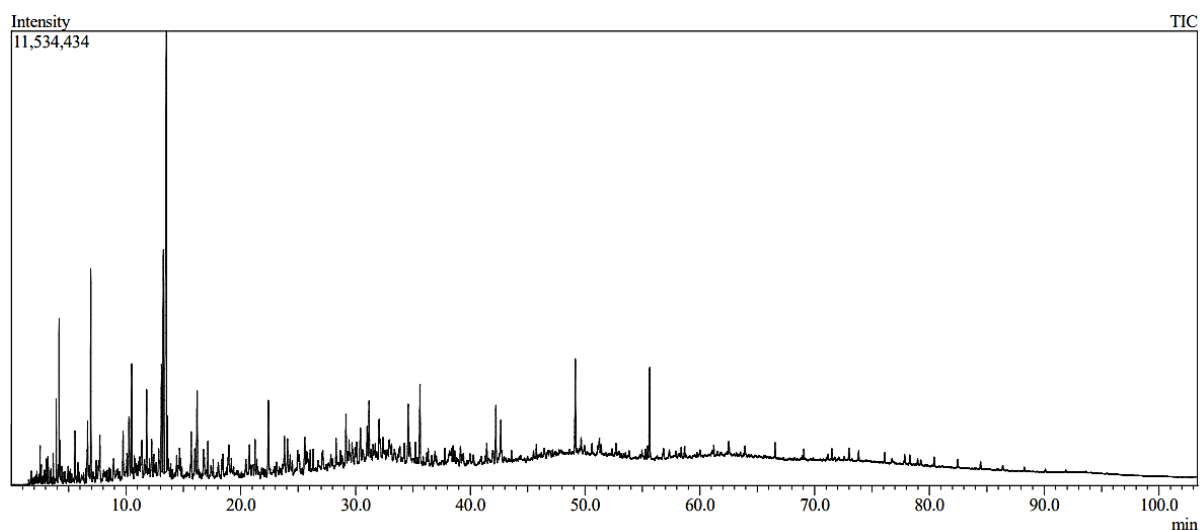
Figure 3.2. Chromatogram of the tyre derived oil.

Figure 3.3 highlights the most abundant compounds in the TDO, of which; some are highly valuable, such as toluene, xylene, mesitylene, cymene and limonene. They are used to produce plastics, resins, surfactants and pharmaceuticals.

Peak#	R.Time	Area%	Similarity	Base m/z	Name
1	4.171	4.34	95	91.05	Toluene
2	6.933	9.08	97	91.05	p-Xylene
3	10.500	4.68	95	105.10	Benzene, 1-ethyl-2-methyl-
4	11.799	4.03	81	105.10	Mesitylene
5	13.093	6.97	84	95.10	Cyclohexene, 1-methyl-4-(1-methylethyl)-, (R)-
6	13.260	17.07	97	119.10	o-Cymene
7	13.525	40.51	96	68.10	D-Limonene
8	16.200	4.92	83	132.10	p-(1-Propenyl)-toluene
9	49.151	4.61	95	57.05	Heptadecanenitrile
10	55.625	3.78	96	57.05	Octadecanenitrile
		100.00			

Figure 3.3. Chromatogram of the tyre derived oil (0 – 60 min) showing the most abundant compounds.

The chemical composition of the TDO confirms the functional groups detected in the FTIR analysis. The compounds were identified using the NIST 20 library. The compounds have been classified into alcohols, alkanes, alkenes, alkynes, terpenes, aromatics, organofluorines, organonitriles, acids, organosulphides, acetates, esters, heteroaromatics and benzene derivatives. The classification was essential, given the vast number of compounds. Table 3.4 shows the assigned tentative compounds and their peak percentage areas compared to the total area of all peaks on the chromatogram, which gives

the relative concentration of the TDO. In the present work, the total identified peak percentage area was 59.16 %, whereas other researchers reported 75.99 % (Islam et al., 2010), 75.03 % (Laresgoiti et al., 2004), 68.82 % (Rofiqul Islam et al., 2008), 23.67 % (Taleb et al., 2020), 83.84 % (Uyumaz et al., 2019) and 71.27 % (Alvarez et al., 2017). The unidentified peaks are due to the presence of heavier and more complex products, which are more difficult to identify (Laresgoiti et al., 2004; Kumar Singh et al., 2018).

The aromatic fraction comprises of compounds such as benzene, toluene, ethylbenzene and xylene (BTEX), which can be refined and used in petrochemical industries as feedstock chemicals (Cunliffe and Williams, 1998). The presence of polycyclic and mono-aromatic hydrocarbons in the TDO were associated with secondary reactions during the pyrolysis process. These compounds are known to originate from the decomposition of primary products, with some of the higher molecular weight compounds formed via Diels Alder reactions (Williams and Taylor, 1993).

The presence of oxygen, nitrogen and sulphur-containing compounds in the TDO were attributed to the thermal degradation of accelerators such as benzothiozolyl disulphide, 2-(4-morpholinylthio)-benzothiazole, N,N-caprolactamdisulphide, 2-mercaptobenzothiazole and N,N-di-isopropyl-2-benzothiazole-sulfenamide incorporated into tyres during the formulation process (Quek and Balasubramanian, 2013; Alvarez et al., 2017). During the pyrolysis of tyres, the C-S and N-S bonds of these additives undergo cleavage to form benzothiazole and benzothiazole derivatives (Quek and Balasubramanian, 2013), which were found in the TDO. Benzothiazole offers a wide range of industrial applications, and several researchers have identified benzothiazole in significant concentrations in tyre derived oils. In the present work, the peak percentage area of benzothiazole was 0.80 %, whereas other researchers reported 0.93 % (Laresgoiti et al., 2004), 0.56 % (Taleb et al., 2020), 1.42 % (Uyumaz et al., 2019) and 1.54 % (Alvarez et al., 2017). Other heteroatomic compounds that have been identified in tyre derived oils include quinolines, thiophenes and benzothiophenes, to name the most common.

The terpene content is partly responsible for the potential value associated with tyre derived oils, particularly DL-limonene (a mixture of *d*- and *l*- limonene) occurring in high concentrations. In the present work, the peak percentage area of DL-limonene was 6.55 %, whereas other researchers reported 11.11 % (Islam et al., 2010), 5.12 % (Laresgoiti et al., 2004), 29.54 % (Rofiqul Islam et al., 2008), 0.18 % (Taleb et al., 2020), 4.31 % (Uyumaz et al., 2019) and 24.29 % (Alvarez et al., 2017). DL-Limonene is one of the major market value compounds in TDO. This compound has a range of uses as an industrial solvent, application in resins and adhesives, a dispersing agent for pigments, a fragrance in cleaning products and as an environmentally friendly solvent (Erasto and Viljoen, 2008; Danon et al., 2015).

Table 3.4. Tentative composition of tyre derived oil.

Name	Formula	Peak Area %						
		Present Work	(Islam et al., 2010)	(Laresgoiti et al., 2004)	(Rofiqul Islam et al., 2008)	(Taleb et al., 2020)	(Uyumaz et al., 2019)	(Alvarez et al., 2017)
Alcohols		**2.18**	**-**	**-**	**-**	**-**	**-**	**0.99**
1-Butanol, 3-methyl-	$C_5H_{12}O$	0.02	-	-	-	-	-	-
Cyclopropaneethanol, 2-methylene-	$C_6H_{10}O$	0.02	-	-	-	-	-	-
2-Cyclohexen-1-ol, 1-methyl-	$C_7H_{12}O$	0.15	-	-	-	-	-	-
Cyclohexanol, 4-methyl-, trans-	$C_7H_{14}O$	0.29	-	-	-	-	-	-
Cyclohexanemethanol, 4-methylene-	$C_8H_{14}O$	0.04	-	-	-	-	-	-
Cyclohexanol, 2,6-dimethyl-	$C_8H_{16}O$	0.04	-	-	-	-	-	-
5-Octen-2-yn-4-ol	$C_8H_{12}O$	0.13	-	-	-	-	-	-
2,2-Dimethylhexanol	$C_8H_{18}O$	-	-	-	-	-	-	0.52
Benzenepropanol	$C_9H_{12}O$	-	-	-	-	-	-	0.06
trans,cis-2,6-Nonadien-1-ol	$C_9H_{16}O$	0.17	-	-	-	-	-	-
(1,2,3-Trimethyl-cyclopent-2-enyl)-methanol	$C_9H_{16}O$	0.07	-	-	-	-	-	-
(1S,3S,4S,5R)-1-Isopropyl-4-methylbicyclo[3.1.0]hexan-3-ol	$C_{10}H_{18}O$	0.12	-	-	-	-	-	-
3,6-Octadien-1-ol, 3,7-dimethyl-, (Z)-	$C_{10}H_{18}O$	0.02	-	-	-	-	-	-
9-Methyltricyclo[4.2.1.1(2,5)]deca-3,7-diene-9,10-diol	$C_{11}H_{14}O_2$	0.17	-	-	-	-	-	-
1-Dodecanol	$C_{12}H_{26}O$	0.08	-	-	-	-	-	-
5,8-Dimethyl-1,2,3,4-tetrahydro-1-naphthol	$C_{12}H_{16}O$	0.08	-	-	-	-	-	-
6,11-Dimethyl-2,6,10-dodecatrien-1-ol	$C_{14}H_{24}O$	-	-	-	-	-	-	0.29
5H-Dibenzo[a,d]cyclohepten-5-ol, 10,11-dihydro-	$C_{15}H_{14}O$	0.09	-	-	-	-	-	-
4-Phenanthrenol, 1,2,3,4-tetrahydro-4-methyl-	$C_{15}H_{16}O$	0.06	-	-	-	-	-	-
1,6,10-Dodecatrien-3-ol, 3,7,11-trimethyl-	$C_{15}H_{26}O$	-	-	-	-	-	-	0.12
n-Pentadecanol	$C_{15}H_{32}O$	0.13	-	-	-	-	-	-
1-Decanol, 2-hexyl-	$C_{16}H_{34}O$	0.14	-	-	-	-	-	-
trans-Geranylgeraniol	$C_{20}H_{34}O$	0.17	-	-	-	-	-	-
Dihydrotachysterol	$C_{28}H_{46}O$	0.21	-	-	-	-	-	-
Alkanes		**4.03**	**1.21**	**5.80**	**-**	**0.85**	**-**	**4.27**
Cyclopentane, methyl-	C_6H_{12}	0.02	-	-	-	-	-	-
Cyclohexane	C_6H_{12}	-	-	-	-	-	-	0.02
Pentane, 2-methyl-	C_6H_{14}	0.03	-	-	-	-	-	-

Compound	Formula							
Hexane	C_6H_{14}	-	-	-	-	-	-	0.08
Cyclopentane, 1,2-dimethyl-, cis-	C_7H_{14}	0.06	-	-	-	-	-	-
Cyclohexane, methyl-	C_7H_{14}	0.07	-	-	-	-	-	-
Cyclopentane, ethyl-	C_7H_{14}	0.03	-	-	-	-	-	-
Ethylcyclopentane	C_7H_{14}	-	-	0.10	-	-	-	-
Dimethylcyclopentane	C_7H_{14}	-	-	0.14	-	-	-	-
Heptane	C_7H_{16}	0.04	-	-	-	-	-	-
Pentane, 2,4-dimethyl-	C_7H_{16}	0.02	-	-	-	-	-	-
Hexane, 3-methyl-	C_7H_{16}	0.04	-	-	-	-	-	-
Cyclohexane, 1,3-dimethyl-, cis-	C_8H_{16}	0.15	-	-	-	-	-	-
Cyclohexane, 1,3-dimethyl-, trans-	C_8H_{16}	0.07	-	-	-	-	-	-
Octane	C_8H_{16}	0.04	-	-	-	0.66	-	-
Dimethylcyclohexane	C_8H_{16}	-	-	0.10	-	-	-	-
Ethylcyclohexane	C_8H_{16}	-	-	0.41	-	-	-	-
Trimethylpentane	C_8H_{18}	-	-	0.41	-	-	-	-
Hexane, 2,2-dimethyl-	C_8H_{18}	0.04	-	-	-	-	-	-
Dimethylhexane	C_8H_{18}	-	-	0.44	-	-	-	-
Cyclohexane, 1,2,3-trimethyl-	C_9H_{18}	0.08	-	-	-	-	-	-
2,2,4,4-tetramethyl-pentane	C_9H_{20}	-	-	-	-	-	-	0.90
Octane, 3-methyl-	C_9H_{20}	0.05	-	-	-	-	-	-
Nonane	C_9H_{20}	0.05	-	-	-	-	-	-
Decane	$C_{10}H_{22}$	-	-	-	-	-	-	-
Heptane, 4-propyl-	$C_{10}H_{22}$	-	-	-	-	-	-	0.26
Norbornane, 2-isobutyl-	$C_{11}H_{20}$	0.05	-	-	-	-	-	-
Cycloundecane	$C_{11}H_{22}$	-	-	0.18	-	-	-	-
n-C11	$C_{11}H_{24}$	-	-	0.23	-	-	-	-
Cyclohexane, 1-methyl-4-(1-methylbutyl)-	$C_{12}H_{24}$	0.04	-	-	-	-	-	-
Dodecane	$C_{12}H_{26}$	0.09	-	-	-	-	-	-
Undecane, 2,6-dimethyl-	$C_{13}H_{28}$	0.11	-	-	-	-	-	-
n-C14	$C_{14}H_{30}$	-	-	1.04	-	-	-	-
Aromadendrane	$C_{15}H_{26}$	-	0.71	-	-	-	-	-
Patchoulane	$C_{15}H_{26}$	-	0.50	-	-	-	-	-
n-C15	$C_{15}H_{32}$	-	-	1.15	-	-	-	-
Pentadecane	$C_{15}H_{32}$	-	-	-	-	0.19	-	0.89
n-C16	$C_{16}H_{34}$	-	-	0.49	-	-	-	-
Hexadecane	$C_{16}H_{34}$	0.75	-	-	-	-	-	0.08

Nonane, 2,2,4,6,8,8-heptamethyl-	$C_{16}H_{34}$	-	-	-	-	-	-	0.51
Heptadecane	$C_{17}H_{36}$	0.57	-	-	-	-	-	0.30
Octadecane	$C_{18}H_{38}$	-	-	-	-	-	-	0.76
Octadecane, 3-methyl-	$C_{19}H_{40}$	0.12	-	-	-	-	-	-
Nonadecane	$C_{19}H_{40}$	-	-	-	-	-	-	0.11
n-C19	$C_{19}H_{40}$	-	-	0.18	-	-	-	-
n-C20	$C_{20}H_{42}$	-	-	0.27	-	-	-	-
Eicosane	$C_{20}H_{42}$	0.25	-	-	-	-	-	0.10
n-C21	$C_{21}H_{44}$	-	-	0.24	-	-	-	-
Heneicosane	$C_{21}H_{44}$	0.27	-	-	-	-	-	0.26
n-C22	$C_{22}H_{46}$	-	-	0.18	-	-	-	-
n-C23	$C_{23}H_{48}$	-	-	0.24	-	-	-	-
Tetracosane	$C_{24}H_{50}$	0.24	-	-	-	-	-	-
Stigmastane	$C_{29}H_{52}$	0.05	-	-	-	-	-	-
Dotriacontane	$C_{32}H_{66}$	0.07	-	-	-	-	-	-
Tetratriacontane	$C_{34}H_{70}$	0.10	-	-	-	-	-	-
Hexatriacontane	$C_{36}H_{74}$	0.54	-	-	-	-	-	-
Alkenes		**8.15**	**22.39**	**9.17**	**14.33**	**-**	**1.62**	**13.41**
1,3-Pentadiene	C_5H_8	0.02	-	-	-	-	-	-
1,3-butadiene, 2-methyl-	C_5H_8	-	2.91	-	1.39	-	-	-
2-Butene, 2-methyl-	C_5H_{10}	0.04	2.96	-	0.29	-	-	-
4-Methyl-1,3-pentadiene	C_6H_{10}	0.02	-	-	-	-	-	-
1,3-Pentadiene, 2-methyl-, (E)-	C_6H_{10}	0.03	-	-	-	-	-	-
2,4-Hexadiene	C_6H_{10}	0.14	-	-	-	-	-	-
1,3-Butadiene, 2,3-dimethyl	C_6H_{10}	-	1.37	-	-	-	-	-
Cyclohexene	C_6H_{10}	0.04	-	-	-	-	-	-
1-Pentene, 2-methyl-	C_6H_{12}	0.02	-	-	-	-	-	-
1-Butene, 2,3-dimethyl-	C_6H_{12}	0.03	-	-	-	-	-	-
2-Butene, 2,3-dimethyl-	C_6H_{12}	-	0.18	-	-	-	-	-
2-Pentene, 3-methyl-, (Z)-	C_6H_{12}	0.04	-	-	-	-	-	-
1-Butene, 3,3-dimethyl-	C_6H_{12}	0.04	-	-	-	-	-	-
2-Pentene, 3-methyl-	C_6H_{12}	0.04	-	-	-	-	-	-
2-Pentene, 4-methyl-	C_6H_{12}	-	0.66	-	-	-	-	-
2-Propenylidene-cyclobutene	C_7H_8	-	3.03	-	-	-	-	-
2-Methyl-cyclohexa-1,3-diene	C_7H_{10}	0.04	-	-	-	-	0.09	-

36

Compound	Formula							
1,3-Cycloheptadiene	C_7H_{10}	0.04	-	-	-	-	-	0.02
1,3,5-Hexatriene, 2-methyl-	C_7H_{10}	-	-	-	-	-	-	0.02
1,3,5-Hexatriene, 3-methyl-	C_7H_{10}	-	-	-	-	-	-	0.04
Methylhexadiene	C_7H_{12}	-	-	0.20	-	-	-	-
Methylcyclohexene	C_7H_{12}	-	-	0.40	-	-	-	-
Cyclopentene, 1,5-dimethyl-	C_7H_{12}	0.42	-	-	-	-	-	-
1,3-Pentadiene, 2,3-dimethyl-	C_7H_{12}	0.14	-	-	-	-	-	-
1,3-Pentadiene, 2,4-dimethyl-	C_7H_{12}	-	-	-	-	-	-	0.02
Cyclopentene, 1,5-dimethyl-	C_7H_{12}	0.07	-	-	-	-	-	0.02
1-Methylethylidene	C_7H_{12}	-	-	-	-	-	0.42	-
3-Heptene	C_7H_{14}	-	0.59	-	-	-	-	-
1-Pentene, 2,3-dimethyl-	C_7H_{14}	-	-	-	-	-	-	0.01
1-Pentene, 3,4-dimethyl-	C_7H_{14}	0.04	-	-	-	-	-	-
1,3,5,7-Cyclooctatetraene	C_8H_8	-	-	-	-	-	-	0.41
Ethylene, 1,1-dicyclopropyl-	C_8H_{12}	-	0.24	-	-	-	-	-
2,3-Dimethyl-cyclohexa-1,3-diene	C_8H_{12}	0.08	-	-	-	-	0.12	-
Spiro[2.4]heptane, 4-methylene-	C_8H_{12}	0.11	-	-	-	-	-	-
Cyclopentene, 3-ethylidene-1-methyl-	C_8H_{12}	0.07	-	-	-	-	-	-
1,3-Cyclopentadiene, 2,5,5-trimethyl-	C_8H_{12}	-	-	-	-	-	-	0.05
Octa-2,4,6-triene	C_8H_{12}	-	-	-	-	-	0.13	0.10
1-Cyclopentene, 1,2-dimethyl-4-methylene-	C_8H_{12}	-	-	-	-	-	-	0.04
Cyclohexene, 4-ethenyl-	C_8H_{12}	-	-	-	-	-	-	0.15
Dimethylhexadiene	C_8H_{14}	-	-	0.10	-	-	-	-
Dimethylcyclohexene	C_8H_{14}	-	-	5.03	-	-	-	-
Cyclooctene	C_8H_{14}	-	0.20	-	-	-	-	-
1,4-Pentadiene, 2,3,3-trimethyl-	C_8H_{14}	-	-	-	-	-	-	0.02
1,4-Heptadiene, 4-methyl-	C_8H_{14}	-	0.37	-	-	-	-	-
Cyclohexene, 1,2-dimethyl-	C_8H_{14}	-	-	-	-	-	-	0.02
Cyclohexene, 1,3-dimethyl-	C_8H_{14}	0.08	-	-	-	-	-	-
Cyclohexene, 3,5-dimethyl-	C_8H_{14}	0.33	-	-	-	-	-	-
Methyl ethyl cyclopentene	C_8H_{14}	0.05	-	-	-	-	-	-
2-Pentene, 2,4,4-trimethyl-	C_8H_{16}	0.08	-	-	-	-	-	-
1-Pentene, 2,4,4-trimethyl-	C_8H_{16}	0.10	-	-	-	-	-	-
1-Heptene, 2-methyl-	C_8H_{16}	0.07	-	-	-	-	-	-
1-Octene	C_8H_{16}	0.08	-	-	-	-	-	-
Octene	C_8H_{16}	-	-	0.09	-	-	-	-

Compound	Formula							
5-Methylenecycloocta-1,3-diene	C$_9$H$_{12}$	0.20	-	-	-	-	-	-
3,3-Dimethyl-6-methylenecyclohexene	C$_9$H$_{14}$	0.30	-	-	-	-	-	-
1,5-Hexadiene, 2,5-dimethyl-3-methylene-	C$_9$H$_{14}$	-	-	-	-	-	-	0.18
1,3-Cyclopentadiene, 1,2,5,5-tetramethyl-	C$_9$H$_{14}$	-	-	-	-	-	-	0.07
Bicyclo[3.1.0]hexane, 6-isopropylidene-	C$_9$H$_{14}$	0.11	-	-	-	-	-	-
1,3,5-Heptatriene, 2,6-dimethyl-	C$_9$H$_{14}$	-	-	-	-	-	-	0.10
2,3,5-Heptatriene, 1,6-dimethyl-	C$_9$H$_{15}$	-	-	-	-	-	-	0.05
1,1-dimethyl-4-methylenecyclohexane	C$_9$H$_{16}$	-	-	-	-	-	-	0.11
3,4-Octadiene, 7-methyl-	C$_9$H$_{16}$	-	1.08	-	-	-	-	-
1,3-Hexadiene, 3-ethyl-2-methyl-, (Z)-	C$_9$H$_{16}$	0.14	-	-	-	-	-	-
1,3-Hexadiene, 2,3,5-trimethyl-	C$_9$H$_{16}$	0.06	-	-	-	-	-	-
Cyclopentene, 3-methyl-1-(1-methylethyl)-	C$_9$H$_{16}$	0.09	-	-	-	-	-	-
Cyclohexene, 3-(1-methylethyl)	C$_9$H$_{16}$	-	-	-	-	-	-	0.05
Methyloctene	C$_9$H$_{18}$	-	-	2.20	-	-	-	-
Nonene	C$_9$H$_{18}$	-	-	0.20	-	-	-	-
1-Heptene, 2,6-dimethyl-	C$_9$H$_{18}$	0.08	-	-	-	-	-	-
Triquinacene	C$_{10}$H$_{10}$	-	-	-	-	-	0.58	-
1,3-Cyclopentadiene, 1,2,3,4-tetramethyl-5-methylene-	C$_{10}$H$_{14}$	-	-	-	-	-	0.28	-
1,3-butadienylidenecyclohexane	C$_{10}$H$_{14}$	-	-	-	-	-	-	0.20
1-butenylidenecyclohexane	C$_{10}$H$_{16}$	-	-	-	-	-	-	0.63
2,6-Dimethyl-1,5,7-octatriene	C$_{10}$H$_{16}$	-	-	-	0.96	-	-	-
1,5-Heptadiene, 2,5-dimethyl-3-methylene-	C$_{10}$H$_{16}$	-	-	-	0.81	-	-	0.87
1,5-Cyclodecadiene, (E,Z)-	C$_{10}$H$_{16}$	-	-	-	2.14	-	-	-
Trimethylheptatriene	C$_{10}$H$_{16}$	-	-	0.25	-	-	-	-
Spiro[2.4]heptane, 1,5-dimethyl-6-methylene-	C$_{10}$H$_{16}$	0.09	-	-	-	-	-	-
1,5-Cyclooctadiene, 1,2-dimethyl-	C$_{10}$H$_{16}$	0.07	-	-	-	-	-	-
1,5-Cyclooctadiene, 1,5-dimethyl-	C$_{10}$H$_{16}$	-	-	-	4.85	-	-	-
1,3-Cyclohexadiene, 1,3,5,5-tetramethyl-	C$_{10}$H$_{16}$	0.11	-	-	-	-	-	0.27
1,4-Cyclohexadiene, 3,3,6,6-tetramethyl-	C$_{10}$H$_{16}$	0.39	-	-	-	-	-	0.55
1,3-Cyclopentadiene, 5,5-dimethyl-2-propyl-	C$_{10}$H$_{16}$	-	-	-	-	-	-	0.17
Bicyclo[3.1.1]heptane, 6,6-dimethyl-2-methylene-	C$_{10}$H$_{16}$	-	0.68	-	-	-	-	-
Bicyclo[3.1.1]heptane, 6,6-dimethyl-2-methylene-, (1S)-	C$_{10}$H$_{16}$	-	-	-	0.61	-	-	-
1,3-Cyclopentadiene, 5,5-dimethyl-1-propyl-	C$_{10}$H$_{16}$	0.11	-	-	-	-	-	-
Cyclopropane, 1,1-dimethyl-2-(2,4-pentadienyl)-	C$_{10}$H$_{16}$	-	-	-	3.28	-	-	-
1,3,6-Heptatriene, 2,4,6-trimethyl-	C$_{10}$H$_{16}$	-	-	-	-	-	-	0.22
1,3,6-Heptatriene, 2,5,5-trimethyl-	C$_{10}$H$_{16}$	-	-	-	-	-	-	0.20

Name	Formula							
1,3,6-Heptatriene, 2,5,6-trimethyl-	$C_{10}H_{16}$	0.47	-	-	-	-	-	0.41
Cyclohexene, 4-methyl-1-(1-methylethenyl)-	$C_{10}H_{16}$	-	-	-	-	-	-	0.28
Cyclohexene, 5-methyl-3-(1-methylethenyl)-	$C_{10}H_{16}$	-	-	-	-	-	-	0.14
1-Cyclohexene, 4-ethyl-3-ethylidene-	$C_{10}H_{16}$	-	-	-	-	-	-	0.43
1-Cyclohexene, 1-methyl-4-(1-methylethylidene)-	$C_{10}H_{16}$	-	-	-	-	-	-	0.32
1-Cyclohexene, 4-methyl-3-(1-methylethylidene)-	$C_{10}H_{16}$	-	-	-	-	-	-	0.23
1,4-Hexadiene, 5-methyl-3-(1-methylethylidene)-	$C_{10}H_{16}$	-	-	-	-	-	-	0.35
1,3,6-Octatriene, 3,7-dimethyl-	$C_{10}H_{16}$	-	-	-	-	-	-	0.27
2,4,6-Octatriene, 2,6-dimethyl-	$C_{10}H_{16}$	-	-	-	-	-	-	0.39
o-Menth-8-ene	$C_{10}H_{18}$	0.05	-	-	-	-	-	-
Cyclopentene, 1-isopropyl-4,5-dimethyl-	$C_{10}H_{18}$	0.10	-	-	-	-	-	-
Cyclohexene, 1-methyl-3-(1-methylethyl)-	$C_{10}H_{18}$	0.14	-	-	-	-	-	-
Cyclohexene, 4-methyl-1-(1-methylethyl)-	$C_{10}H_{18}$	0.28	-	-	-	-	-	-
1-Cyclohexene, 1-methyl-4-isopropyl-	$C_{10}H_{18}$	-	-	-	-	-	-	0.94
1,6-Octadiene, 5,7-dimethyl-, (R)-	$C_{10}H_{18}$	0.07	-	-	-	-	-	-
1,6-Octadiene, 2,6-dimethyl-, (Z)-	$C_{10}H_{18}$	0.09	-	-	-	-	-	-
1,6-Octadiene, 2,6-dimethyl-	$C_{10}H_{18}$	-	-	-	-	-	-	0.55
1,7-Octadiene, 2,7-dimethyl-	$C_{10}H_{18}$	-	-	-	-	-	-	0.46
2,6-Dimethyl-2-trans-6-octadiene	$C_{10}H_{18}$	0.20	-	-	-	-	-	-
1,3-Hexadiene, 3-ethyl-2,5-dimethyl-	$C_{10}H_{18}$	0.21	-	-	-	-	-	-
cis-2,6-Dimethyl-2,6-octadiene	$C_{10}H_{18}$	0.50	-	-	-	-	-	-
1,4-Hexadiene, 3-ethyl-4,5-dimethyl-	$C_{10}H_{18}$	0.14	-	-	-	-	-	-
2-Octene, 2,6-dimethyl-	$C_{10}H_{20}$	0.28	-	-	-	-	-	-
Isopropylmethylcyclohexene	$C_{10}H_{20}$	-	-	0.51	-	-	-	-
1-Decene	$C_{10}H_{20}$	-	-	-	-	-	-	0.12
Bicyclo[4.2.1]nona-2,4,7-triene, 7-ethyl-	$C_{11}H_{14}$	0.05	-	-	-	-	-	-
Hept-2-ene, 2,4,4,6-tetramethyl-	$C_{11}H_{22}$	0.41	-	-	-	-	-	-
1-Undecene	$C_{11}H_{22}$	0.12	-	-	-	-	-	-
3-Undecene, (Z)-	$C_{11}H_{22}$	0.04	-	-	-	-	-	-
Hept-2-ene, 2,4,4,6-tetramethyl-	$C_{11}H_{22}$	0.09	-	-	-	-	-	1.12
Dispiro[2.0.2.5]undecane, 8-methylene-	$C_{12}H_{18}$	-	0.98	-	-	-	-	-
1,5-diethenyl-3-methyl-2-methylene-cyclohexane	$C_{12}H_{18}$	-	0.25	-	-	-	-	-
1-Dodecene	$C_{12}H_{24}$	-	-	-	-	-	-	0.12
3,5-Dodecadiene, 2-methyl-	$C_{13}H_{24}$	-	1.99	-	-	-	-	-
1-Tridecene	$C_{13}H_{26}$	0.10	-	-	-	-	-	-
Cyclobutene, 4,4-dimethyl-1-(2,7-octadienyl)-	$C_{14}H_{22}$	-	0.44	-	-	-	-	-

Name	Formula							
Spiro[bicyclo[6.1.0]nonane-9,1'-cyclopentane], 3'-methylene-	$C_{14}H_{22}$	-	0.27	-	-	-	-	-
1,5,9,11-Tridecatetraene, 12-methyl-, (E,E)-	$C_{14}H_{22}$	-	0.15	-	-	-	-	-
2,6,10-trimethyl-1,5,9-undecatriene	$C_{14}H_{22}$	-	-	-	-	-	-	0.53
1,5,9-Decatriene, 2,3,5,8-tetramethyl-	$C_{14}H_{24}$	-	-	-	-	-	-	0.71
1,6,10-Dodecatriene, 7,11-dimethyl-3-methylene-	$C_{15}H_{24}$	-	2.11	-	-	-	-	-
1,3,6,10-Dodecatetraene, 3,7,11-trimethyl-	$C_{15}H_{24}$	-	1.93	-	-	-	-	-
2-Epi-.alpha.-funebrene	$C_{15}H_{24}$	0.15	-	-	-	-	-	-
Cyclohexane, 1-ethenyl-1-methyl-2-(1-methylethenyl)-4-(1-methylethylidene)-	$C_{15}H_{24}$	0.20	-	-	-	-	-	-
1H-Benzocycloheptene, 2,4a,5,6,7,8,9,9a-octahydro-3,5,5-trimethyl-9-methylene-	$C_{15}H_{24}$	-	-	-	-	-	-	0.11
1,2,3,5,6,7,8,8a-octahydro-1,4-dimethyl-7-(1-methylethenyl)-azulene	$C_{15}H_{24}$	-	-	-	-	-	-	0.57
Ledane	$C_{15}H_{26}$	-	-	-	-	-	-	0.11
Pentadecene	$C_{15}H_{30}$	-	-	0.19	-	-	-	-
1-Pentadecene	$C_{15}H_{30}$	-	-	-	-	-	-	0.35
1,2,3,1',2',3'-Hexamethyl-bicyclopentyl-2,2'-diene	$C_{16}H_{26}$	0.17	-	-	-	-	-	-
2,4,4,6,6,8,8-Heptamethyl-1-nonene	$C_{16}H_{32}$	0.07	-	-	-	-	-	-
1-Hexadecene	$C_{16}H_{32}$	-	-	-	-	-	-	0.08
1-Octadecene	$C_{18}H_{36}$	-	-	-	-	-	-	0.23
1-Nonadecene	$C_{19}H_{38}$	0.27	-	-	-	-	-	-
Alkynes		**0.18**	**8.01**	**0.12**	**2.24**	**-**	**-**	**-**
2,4-Hexadiyne	C_6H_6	0.09	-	-	-	-	-	-
1,7-Octadiyne	C_8H_{10}	-	2.34	-	-	-	-	-
2-Hepten-4-yne, 2-methyl-	C_8H_{12}	-	-	-	0.38	-	-	-
Methylheptyne	C_8H_{14}	-	-	0.12	-	-	-	-
3-Nonen-1-yne, (E)-	C_9H_{14}	-	-	-	0.40	-	-	-
1,3-Decadiyne	$C_{10}H_{14}$	-	-	-	0.41	-	-	-
3-Decen-1-yne, (Z)-	$C_{10}H_{16}$	-	0.16	-	0.21	-	-	-
3-Undecene-1,5-diyne	$C_{11}H_{14}$	-	-	-	0.57	-	-	-
3-Undecen-1-yne, (Z)-	$C_{11}H_{18}$	-	0.35	-	-	-	-	-
2-Undecyne	$C_{11}H_{20}$	0.09	-	-	-	-	-	-
3-Dodecen-1-yne, (Z)-	$C_{12}H_{20}$	-	0.19	-	0.27	-	-	-
5,9-Tetradecadiyne	$C_{14}H_{22}$	-	3.28	-	-	-	-	-
4-Hexadecen-6-yne, (E)-	$C_{16}H_{28}$	-	0.42	-	-	-	-	-

3-Heptadecen-5-yne, (Z)-	$C_{17}H_{30}$	-	1.27	-	-	-	-	-

Terpenes		**11.97**	**11.43**	**8.54**	**32.67**	**2.02**	**5.03**	**27.42**
p-Cymene	$C_{10}H_{14}$	-	-	-	-	1.09	-	-
m-Cymene	$C_{10}H_{14}$	-	-	-	-	0.58	-	-
o-Cymene	$C_{10}H_{14}$	2.56	-	-	-	-	-	-
Cymene	$C_{10}H_{14}$	-	-	2.84	-	-	-	-
1,2,8-p-Menthatriene	$C_{10}H_{14}$	-	-	-	-	-	-	0.65
1,3,8-p-Menthatriene	$C_{10}H_{14}$	-	-	-	-	-	-	0.42
.beta.-Myrcene	$C_{10}H_{16}$	-	-	-	2.28	-	-	-
D-Limonene	$C_{10}H_{16}$	6.55	-	-	-	-	-	22.84
L-Limonene	$C_{10}H_{16}$	-	-	-	-	-	3.71	1.45
DL-Limonene	$C_{10}H_{16}$	-	11.11	5.12	29.54	0.18	0.60	-
Isolimonene	$C_{10}H_{16}$	-	-	-	-	-	0.11	0.05
(+)-trans-Isolimonene	$C_{10}H_{16}$	-	-	-	-	-	0.10	-
Camphene	$C_{10}H_{16}$	-	-	-	-	-	-	0.03
.alpha.-Ocimene	$C_{10}H_{16}$	-	-	-	0.41	-	-	-
.beta.-cis-Ocimene	$C_{10}H_{16}$	-	-	-	0.44	-	-	-
.alpha.-Terpinene	$C_{10}H_{16}$	0.38	-	-	-	-	0.25	-
.gamma.-Terpinene	$C_{10}H_{16}$	0.05	-	-	-	-	-	-
p-Mentha-3,8-diene	$C_{10}H_{16}$	0.02	-	-	-	-	-	-
Pinene	$C_{10}H_{16}$	-	-	0.58	-	-	-	-
.alpha.-Terpinolene	$C_{10}H_{16}$	-	-	-	-	-	0.26	-
(+)-Carvomenthene	$C_{10}H_{18}$	1.12	-	-	-	-	-	-
Chamazulene	$C_{14}H_{16}$	0.08	-	-	-	0.17	-	-
Cadalene	$C_{15}H_{18}$	0.07	-	-	-	-	-	-
Cadina-1(10),6,8-triene	$C_{15}H_{22}$	0.11	-	-	-	-	-	-
.alpha.-Curcumene	$C_{15}H_{22}$	0.24	-	-	-	-	-	0.29
α-Selinene	$C_{15}H_{24}$	-	-	-	-	-	-	0.29
Thujopsene	$C_{15}H_{24}$	-	-	-	-	-	-	0.66
Aromadendrene	$C_{15}H_{24}$	-	-	-	-	-	-	0.47
α-Farnesene	$C_{15}H_{24}$	-	-	-	-	-	-	0.27
.alpha.-Cuprenene	$C_{15}H_{24}$	0.08	-	-	-	-	-	-
.beta.-Chamigrene	$C_{15}H_{24}$	0.38	-	-	-	-	-	-
Caryophyllene	$C_{15}H_{24}$	-	0.32	-	-	-	-	-
1,2-Dihydrothujopsene-(I1)	$C_{15}H_{26}$	0.22	-	-	-	-	-	-

Gerany-p-cymene	$C_{20}H_{30}$	0.11	-	-	-	-	-	-
Aromatics		**22.36**	**29.15**	**47.05**	**13.32**	**17.88**	**72.83**	**11.81**
Benzene	C_6H_6	-	5.97	0.98	0.13	-	-	0.12
Toluene	C_7H_8	0.71	5.82	4.40	6.03	0.18	1.28	0.14
Styrene	C_8H_8	0.15	-	2.45	-	0.12	1.38	-
Ethylbenzene	C_8H_{10}	0.56	-	2.79	-	0.09	0.84	0.16
p-Xylene	C_8H_{10}	-	7.29	-	3.14	1.27	0.96	-
m-Xylene	C_8H_{10}	-	1.56	-	0.92	-	-	-
o-Xylene	C_8H_{10}	1.39	3.60	-	1.24	-	-	0.76
Xylene	C_8H_{10}	-	-	3.48	-	-	-	-
Benzene, 1,3-dimethyl-	C_8H_{10}	0.33	-	-	-	-	-	-
Benzene, 1,4-dimethyl-	C_8H_{10}	-	-	-	-	-	3.33	-
Benzene, 1-propynyl-	C_9H_8	-	1.23	-	0.96	0.58	-	-
Indene	C_9H_8	-	-	-	-	-	1.46	0.30
1H-indene	C_9H_8	-	-	0.90	-	-	-	-
Indane	C_9H_{10}	0.12	-	-	-	0.15	-	0.13
Benzene, 1-ethenyl-2-methyl-	C_9H_{10}	0.08	-	-	-	-	-	-
Benzene, 1-ethenyl-3-methyl-	C_9H_{10}	-	-	-	-	-	0.93	-
Benzene, 1-ethenyl-4-methyl-	C_9H_{10}	-	-	-	-	0.70	-	-
Ethenylmethylbenzene	C_9H_{10}	-	-	0.31	-	-	1.22	-
Methylethenylbenzene	C_9H_{10}	-	-	1.56	-	-	-	-
Benzene, (1-methylethenyl)-	C_9H_{10}	-	-	-	-	-	1.16	-
Propenylbenzene	C_9H_{10}	-	-	0.23	-	-	-	-
Benzene, 2-Propenyl-	C_9H_{10}	-	-	-	-	-	0.71	0.24
Dihydro-1H-indene	C_9H_{10}	-	-	0.58	-	-	-	-
.alpha.-Methylstyrene	C_9H_{10}	-	-	-	-	-	-	0.02
Cumene	C_9H_{12}	-	-	0.61	-	-	-	0.09
C3-benzene	C_9H_{12}	-	-	1.39	-	-	-	-
Benzene, (1-methylethyl)-	C_9H_{12}	0.29	-	-	-	-	0.30	-
Benzene, 1-ethyl-2-methyl-	C_9H_{12}	0.82	-	-	-	-	3.88	0.39
Benzene, 1-ethyl-3-methyl-	C_9H_{12}	-	-	-	-	1.25	2.41	0.88
Benzene, 1-ethyl-4-methyl-	C_9H_{12}	-	-	-	-	0.13	-	-
Ethylmethylbenzene	C_9H_{12}	-	-	2.05	-	-	-	-
Mesitylene	C_9H_{12}	1.14	-	-	-	-	-	-
Propylbenzene	C_9H_{12}	-	-	0.61	-	-	0.31	-

Compound	Formula							
Trimethylbenzene	C_9H_{12}	-	-	0.27	-	-	-	-
Benzene, 1,2,3-trimethyl-	C_9H_{12}	-	-	-	-	2.30	2.41	-
Benzene, 1,2,4-trimethyl-	C_9H_{12}	-	-	-	-	-	1.95	0.23
Benzene, 1,3,5-trimethyl-	C_9H_{12}	-	-	-	-	-	0.68	-
Naphthalene	$C_{10}H_8$	-	-	0.73	-	0.83	2.06	-
Naphthalene, 1,2-dihydro-	$C_{10}H_{10}$	0.14	-	-	-	-	0.33	-
Methyl-1H-indene	$C_{10}H_{10}$	-	-	0.57	-	-	-	-
1-Methylindene	$C_{10}H_{10}$	-	-	-	-	-	0.11	-
2-Methylindene	$C_{10}H_{10}$	0.18	-	-	-	-	3.12	-
3-Methylindene	$C_{10}H_{10}$	-	-	-	-	-	2.55	0.13
5-Methylindane	$C_{10}H_{10}$	-	-	-	-	-	-	0.12
Bicyclo[4.2.0]octa-1,3,5-triene, 2,4-dimethyl-	$C_{10}H_{12}$	-	-	-	-	0.15	-	-
Tetrahydronaphthalene	$C_{10}H_{12}$	-	-	0.28	-	-	-	-
1,4,5,8-Tetrahydronaphthalene	$C_{10}H_{12}$	-	-	-	0.12	-	-	-
Dihydromethyl-1H-indene	$C_{10}H_{12}$	-	-	3.55	-	-	-	-
p-(1-Propenyl)-toluene	$C_{10}H_{12}$	0.04	-	-	-	-	-	-
Benzene, (2-methylcyclopropyl)-	$C_{10}H_{12}$	-	-	-	-	-	1.14	-
Benzene, 1-methyl-2-(2-propenyl)-	$C_{10}H_{12}$	0.38	-	-	-	-	-	-
Benzene, Methyl(1-Methylethenyl)-	$C_{10}H_{12}$	-	-	-	-	-	0.17	-
Benzene, 1-methyl-4-(1-methylethenyl)-	$C_{10}H_{12}$	-	-	-	-	1.19	2.00	-
p-(1-Propenyl)-toluene	$C_{10}H_{12}$	0.86	-	-	-	-	-	-
1H-Indene, 2,3-dihydro-5-methyl-	$C_{10}H_{12}$	0.19	-	-	-	-	0.66	-
Benzene, 1-ethenyl-3,5-dimethyl-	$C_{10}H_{12}$	-	-	-	-	-	0.26	-
Benzene, 2-ethenyl-1,4-dimethyl-	$C_{10}H_{12}$	-	-	-	-	-	0.64	-
Benzene, 4-ethenyl-1,2-dimethyl	$C_{10}H_{12}$	-	-	-	-	-	0.48	-
Benzene, 1-ethenyl-4-ethyl-	$C_{10}H_{12}$	0.24	-	-	-	-	-	-
Benzene, 2-butenyl-	$C_{10}H_{12}$	-	-	-	0.78	-	0.23	-
2,4-Dimethylstyrene	$C_{10}H_{12}$	-	-	-	-	-	0.35	-
.alpha.-Dimethylstyrene	$C_{10}H_{12}$	-	-	-	-	-	-	1.00
C4-benzene	$C_{10}H_{14}$	-	-	0.17	-	-	-	-
Tetramethylbenzene	$C_{10}H_{14}$	-	-	0.48	-	-	-	-
Benzene, 1,2,4,5-tetramethyl-	$C_{10}H_{14}$	-	-	-	-	-	0.77	-
Benzene, 1,2,3,5-tetramethyl-	$C_{10}H_{14}$	0.07	-	-	-	-	-	0.19
Butylbenzene	$C_{10}H_{14}$	-	-	0.67	-	-	-	-
Ethyldimethylbenzene	$C_{10}H_{14}$	-	-	0.48	-	-	-	-
Benzene, 1-methyl-3-propyl-	$C_{10}H_{14}$	0.19	-	-	-	-	0.45	-

Name	Formula							
Benzene, 1-methyl-4-propyl-	$C_{10}H_{14}$	0.11	-	-	-	-	-	-
Benzene, 2-ethyl-1,4-dimethyl-	$C_{10}H_{14}$	0.63	-	-	-	-	-	-
Benzene, 4-ethyl-1,2-dimethyl-	$C_{10}H_{14}$	-	-	-	-	-	0.18	-
Benzene, (1-methylpropyl)-	$C_{10}H_{14}$	-	-	-	-	-	0.22	-
Benzene, 1-methyl-4-(1-methylethyl)-	$C_{10}H_{14}$	-	-	-	-	-	-	0.54
Benzene, 1,2-diethyl-	$C_{10}H_{14}$	-	-	-	-	-	0.10	-
Isodurene	$C_{10}H_{14}$	0.13	-	-	-	-	-	-
m-Xylene, 5-ethyl-	$C_{10}H_{14}$	-	-	-	-	-	0.66	-
Benzocycloheptatriene	$C_{11}H_{10}$	0.43	-	-	-	-	-	-
Naphthalene, 1-methyl-	$C_{11}H_{10}$	0.18	-	-	-	-	1.84	-
Naphthalene, 2-methyl-	$C_{11}H_{10}$	-	-	-	-	3.16	2.68	0.33
Methylnaphthalene	$C_{11}H_{10}$	-	-	1.83	-	-	-	-
Naphthalene, 1,2-dihydro-4-methyl-	$C_{11}H_{12}$	-	-	-	-	0.98	-	-
Naphthalene, 3-methyl-1,2-dihydro-	$C_{11}H_{12}$	-	-	-	-	-	-	0.42
Naphthalene, 6-methyl-1,2-dihydro	$C_{11}H_{12}$	-	-	-	-	-	-	0.21
1,2-Dimethylindane	$C_{11}H_{12}$	-	-	-	-	-	-	0.29
Dimethyl-1H-indene	$C_{11}H_{12}$	-	-	0.64	-	-	-	-
Ethyl-1H-indene	$C_{11}H_{12}$	-	-	0.32	-	-	-	-
1H-Indene, 1,3-dimethyl-	$C_{11}H_{12}$	0.88	-	-	-	1.23	2.08	-
1H-Indene, 4,7-dimethyl-	$C_{11}H_{12}$	0.46	-	-	-	-	1.71	-
Cyclopentenylbenzene	$C_{11}H_{12}$	-	-	0.70	-	-	-	-
1,1a,7,7a-Tetrahydro-2H-cyclopropa[b]naphthalene	$C_{11}H_{12}$	-	-	-	-	-	1.71	-
2,4,6-Trimethylstyrene	$C_{11}H_{14}$	-	-	-	-	-	-	0.10
2,2-Dimethylindene, 2,3-dihydro-	$C_{11}H_{14}$	-	-	-	-	0.23	0.58	-
Methylbutenylbenzene	$C_{11}H_{14}$	-	-	0.54	-	-	-	-
Tetrahydromethylnaphthalene	$C_{11}H_{14}$	-	-	0.31	-	-	-	-
Naphthalene, 1,2,3,4-tetrahydro-1-methyl-	$C_{11}H_{14}$	-	-	-	-	-	-	0.27
Dihydrodimethyl-1H-indene	$C_{11}H_{14}$	-	-	0.20	-	-	-	-
Cyclopentylbenzene	$C_{11}H_{14}$	-	-	0.17	-	-	-	-
Benzene, 2-ethenyl-1,3,5-trimethyl-	$C_{11}H_{14}$	0.21	-	-	-	-	-	-
1H-Indene, 2,3-dihydro-1,6-dimethyl-	$C_{11}H_{14}$	0.57	-	-	-	-	0.51	-
1H-Indene, 2,3-dihydro-4,7-dimethyl-	$C_{11}H_{14}$	0.07	-	-	-	-	-	-
2-Ethyl-2,3-dihydro-1H-indene	$C_{11}H_{14}$	0.09	-	-	-	-	-	-
Benzene, 1-methyl-3-(1-methyl-2-propenyl)-	$C_{11}H_{14}$	-	-	-	-	-	-	0.31
Benzene, 1-methyl-4-(1-methyl-2-propenyl)-	$C_{11}H_{14}$	0.10	-	-	-	-	-	-
Benzene, 1-methyl-4-(1-methylpropyl)-	$C_{11}H_{16}$	0.27	-	-	-	-	0.38	-

Compound	Formula							
Benzene, 1-methyl-4-(2-methylpropyl)-	$C_{11}H_{16}$	0.25	-	-	-	-	-	-
Benzene, 1,4-dimethyl-2-(1-methylethyl)-	$C_{11}H_{16}$	0.14	-	-	-	-	-	-
Benzene, 2,4-dimethyl-1-(1-methylethyl)-	$C_{11}H_{16}$	0.04	-	-	-	-	-	-
Benzene, 1-ethyl-4-(1-methylethyl)-	$C_{11}H_{16}$	-	-	-	-	-	-	0.28
Benzene, 2,4-diethyl-1-methyl-	$C_{11}H_{16}$	-	-	-	-	-	-	1.00
Benzene, pentyl-	$C_{11}H_{16}$	0.11	-	-	-	-	-	-
Biphenylene	$C_{12}H_8$	-	-	-	-	0.29	-	-
Biphenyl	$C_{12}H_{10}$	-	-	0.91	-	-	-	-
Acenaphthene	$C_{12}H_{10}$	0.08	-	0.21	-	-	-	-
Ethylnaphthalene	$C_{12}H_{12}$	-	-	0.92	-	-	-	-
Naphthalene, 2-ethyl-	$C_{12}H_{12}$	-	-	-	-	-	0.52	-
Naphthalene, 1,2-dimethyl-	$C_{12}H_{12}$	0.43	-	-	-	-	-	-
Naphthalene, 1,3-dimethyl-	$C_{12}H_{12}$	-	-	-	-	-	2.32	-
Naphthalene, 1,5-dimethyl-	$C_{12}H_{12}$	0.57	-	-	-	-	-	0.35
Naphthalene, 1,6-dimethyl-	$C_{12}H_{12}$	-	-	-	-	-	1.83	-
Naphthalene, 1,7-dimethyl-	$C_{12}H_{12}$	-	-	-	-	-	1.86	-
Naphthalene, 2,3-dimethyl-	$C_{12}H_{12}$	-	-	-	-	-	0.85	-
Dimethylnaphthalene	$C_{12}H_{12}$	-	-	2.06	-	-	-	-
1,2,3-Trimethylindene	$C_{12}H_{14}$	0.54	-	0.62	-	0.62	-	0.26
1H-Indene, 1,1,3-trimethyl-	$C_{12}H_{14}$	0.26	-	-	-	-	1.04	0.13
Tetrahydrodimethylnaphthalene	$C_{12}H_{16}$	-	-	0.61	-	-	-	-
Tetrahydroethylnaphthalene	$C_{12}H_{16}$	-	-	0.34	-	-	-	-
Naphthalene, 1,2,3,4-tetrahydro-1,5-dimethyl-	$C_{12}H_{16}$	0.04	-	-	-	-	-	-
Benzene, 1-(2-butenyl)-2,3-dimethyl-	$C_{12}H_{16}$	0.13	-	-	-	-	-	-
Naphthalene, 1,2,3,4-tetrahydro-1,8-dimethyl-	$C_{12}H_{16}$	0.08	-	-	-	-	-	-
Naphthalene, 1,2,3,4-tetrahydro-5,7-dimethyl-	$C_{12}H_{16}$	0.05	-	-	-	-	-	-
1H-Indene, 1-ethyl-2,3-dihydro-1-methyl-	$C_{12}H_{16}$	0.22	-	-	-	-	-	-
Naphthalene, 1,2,3,4-tetrahydro-2,6-dimethyl-	$C_{12}H_{16}$	0.06	-	-	-	-	-	-
Naphthalene, 1,2,3,4-tetrahydro-1,5-dimethyl-	$C_{12}H_{16}$	0.23	-	-	-	-	-	-
Naphthalene, 6-ethyl-1,2,3,4-tetrahydro-	$C_{12}H_{16}$	0.15	-	-	-	-	-	-
C6-benzene	$C_{12}H_{18}$	-	-	0.26	-	-	-	-
Benzene, 1,4-dimethyl-2-(2-methylpropyl)-	$C_{12}H_{18}$	0.16	-	-	-	-	-	-
Benzene, 2,4-dimethyl-1-(1-methylpropyl)-	$C_{12}H_{18}$	0.09	-	-	-	-	-	-
Fluorene	$C_{13}H_{10}$	-	-	0.36	-	0.31	-	-
9H-Fluorene	$C_{13}H_{10}$	-	-	-	-	-	2.21	-
1H-Phenalene	$C_{13}H_{10}$	-	-	-	-	0.22	-	-

Compound	Formula	C1	C2	C3	C4	C5	C6	C7
1,1'-Biphenyl, 3-methyl-	$C_{13}H_{12}$	-	-	-	-	-	0.80	-
1,1'-Biphenyl, 4-methyl-	$C_{13}H_{12}$	-	-	-	-	-	0.91	0.33
Methyldiphenyl	$C_{13}H_{12}$	-	-	0.76	-	-	-	-
3-(2-Methyl-propenyl)-1H-indene	$C_{13}H_{14}$	0.05	-	-	-	-	-	-
Naphthalene, 1,4,6-trimethyl-	$C_{13}H_{14}$	-	-	-	-	0.40	1.63	-
Naphthalene, 1,6,7-trimethyl-	$C_{13}H_{14}$	0.92	-	-	-	-	1.78	0.49
Naphthalene, 2,3,6-trimethyl-	$C_{13}H_{14}$	0.67	-	-	-	-	-	0.51
Trimethylnaphthalene	$C_{13}H_{14}$	-	-	1.20	-	-	-	-
2,3,5-Trimethylnaphthalene	$C_{13}H_{14}$	-	-	-	-	-	0.58	-
3-(2-Methyl-propenyl)-1H-indene	$C_{13}H_{14}$	0.24	-	-	-	-	-	-
Trimethylazulene	$C_{13}H_{14}$	-	-	0.40	-	-	-	-
Naphthalene, 1,2-dihydro-2,5,8-trimethyl-	$C_{13}H_{16}$	-	-	-	-	-	-	0.19
Naphthalene, 1,2-dihydro-3,5,8-trimethyl-	$C_{13}H_{16}$	-	-	-	-	-	-	0.16
1H-Indene, 2,3-dihydro-1,1,5,6-tetramethyl-	$C_{13}H_{18}$	0.23	-	-	-	-	-	-
Benzene, 2-(2-butenyl)-1,3,5-trimethyl-	$C_{13}H_{18}$	0.15	-	-	-	-	-	-
Benzene, 3,3-Dimethyl-4-pentenyl-	$C_{13}H_{18}$	-	3.68	-	-	-	-	-
1-Methyl-2-cyclohexylbenzene	$C_{13}H_{18}$	0.14	-	-	-	-	-	-
Naphthalene, 1,2,3,4-tetrahydro-2,5,8-trimethyl-	$C_{13}H_{18}$	0.14	-	-	-	-	-	-
Anthracene	$C_{14}H_{10}$	-	-	0.22	-	-	-	-
Phenanthrene	$C_{14}H_{10}$	-	-	0.21	-	-	0.51	-
3H-Benz[e]indene, 2-methyl-	$C_{14}H_{12}$	-	-	-	-	-	0.32	-
Methylfluorene	$C_{14}H_{12}$	-	-	0.41	-	-	-	-
1H,2H,3H-Cyclopenta[a]naphthalen-5-ylmethane	$C_{14}H_{14}$	0.13	-	-	-	-	-	-
Dimethyldiphenyl	$C_{14}H_{14}$	-	-	0.47	-	-	-	-
2,2'-Dimethylbiphenyl	$C_{14}H_{14}$	0.07	-	-	-	-	-	-
3,3'-Dimethylbiphenyl	$C_{14}H_{14}$	-	-	-	-	0.66	-	-
Ethyldimethylazulene	$C_{14}H_{16}$	-	-	0.21	-	-	-	-
Naphthalene, 1-methyl-7-(1-methylethyl)-	$C_{14}H_{16}$	0.82	-	-	-	-	-	-
2-Isopropyl-7-methylnaphthalene	$C_{14}H_{16}$	-	-	-	-	0.37	-	-
Naphthalene, 1,2,3,4-tetramethyl-	$C_{14}H_{16}$	0.72	-	-	-	-	-	0.25
Naphthalene. 1,4,5,8-tetramethyl-	$C_{14}H_{16}$	-	-	-	-	-	1.62	0.17
Benzene, (2-ethyl-4-methyl-1,3-pentadienyl)-, (E)-	$C_{14}H_{18}$	0.17	-	-	-	-	-	-
1,4,6,7-Tetramethyl1,2,3,4-tetrahydronaphthalene	$C_{14}H_{20}$	0.15	-	-	-	-	-	-
Naphthalene, 1,2,3,4-tetrahydro-5,6,7,8-tetramethyl-	$C_{14}H_{20}$	0.85	-	-	-	-	-	-
Methylphenanthrene	$C_{15}H_{12}$	-	-	1.36	-	-	-	-
Phenanthrene, 2-methyl-	$C_{15}H_{12}$	-	-	-	-	-	0.87	-

Compound	Formula							
Benzene, 2,4-dimethyl-1-(phenylmethyl)-	$C_{15}H_{16}$	0.07	-	-	-	-	-	-
1,1'-Biphenyl, 4-(1-methylethyl)-	$C_{15}H_{16}$	0.12	-	-	-	-	-	-
Benzene, 1,1'-(1,3-propanediyl)bis-	$C_{15}H_{16}$	-	-	-	-	-	-	0.19
Benzene, 1-(1,5-dimethylhexyl)-4-methyl-	$C_{15}H_{24}$	0.05	-	-	-	-	-	-
1,2,4-Metheno-1H-indene, octahydro-1,7a-dimethyl-5-(1-methylethyl)-, [1S-(1.alpha.,2.alpha.,3a.beta.,4.alpha.,5.alpha.,7a.beta.,8S*)]-	$C_{15}H_{24}$	0.07	-	-	-	-	-	-
Benzene, 1-(1,5-dimethylhexyl)-4-methyl-	$C_{15}H_{24}$	0.18	-	-	-	-	-	-
Pyrene	$C_{16}H_{10}$	-	-	-	-	0.27	-	-
Dimethylphenanthrene	$C_{16}H_{14}$	-	-	0.35	-	-	-	-
Phenanthrene, 1,7-dimethyl-	$C_{16}H_{14}$	-	-	-	-	0.20	-	-
Anthracene, 9,10-dihydro-9,10-dimethyl-	$C_{16}H_{16}$	0.46	-	-	-	-	-	-
(3,4-Divinylcyclohexyl)benzene	$C_{16}H_{20}$	-	-	-	-	-	-	0.13
Phenanthrene, 2,3,5-trimethyl-	$C_{17}H_{16}$	0.17	-	-	-	-	-	-
Trimethylphenanthrene	$C_{17}H_{16}$	-	-	0.19	-	-	-	-
Retene	$C_{18}H_{18}$	0.11	-	-	-	-	-	-
Isopropylmethylphenanthrene	$C_{18}H_{18}$	-	-	0.73	-	-	-	-
Benzene, (1,1,4,6,6-pentamethylheptyl)-	$C_{18}H_{30}$	0.08	-	-	-	-	-	-
Organofluorines		**0.15**	**-**	**-**	**-**	**-**	**-**	**-**
1,2-Dimethyl-4-trifluoroacetoxycyclohexane	$C_{10}H_{15}F_3O_2$	0.11	-	-	-	-	-	-
1,2-Dimethyl-4-heptafluorobutyryloxycyclohexane	$C_{12}H_{15}F_7O_2$	0.03	-	-	-	-	-	-
(Z)-Tetradec-11-en-1-yl 2,2,3,3,3-pentafluoropropanoate	$C_{17}H_{27}F_5O_2$	0.01	-	-	-	-	-	-
Organonitriles		**1.80**	**-**	**0.32**	**-**	**-**	**0.34**	**0.34**
Benzonitrile	C_7H_5N	-	-	0.32	-	-	-	-
Heptadecanenitrile	$C_{17}H_{33}N$	0.87	-	-	-	-	0.34	-
Hexadecanenitrile	$C_{16}H_{31}N$	-	-	-	-	-	-	0.34
9-Octadecenenitrile, (Z)-	$C_{18}H_{33}N$	0.09	-	-	-	-	-	-
Octadecanenitrile	$C_{18}H_{35}N$	0.83	-	-	-	-	-	-
Acids		**0.29**	**-**	**0.88**	**0.43**	**0.26**	**-**	**7.57**
3-Methyl-2-pentenoic acid	$C_6H_{10}O_2$	-	-	-	0.43	-	-	-
Benzoic acid	$C_7H_6O_2$	-	-	0.28	-	-	-	-
2-Bromo-4,5-dimethoxycinnamic acid	$C_{11}H_{11}BrO_4$	-	-	-	-	0.26	-	-

Tetradecanoic acid	$C_{14}H_{28}O_2$	-	-	-	-	-	-	4.61
Pentadecanoic acid	$C_{15}H_{30}O_2$	-	-	0.60	-	-	-	2.96
n-Hexadecanoic acid	$C_{16}H_{32}O_2$	0.19	-	-	-	-	-	-
Octadecanoic acid	$C_{18}H_{36}O_2$	0.10	-	-	-	-	-	-
Organosulphides		**0.63**	**-**	**-**	**-**	**-**	**-**	**-**
Disulphide, bis(1,1,3,3-tetramethylbutyl)	$C_{16}H_{34}S_2$	0.63	-	-	-	-	-	-
Organochlorines		**-**	**0.95**	**-**	**1.00**	**-**	**-**	**-**
1,7-Dichloroheptane	$C_7H_{14}Cl_2$	-	0.95	-	-	-	-	-
Octanoyl-chloride	$C_8H_{15}ClO$	-	-	-	0.35	-	-	-
Dodecane, 1-chloro-	$C_{12}H_{25}Cl$	-	-	-	0.65	-	-	-
Acetates		**0.57**	**-**	**-**	**-**	**-**	**-**	**-**
(S,E)-2,5-Dimethyl-4-vinylhexa-2,5-dien-1-yl acetate	$C_{12}H_{18}O_2$	0.09	-	-	-	-	-	-
5-Isopropyl-2-methylphenethyl acetate	$C_{14}H_{20}O_2$	0.26	-	-	-	-	-	-
(E)-2-Methyl-6-(p-tolyl)hept-2-en-1-yl acetate	$C_{17}H_{24}O_2$	0.12	-	-	-	-	-	-
Retinol, acetate	$C_{22}H_{32}O_2$	0.11	-	-	-	-	-	-
Esters		**1.88**	**1.84**	**0.23**	**-**	**0.46**	**-**	**-**
Allyl isovalerate	$C_8H_{14}O_2$	-	-	-	-	0.13	-	-
1H-Indene-4-carboxylic acid, 2,3-dihydro-1,1- dimethyl-, methyl ester	$C_{13}H_{16}O_2$	-	-	-	-	0.33	-	-
Pentafluoropropionic acid, dodecyl ester	$C_{15}H_{25}F_5O_2$	0.26	-	-	-	-	-	-
Bis(2-ethylhexyl) methylphosphonate	$C_{17}H_{37}O_3P$	0.24	-	-	-	-	-	-
Succinic acid, 4,4-dimethylpent-2-yl 2-methylhex-3-yl ester	$C_{18}H_{34}O_4$	0.07	-	-	-	-	-	-
Heptadecanoic acid, methyl ester	$C_{18}H_{36}O_2$	-	-	0.23	-	-	-	-
Trichloroacetic acid, hexadecyl ester	$C_{18}H_{33}Cl_3O_2$	0.26	-	-	-	-	-	-
2,5-Octadecadienoic acid, methyl ester	$C_{19}H_{34}O_2$	-	1.84	-	-	-	-	-
5-Bromovaleric acid, 3-tetradecyl ester	$C_{19}H_{37}BrO_2$	0.09	-	-	-	-	-	-
Sulphurous acid, cyclohexylmethyl pentadecyl ester	$C_{22}H_{44}O_3S$	0.51	-	-	-	-	-	-
10,12-Tricosadiynoic acid, methyl ester	$C_{24}H_{40}O_2$	0.22	-	-	-	-	-	-
Octanoic acid, hexadecyl ester	$C_{24}H_{48}O_2$	0.22	-	-	-	-	-	-
Heteroaromatics		**3.11**	**0.34**	**2.01**	**-**	**1.8**	**2.91**	**3.55**

48

2-Methylthiophene	C_5H_6S	-	-	-	-	-	-	0.03
Thiophene, 2,3-dimethyl-	C_6H_8S	-	-	-	-	-	0.11	-
Thiophene, 3,4-dimethyl-	C_6H_8S	0.02	-	-	-	-	-	-
Pyridine, 2-methyl-	C_6H_7N	0.14	-	-	-	-	-	-
Benzothiazole	C_7H_5NS	0.80	-	0.93	-	0.56	1.42	1.54
2(3H)-Benzothiazolone	C_7H_5NOS	-	-	-	-	-	-	0.08
Thiophene, 3-(2-butenyl)-	$C_8H_{10}S$	-	-	-	-	-	-	0.16
Thiophene, 2,5-diethyl-	$C_8H_{12}S$	0.15	-	-	-	-	-	-
2-Pyrazoline, 1-isobutyl-3-methyl-	$C_8H_{16}N_2$	0.11	-	-	-	-	-	-
Benzo[b]thiophene, 2,7-dimethyl-	$C_{10}H_{10}S$	0.22	-	-	-	-	-	0.12
Benzo[b]thiophene, 3,5-dimethyl-	$C_{10}H_{10}S$	-	-	-	-	0.61	-	-
Quinoline, 2,4-dimethyl-	$C_{11}H_{11}N$	0.34	-	-	-	0.63	1.38	-
Quinoline, 2,8-dimethyl	$C_{11}H_{11}N$	-	-	-	-	-	-	0.46
Ethylquinoline	$C_{11}H_{11}N$	-	-	1.08	-	-	-	-
1-Phenyl-2-ethylprop-1-ene (1-3)sultine	$C_{11}H_{12}O_2S$	-	0.34	-	-	-	-	-
Benzothiazole, 2-butyl-	$C_{11}H_{13}NS$	0.08	-	-	-	-	-	-
Thiophene, 2-heptyl-	$C_{11}H_{18}S$	0.27	-	-	-	-	-	-
Amobarbital	$C_{11}H_{18}N_2O_3$	0.08	-	-	-	-	-	-
3-Acetyl-2,5-dimethylbenzo(b)thiophene	$C_{12}H_{12}OS$	0.14	-	-	-	-	-	0.16
Benzo[b]thiophene, 2-ethyl-5,7-dimethyl-	$C_{12}H_{14}S$	0.18	-	-	-	-	-	-
2,2,4-Trimethyl-1,2-dihydroquinoline	$C_{12}H_{15}N$	-	-	-	-	-	-	0.83
2,2,4-Trimethyl-1,2,3,4-tetrahydroquinoline	$C_{12}H_{17}N$	0.33	-	-	-	-	-	-
Benzothiazole, 2-phenyl-	$C_{13}H_9NS$	0.11	-	-	-	-	-	0.17
Isoxaben	$C_{18}H_{24}N_2O_4$	0.05	-	-	-	-	-	-
Apparicine, Nb-methyltetrahydro-	$C_{19}H_{26}N_2$	0.07	-	-	-	-	-	-
Ketones		**-**	**-**	**0.48**	**-**	**0.21**	**0.49**	**0.25**
2-Hexanone	$C_6H_{12}O$	-	-	-	-	0.12	-	-
3-Hexanone	$C_6H_{12}O$	-	-	-	-	0.09	-	-
Methylpentanone	$C_6H_{12}O$	-	-	0.18	-	-	-	-
4-Methylpentanone, 4-hydroxy-	$C_6H_{12}O_2$	-	-	-	-	-	-	0.25
2-Pentanone, 4-hydroxy-4-methyl-	$C_6H_{12}O_2$	-	-	-	-	-	0.49	-
Methylphenylethanone	$C_9H_{10}O$	-	-	0.30	-	-	-	-
Benzene Derivatives		**1.88**	**0.67**	**0.43**	**4.83**	**0.19**	**0.62**	**1.66**

Compound	Formula	1	2	3	4	5	6	7
Phenol	C_6H_6O	-	-	0.24	-	-	-	-
Phenol, 3-methyl-	C_7H_8O	-	-	-	-	-	0.23	-
Parachlorophenol	C_6H_5ClO	-	-	-	0.58	-	-	-
1-Azido-2-methyl-benzene	$C_7H_7N_3$	-	-	-	3.45	-	-	-
3,4-Dimethylthiophenol	$C_8H_{10}S$	0.43	-	-	-	-	-	-
Dimethylphenol	$C_8H_{10}O$	-	-	0.19	-	-	-	-
1H-Indene, 1-chloro-2,3-dihydro-	C_9H_9Cl	0.06	-	-	-	-	-	-
Benzofuran, 2,3-dihydro-2-methyl-	$C_9H_{10}O$	-	-	-	-	0.19	-	-
Phenol, 4-propyl-	$C_9H_{12}O$	0.09	-	-	-	-	-	-
5-Nitro-1,2,3,4-tetrahydronaphthalene	$C_{10}H_{11}NO_2$	-	0.67	-	-	-	-	-
Phenol, m-tert-butyl-	$C_{10}H_{14}O$	0.22	-	-	-	-	-	-
N-Benzylpalmitamide	$C_{11}H_{13}NS$	0.12	-	-	-	-	-	-
5-Methyl-6-phenyltetrahydro-1,3-oxazine-2- thione	$C_{11}H_{13}NOS$	-	-	-	0.80	-	-	-
Diphenylamine	$C_{12}H_{11}N$	-	-	-	-	-	-	0.18
1,4-Benzenediamine, N-phenyl-	$C_{12}H_{12}N_2$	0.09	-	-	-	-	-	-
5-Methoxy-2,2-Dimethylindan-1-one	$C_{12}H_{14}O_2$	-	-	-	-	-	0.39	-
1,3,5-Trimethyl-2-(2-nitroallyl)benzene	$C_{12}H_{15}NO_2$	0.12	-	-	-	-	-	-
Phenol, 2,4-bis(1-methylethyl)-	$C_{12}H_{18}O$	0.12	-	-	-	-	-	-
Phenol, 2-(1,1,3,3-tetramethylbutyl)-	$C_{14}H_{22}O$	0.17	-	-	-	-	-	-
Phenol, 4-(1,1,3,3-tetramethylbutyl)-	$C_{14}H_{22}O$	-	-	-	-	-	-	0.71
6-(p-Tolyl)-2-methyl-2-heptenol, trans-	$C_{15}H_{22}O$	0.14	-	-	-	-	-	-
Phenol, 2-methyl-4-(1,1,3,3-tetramethylbutyl)-	$C_{15}H_{24}O$	0.17	-	-	-	-	-	0.16
4-(1,3-Dimethylbutyl)amino-diphenylamine	$C_{18}H_{24}N_2$	-	-	-	-	-	-	0.61
1,4-Benzenediamine, N-(1,3-dimethylbutyl)-N'-phenyl-	$C_{18}H_{24}N_2$	0.15	-	-	-	-	-	-
Total Identified		**59.16**	**75.99**	**75.03**	**68.82**	**23.67**	**83.84**	**71.27**

3.3. Conclusion

The purpose of this entire chapter was to characterize the untreated TDO to supplement existing literature for TDO as a potential replacement to conventional liquid fuels. Furthermore, to identify high-value compounds within the TDO. The FTIR analysis revealed that the TDO was composed of aliphatics and aromatics as well as oxygen, nitrogen and sulphur-containing compounds. The GC-MS analysis identified a plethora of compounds that were listed with their peak percentage areas in Table 3.4. The main aromatic compounds found in the TDO were limonene, cymene, xylene, toluene, benzothiazole and styrene. The high percentage of aromatics and naphthenic components that were identified make the TDO suitable as an alternative to conventional liquid fuels. However, further treatment is needed (such as hydrogenation, demetallization, and desulphurization) to get high-quality fuel from the tyre derived oil.

3.4. References

- Alvarez, J., Lopez, G., Amutio, M., Mkhize, N., Danon, B., van der Gryp, P., Görgens, J., Bilbao, J. and Olazar, M. (2017). *Evaluation of the properties of tyre pyrolysis oils obtained in a conical spouted bed reactor.*

- Cunliffe, A. and Williams, P. (1998). Composition of oils derived from the batch pyrolysis of tyres. *Journal of Analytical and Applied Pyrolysis*, 44(2), pp.131-152.

- Danon, B., van der Gryp, P., Schwarz, C. and Görgens, J. (2015). A review of dipentene (dl-limonene) production from waste tire pyrolysis. *Journal of Analytical and Applied Pyrolysis*, 112, pp.1-13.

- Erasto, P. and Viljoen, A. (2008). Limonene - a Review: Biosynthetic, Ecological and Pharmacological Relevance. *Natural Product Communications*, 3(7), pp.1193-1202.

- Islam, M., Parveen, M., Haniu, H. and Sarker, M. (2010). Innovation in Pyrolysis Technology for Management of Scrap Tire: a Solution of Energy and Environment. *International Journal of Environmental Science and Development*, pp.89-96.

- Kumar Singh, R., Ruj, B., Jana, A., Mondal, S., Jana, B., Kumar Sadhukhan, A. and Gupta, P. (2018). Pyrolysis of three different categories of automotive tyre wastes: Product yield analysis and characterization. *Journal of Analytical and Applied Pyrolysis*, 135, pp.379-389.

- Laresgoiti, M., Caballero, B., de Marco, I., Torres, A., Cabrero, M. and Chomón, M. (2004). Characterization of the liquid products obtained in tyre pyrolysis. *Journal of Analytical and Applied Pyrolysis*, 71(2), pp.917-934.

- Quek, A. and Balasubramanian, R. (2013). Liquefaction of waste tires by pyrolysis for oil and chemicals—A review. *Journal of Analytical and Applied Pyrolysis*, 101, pp.1-16.

- Rofiqul Islam, M., Haniu, H. and Rafiqul Alam Beg, M. (2008). Liquid fuels and chemicals from pyrolysis of motorcycle tire waste: Product yields, compositions and related properties. *Fuel*, 87(13-14), pp.3112-3122.

- Taleb, D., Hamid, H., Deris, R., Zulkifli, M., Khalil, N. and Ahmad Yahaya, A. (2020). Insights into pyrolysis of waste tire in fixed bed reactor: Thermal behavior. *Materials Today: Proceedings*, 31, pp.178-186.

- Uyumaz, A., Aydoğan, B., Solmaz, H., Yılmaz, E., Yeşim Hopa, D., Aksoy Bahtli, T., Solmaz, Ö. and Aksoy, F. (2019). Production of waste tyre oil and experimental investigation on combustion, engine performance and exhaust emissions. *Journal of the Energy Institute*, 92(5), pp.1406-1418.

- Williams, P. and Taylor, D. (1993). Aromatization of tyre pyrolysis oil to yield polycyclic aromatic hydrocarbons. *Fuel*, 72(11), pp.1469-1474.

CHAPTER 4

4. Desulphurization of Tyre Derived Oil using Unsupported and Supported Alkaline Earth Metal Oxides

4.1. Experimental Method and Design

Chapter 4.1 has been divided into several segments. This chapter presents the materials required (Table 4.1), preparation and characterization of silica-supported alkaline earth metal oxides, experimental procedures, and methods of analysis.

4.1.1. Materials

Table 4.1. Details and percentage purity of the materials required.

Material	Purity (%)	Details
Silica Gel Grade 923 – 30 Å pore size, 100-200 mesh particle size	-	Sigma-Aldrich® products procured from DLD Scientific CC.
Silica Gel Grade 636 – 60 Å pore size, 35-60 mesh particle size	-	
Silica Gel Grade 646 – 150 Å pore size, 35-60 mesh particle size	-	
Magnesium Oxide (MgO)	97	
Barium Oxide (BaO)	97	
Magnesium Acetate Tetrahydrate ($Mg(CH_3COO)_2.4H_2O$)	≥ 98	
Calcium Nitrate Tetrahydrate ($Ca(NO_3)_2.4H_2O$)	99	
Barium Chloride Dihydrate ($BaCl_2.4H_2O$)	≥ 99	
Calcium Oxide (CaO)	99.8	Procured from Radchem (Pty) Ltd.
2-Propanethiol (C_3H_8S)	≥ 98	Sigma-Aldrich® products.
Dichloromethane (CH_2Cl_2)	≥ 99	
Nitrogen Gas	> 99.999	From African Oxygen Limited (Afrox).
Deionized Water	-	Produced using an Elga Purelab Option Q water purification system.
Tyre Derived Oil (TDO)	-	Obtained from Mandini, a tyre pyrolysis company based in Alberton, Johannesburg.

4.1.2. Preparation of Supported Alkaline Earth Metal Oxides

The samples were named as X(Metal Oxide)-Y(Silica Gel), in which X is the weight percentage of the metal oxide and Y is the pore size of the silica gel. The preparation of the supported alkaline earth metal oxides were aided by reviewed literature in Chapter 2.3. Figure 4.1 contains the schematic of the Carbolite MTF 12/38/400 tube furnace that was used for the calcination process.
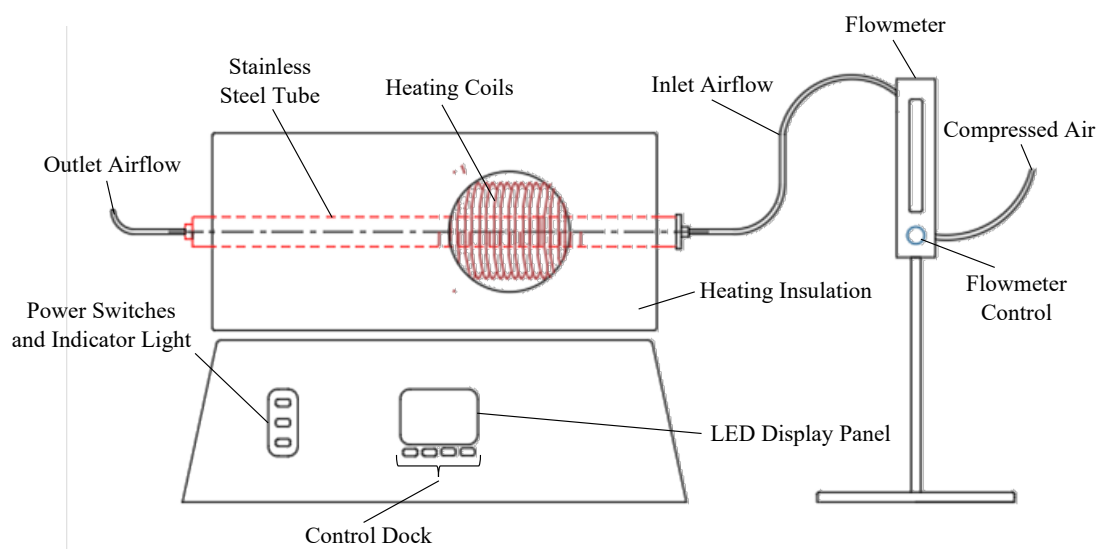
Figure 4.1. Schematic of the tube furnace and its peripherals.

4.1.2.1. Synthesis of Silica-supported Magnesium Oxide

The silica-supported magnesium oxide was prepared by using a simple wet impregnation method. Davisil Grade 636 Silica gel (150.67 g) was added to 250 ml deionized water containing 69.95 g of dissolved magnesium acetate tetrahydrate in a 500 ml beaker. The mixture was magnetically stirred for 2 h at room temperature and then evaporated at 70 °C along with stirring until a thick slurry formed. The thick slurry was then calcined in a tube furnace at 400 °C for 12 h with an air flowrate of 20 cm^3/min to remove gaseous products. The final calcination temperature of 400 °C was attained using a heating ramp rate of 1 °C/min. The procedure described relates to $8MgO-60SiO_2$. The procedure was repeated, with the appropriate quantities, to produce $8MgO-30SiO_2$ and $8MgO-150SiO_2$.

4.1.2.2. Synthesis of Silica-supported Calcium Oxide

The silica-supported calcium oxide was prepared using 54.94 g calcium nitrate tetrahydrate and 150.12 g Davisil Grade 636 Silica gel. The solution was prepared in a 500 ml beaker containing 250 ml deionized water to ensure wet impregnation. The mixture was stirred for 1 h at 60 °C for complete dilution. After that, the mixture was dried at 120 °C for 12 h until a thick slurry formed. The thick slurry

was calcined in a tube furnace at 800 ºC for 4 h. The final calcination temperature of 800 °C was attained using a heating ramp rate of 2 °C/min. An air flowrate of 20 cm^3/min was used during calcination to remove gaseous products. The procedure was repeated, with the appropriate quantities, to produce $8CaO-30SiO_2$ and $8CaO-150SiO_2$.

4.1.2.3. Synthesis of Silica-supported Barium Oxide

Similarly, silica-supported barium oxide was prepared using the wet impregnation method. Davisil Grade 636 Silica gel (120 g) was added to 200 ml deionized water containing 16.62 g of dissolved barium chloride dihydrate in a 500 ml beaker. The mixture was magnetically stirred for 1 h at 60 ºC and then evaporated at 90 °C along with continuous stirring until a thick slurry formed. The thick slurry was then placed in a tube furnace at 900 °C for 4 h. The final calcination temperature of 900 °C was attained using a heating ramp rate of 2 °C/min. An air flowrate of 20 cm^3/min was used during calcination to remove gaseous products. The procedure was repeated, with the appropriate quantities, to produce $8BaO-30SiO_2$ and $8BaO-150SiO_2$.

4.1.3. Characterization of Supported Alkaline Earth Metal Oxides

The samples were dispersed on carbon adhesive tape and were analysed using a Phenom Pharos Desktop Scanning Electron Microscope (SEM) with a Field Emission Gun (FEG) electron source for high-resolution imaging. The SEM was used to study the topography and morphology of the samples. The instrument was equipped with an Energy Dispersive X-ray (EDX) probe for semi-quantitative elemental analysis with an acceleration voltage of 15 kV. The composition (full) mode was used for the Backscatter Electron Detector (BSD).

4.1.4. Desulphurization of Tyre Derived Oil

4.1.4.1. Experimental Method
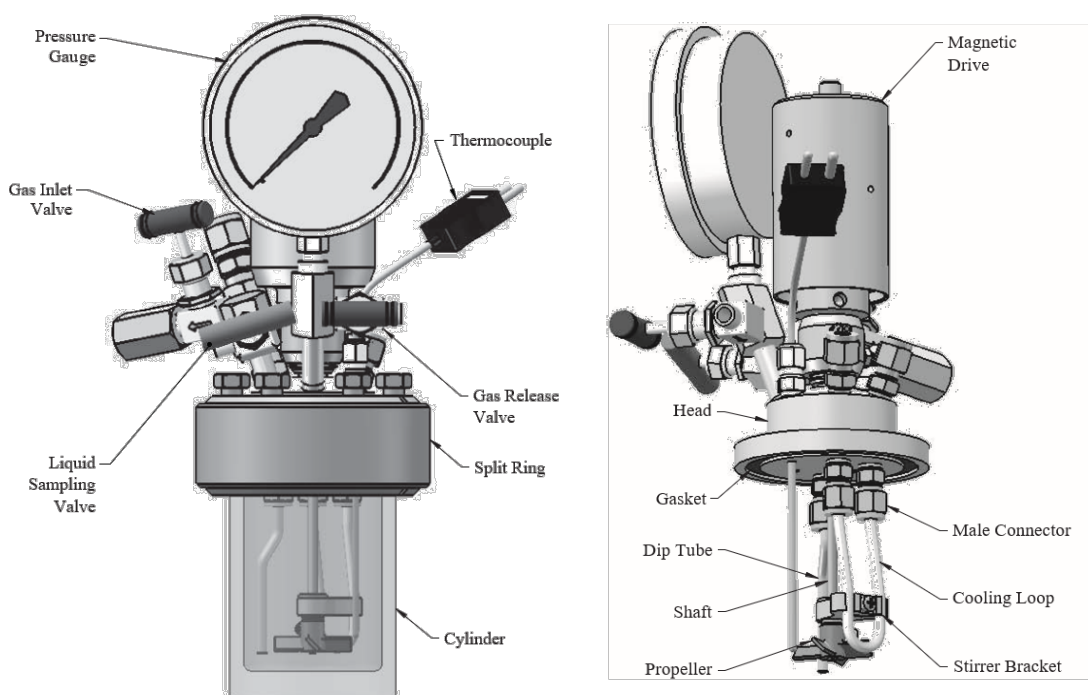
(a) Vessel closure and external parts   (b) Vessel closure and internal parts

Figure 4.2. Schematic of the Parr 5500 series reactor vessel (Parr Instrument Company, 2014).
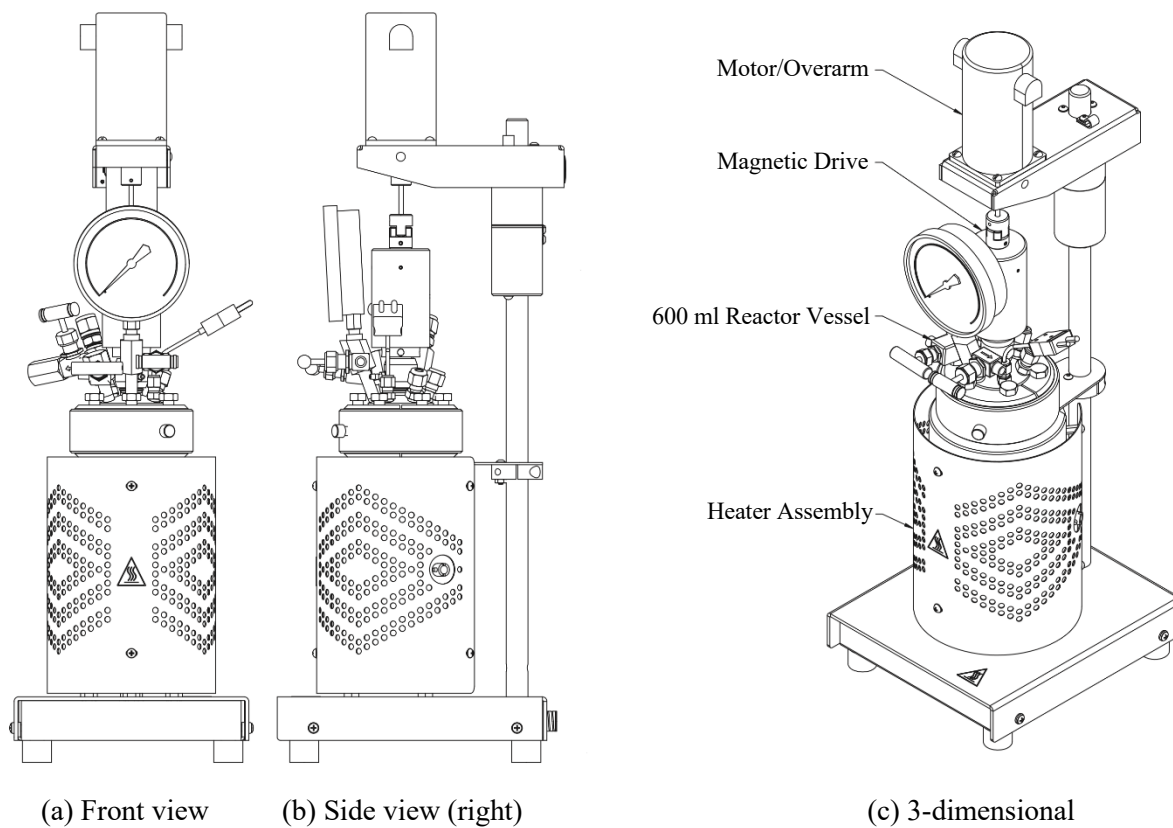
(a) Front view   (b) Side view (right)   (c) 3-dimensional

Figure 4.3. Schematic of the Parr 5500 series batch reactor (Parr Instrument Company, 2014).

Figure 4.3 shows a schematic of the 600 ml Parr 5500 series batch reactor made with 316 stainless steel and equipped with a magnetic stirrer drive. According to the Parr Instrument Company, the permissible working pressures and temperatures are up to 200 bar and 350 °C, respectively. The reactor has a J-type thermocouple encased in a 1/8-inch diameter stainless steel sheath with an accuracy of +/- 2 °C. The thermocouple was connected to the Parr 4848 reactor control unit to provide a full three-term PID control. In addition, the temperature, stirrer speed and temperature limits were adjusted using the reactor control unit.
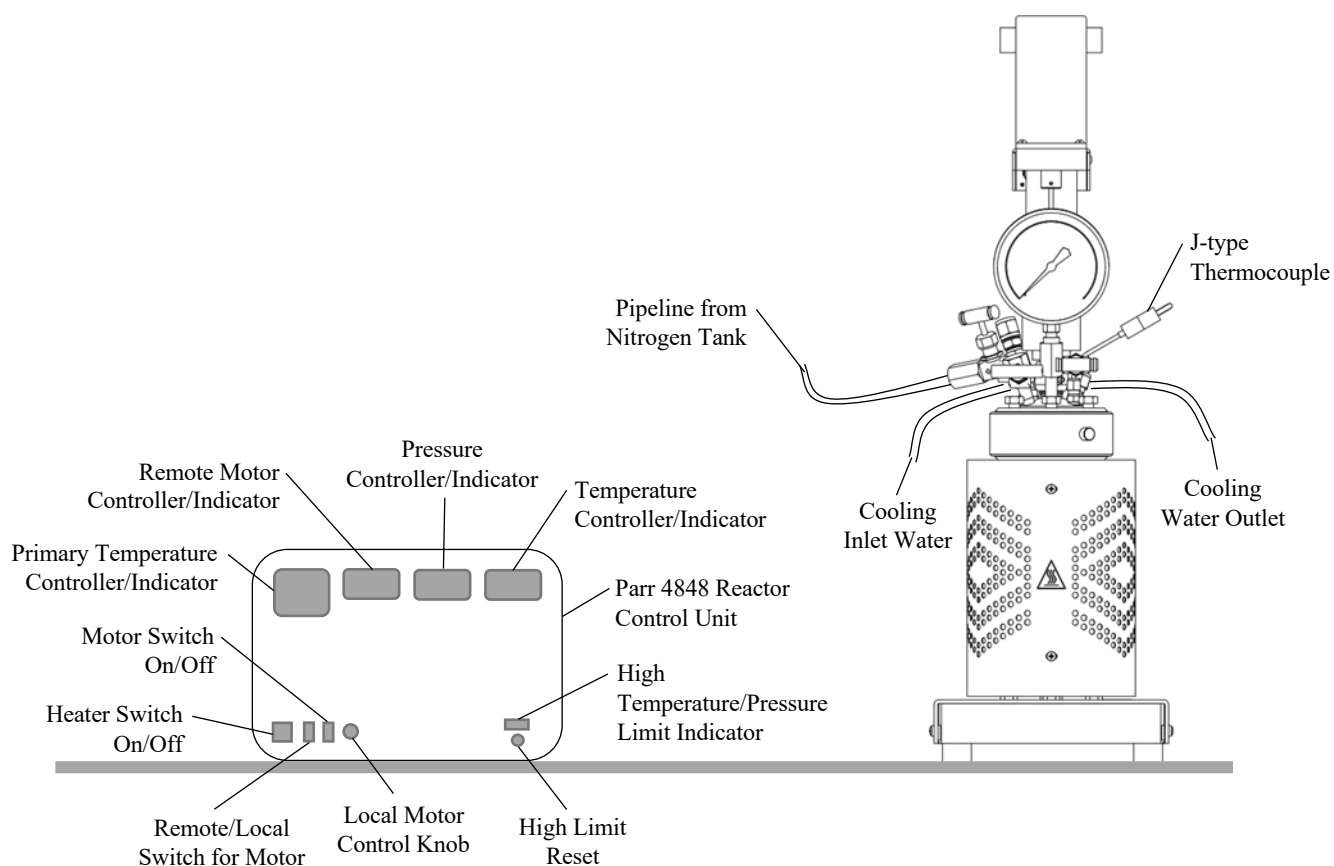
(a) Parr 4848 reactor control unit

(b) 600 ml Parr 5500 series batch reactor
(Parr Instrument Company, 2014)

Figure 4.4. Schematic of the reactor system used for desulphurization.

The experiments followed the Standard Run Order as in Tables 4.2 and 4.3. Run 1 will be used to describe the experimental procedure using calcium oxide as the sorbent. An Ohaus PA214 analytical balance with a repeatability of 0.0001 g was used to weigh 1.0013 g of CaO. A borosilicate measuring cylinder with an accuracy of +/- 0.5 ml was used to measure 80 ml of TDO. The heater assembly was preheated to 240 °C. All electrical cables and water pipes were positioned and tied such that they never contact the heater assembly. The CaO and TDO were loaded into the reactor vessel, resulting in a sorbent-to-oil ratio of 0.0125 g/ml. The reactor head was fitted to the reactor vessel, and the reactor bolts were tightened in a criss-cross pattern. All valves were checked carefully before pressurizing the

reactor to 20 bar to keep the TDO in a liquid state at high temperatures. Heat resistant gloves were used to place the reactor into the heater assembly. The magnetic drive was attached, and the stirrer speed was set to 400 rpm for a reaction time of 30 minutes. The cooling water valve was opened to cool the stirrer components, which prevented the stirrer from seizing at high temperatures. After the 30 min reaction time, the stirrer and heater assembly were switched off. Heat resistant gloves were used to transfer the reactor from the heater assembly into a 5 litre plastic beaker filled with ice to allow for rapid cooling. When the reactor cooled to 25 °C, the gas release valve was gradually opened to depressurize the reactor. The cooling water valve was closed, and the reactor bolts were opened to remove the reactor head from the reactor vessel. The desulphurized oil was filtered from the spent CaO sorbent. The filtration process involved the use of a Büchner funnel and flask, Grade 1 Whatman® filter paper (110 mm Ø) and an Edwards RV3 vacuum pump. A sample of the filtrate was filtered into a 2 ml glass vial, using a 10 ml syringe and a 0.45 µm PTFE syringe filter, for GC-PFDP analysis. The remaining filtrate was stored for recommended experiments and analyses. The reactor vessel and internal components were cleaned using acetone before beginning the next run.

4.1.4.2.   Experimental Design

A 2^3 factorial design was applied with one central point. The measured response, Ds, was the weight percentage of desulphurization. The studied factors were reaction time, reaction temperature and the sorbent-to-oil ratio. A stirring rate of 400 rpm was set for all experiments. The stirring rate was set to prevent the problems of vortexing, poor mixing and poor reaction performance whilst maintaining a uniform distribution of phases, components and temperature within the reactor vessel. The objectives of the design were:

1. To investigate the effect of the experimental factors and their interactions on the outcome, Ds.
2. To develop a mathematical model that is valid within the experimental range.
3. To determine the optimal operating conditions necessary for process scale-up.

Table 4.2. Levels for the 2^3 factorial design.

Parameter	Notation	Levels		
		-1	**0**	**1**
Reaction Temperature (°C)	X_T	240	280	320
Reaction Time (min)	X_{RT}	30	60	90
Sorbent-to-oil Ratio (g/ml)	X_{SO}	0.0125	0.0250	0.0375

In tabular form, the design can be represented as shown in Table 4.3. The column on the left-hand side of Table 4.3, numbers 1 to 8, is called the Standard Run Order. These numbers are also depicted in Figure 4.5. For example, run number 8 is made at the high setting of all three factors.

Table 4.3. Experimental matrix for the 2^3 factorial design.

Run	X_T	X_{RT}	X_{SO}
1	-1	-1	-1
2	-1	-1	1
3	1	-1	-1
4	1	-1	1
5	-1	1	-1
6	-1	1	1
7	1	1	-1
8	1	1	1
9	0	0	0

Figure 4.5 shows a cubic representation of the 2^3 factorial design. The arrows show the direction of increase of the factors. The numbers 1 through 8 at the corners of the design box represent the Standard Run Order. Number 9 at the centre of the design box represents the central point.
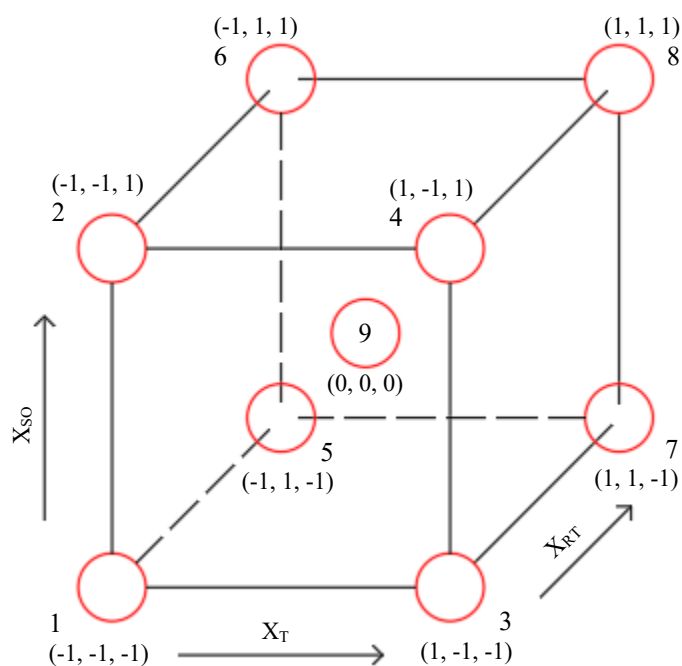
Figure 4.5. Representation of the 2^3 factorial design as a cube.

The experimental design will be used for the unsupported metal oxides and the silica-supported metal oxides with a 60 Å pore size. The metal oxides supported on silica gel with pore sizes of 30 Å and 150 Å will be used to determine whether pore size plays an important role in desulphurization. The operating conditions will be determined based on the desulphurization capability of the metal oxides supported on silica gel with a pore size of 60 Å.

4.1.4.3. Determining the Sulphur Content of Tyre Derived Oil

A gas chromatograph equipped with a PFPD was utilized to determine the sulphur content of the untreated and treated TDO. The PFPD is an inherently equimolar response detector; the sulphur's chemiluminescence response is independent of a compound's molecular structure (Chambers and Duffy, 2003). Therefore, a fixed concentration of sulphur will give the same PFPD response regardless of the parent compound, and this feature allows quantitative determination of the total or speciated sulphur content in complex samples using a single calibrant. Calibration with a known concentration of a single sulphur compound will allow quantitation of the sulphur content in individual chromatographic peaks of unknown compounds.

A calibration curve was created to establish a relationship between the total peak area and the sulphur content in the untreated and treated TDO. A set of calibration standards were made containing a known amount of sulphur. The sulphur-containing compound (2-propanethiol C_3H_8S) and a diluent (dichloromethane CH_2Cl_2) were used to make the calibration standards. According to Table 2.2 from Chapter 2, the sulphur content of TDO can be expected, but not limited to, the range of 0.11 wt.% to 1.27 wt.%. The range was used as a reference for preparing the calibration standards. An Ohaus PA214 analytical balance with a repeatability of 0.0001 g was used to weigh the 2-propanethiol and dichloromethane as presented in Table 4.4. Samples 1 to 12 were prepared in a 5 ml GC vial. Sample 13 was prepared in a 20 ml beaker and an aliquot was stored in a 5 ml GC vial.

Table 4.4. Prepared calibration standards.

Calibration Standards	Mass of 2-Propanethiol C_3H_8S (mg)	Mass of Dichloromethane CH_2Cl_2 (mg)	Sulphur Content (wt. %)
1	21.0	4839.0	0.1819
2	29.3	3639.1	0.3363
3	8.9	4809.6	0.0778
4	37.4	5703.0	0.2743
5	35.5	6203.8	0.2395
6	15.6	5580.7	0.1174
7	8.9	6047.9	0.0619
8	10.6	17750.2	0.0251

The sulphur content of calibration standard 1 was calculated as follows:

$$m_{prop} = 21\ mg = 0.021\ g$$

$$n_{prop} = \frac{m_{prop}}{M_{prop}} = \frac{0.021\ g}{76.162\ g/mol} = 2.757 \times 10^{-4}\ mol$$

Where,

m_{prop} = Mass of 2-Propanethiol

n_{prop} = Moles of 2-Propanethiol

M_{prop} = Molar Mass of 2-Propanethiol

There exists an equimolar relationship between 2-propanethiol (C_3H_8S) and the sulphur present in the 2-propanthiol molecule. Therefore, we have the following relationship to calculate the mass of sulphur:

$$n_{prop} = n_s$$

$$m_s = n_s M_s = 2.757 \times 10^{-4} \, mol \times 32.065 \, g/mol = 8.840 \times 10^{-3} g$$

The mass percentage of sulphur was calculated as follows:

$$Sulphur \; Content \, (wt. \%) = \frac{m_s}{m_{DCM} + m_{prop}} \times 100$$

$$= \frac{8.840 \times 10^{-3} g}{4.8390 \, g + 0.0210 \, g} \times 100 = 0.1819 \, wt. \%$$

Where,

n_s = Moles of Sulphur

m_s = Mass of Sulphur

M_s = Molar Mass of Sulphur

m_{DCM} = Mass of Dichloromethane

The calculation was repeated for the remaining calibration standards and are presented in Table 4.4.

A Shimadzu GC-2014 equipped with a PFDP detector was used to determine the total peak area of the calibration standards. An aliquot of 0.5 µl was injected. Each calibration standard was tested 3 times to evaluate the precision of the calibration process. A calibration curve was prepared by plotting the GC-PFPD response (total peak area) as a function of the sulphur concentration. The correlation coefficient (R^2) and the equation for the calibration curve were determined using Microsoft Excel. The details of the GC-PFPD method are presented in Table 4.5. The equation for the calibration curve was used to calculate the sulphur content in the unknown TDO samples.

The TDO samples were prepared in a 2 ml GC vial using a 10 ml syringe and a 0.45 µm PTFE syringe filter. Due to the difference in density between the calibration standards and the TDO, an aliquot of 0.72 µl of TDO was injected to ensure that an equal amount of mass was analysed. An aliquot of 0.5 µl of the calibration standard was equivalent to 0.72 µl of TDO. The density of the TDO (915.385 kg/m^3 at 25 ºC) was determined using a DSA 5000 M Anton Paar Density and Sound Velocity Meter. The calibration standards' density was taken as the density of dichloromethane because the calibration standards only contained minute quantities of 2-propanethiol. The density of dichloromethane (1325.0 kg/m^3 at 25 ºC) was obtained from the specification sheet from Sigma-Aldrich®. The following calculations show that the injected mass of the TDO samples differ from mass of the calibration standards by 0.51 %:

$$Mass\ of\ Calibration\ Standard = Volume\ Injected \times Density\ of\ Calibration\ Standard$$
$$= 0.50\ \mu l \times 10^{-9} m^3/\mu l \times 1325.0\ kg/m^3 = 6.625 \times 10^{-7}\ kg$$

$$Mass\ of\ TDO\ Sample = Volume\ Injected \times Density\ of\ TDO$$
$$= 0.72\ \mu l \times 10^{-9} m^3/\mu l \times 915.385\ kg/m^3 = 6.591 \times 10^{-7}\ kg$$

$$Percent\ Deviation = \frac{6.625 \times 10^{-7}\ kg - 6.591 \times 10^{-7}\ kg}{6.625 \times 10^{-7}\ kg} \times 100 = 0.51\ \%$$

Table 4.5. Method for the GC-PFDP analysis.

Specification	Details
Column configuration	Zebron ZB-1 column (0.25 mm Internal Diameter, 0.25 μm Film Thickness, 30 m Length) - Dimethyl polysiloxane.
Oven/column temperature	The oven temperature profile started at 40 °C for 1 min, then increased at 10 °C/min to 275 °C and then held isothermally for 5 min.
Carrier gas/flowrate	Helium (> 99.999 % Purity), 1.38 ml/min
Total flow	38.9 ml/min
Head column pressure	102.9 kPa
Transfer line temperature	250 °C
Split ratio	25:1
Flame/Detector Temperature	280 °C

4.2. Results and Discussion

4.2.1. Characterization of Supported Alkaline Earth Metal Oxides

The silica-supported alkaline earth metal oxides were synthesized and characterized as described in Chapter 4.1. Figure 4.6 (a-c) shows the SEM-EDX analysis of the silica gel with pore sizes of 30, 60 and 150 Å. The EDX analysis of the silica gel shows two prominent peaks of oxygen and silicon. The characterization of the silica gel was essential to understand the formation of the metal oxides on the surface of the silica particles. In some cases, the energy peaks of oxygen and silicon overlapped with the energy peaks of iodine and strontium, respectively. The energy peaks of iodine and strontium were resolved, given the known context of the sample. According to Goodge (2017), individual peaks may correspond to several elements, particularly at higher energies.
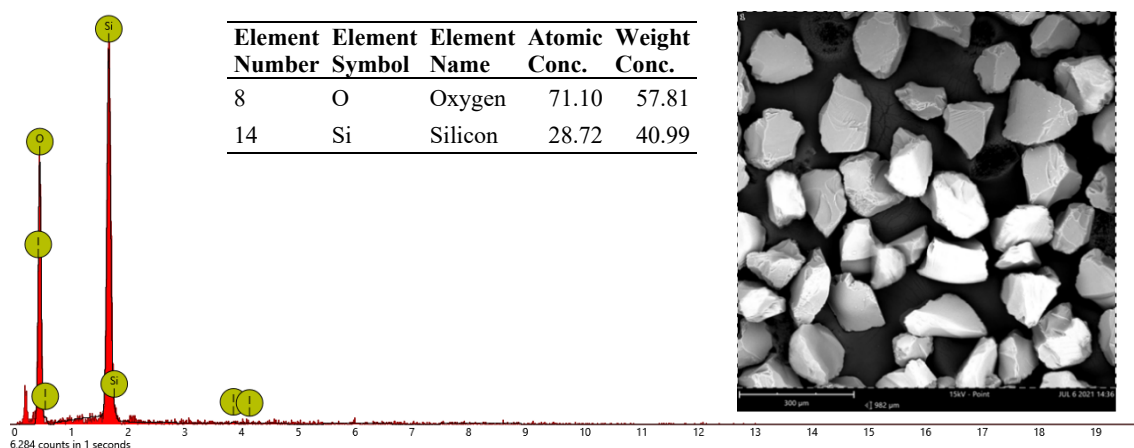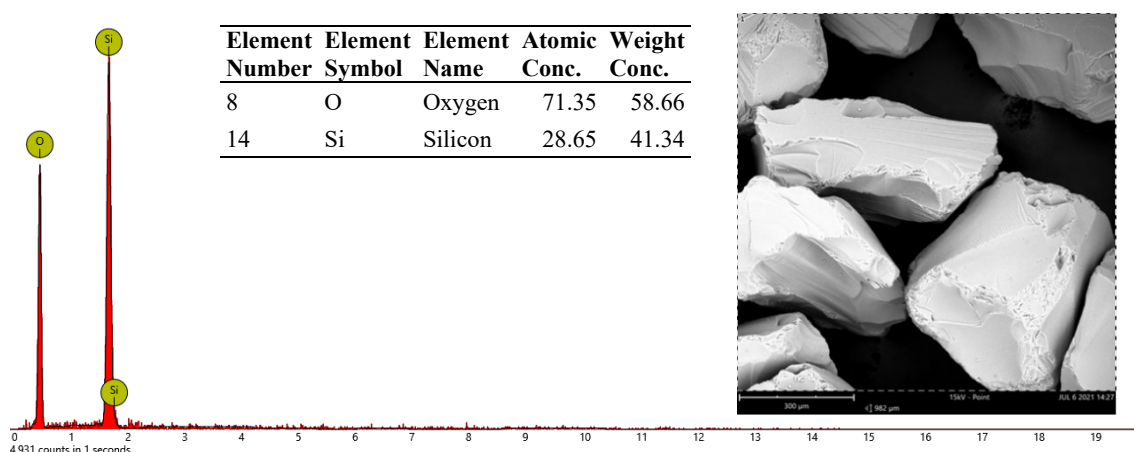
Element Number	Element Symbol	Element Name	Atomic Conc.	Weight Conc.
8	O	Oxygen	71.10	57.81
14	Si	Silicon	28.72	40.99

(a) Silica gel grade 923 – 30 Å pore size, 100-200 mesh particle size

Element Number	Element Symbol	Element Name	Atomic Conc.	Weight Conc.
8	O	Oxygen	71.35	58.66
14	Si	Silicon	28.65	41.34

(b) Silica gel grade 636 – 60 Å pore size, 35-60 mesh particle size

Element Number	Element Symbol	Element Name	Atomic Conc.	Weight Conc.
8	O	Oxygen	71.74	59.12
14	Si	Silicon	28.26	40.88
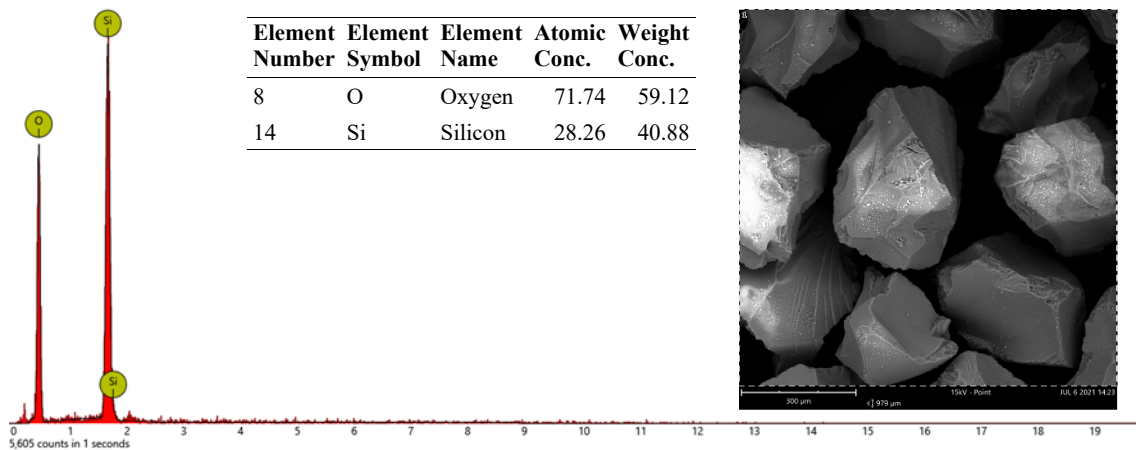
(c) Silica gel grade 646 – 150 Å pore size, 35-60 mesh particle size

Figure 4.6. SEM-EDX analysis of silica gel – a Sigma-Aldrich® product.

The SEM-EDX analysis of the silica-supported magnesium oxides are shown in Figure 4.7 (a-c). The SEM micrographs of the supported magnesium oxides show a rougher surface area than the samples of the raw silica gel. This can be seen by comparing the micrographs of the raw silica gel in Figure 4.6 (a-c) to the micrographs of the supported magnesium oxides in Figure 4.7 (a-c). The EDX analysis shows the presence of oxygen, silicon and magnesium, which confirmed the calcination of magnesium acetate to magnesium oxide as intended. The experimentally determined loading of magnesium oxide on silica gel with pore sizes of 30, 60 and 150 Å was 9.83, 10.56 and 10.81 wt.%, respectively. The experimentally determined weight percentage loading of magnesium oxide on silica gel was calculated (Appendix C-1) using the composition of magnesium. The experimental loading was in good agreement with the theoretical loading of 8 wt. % magnesium oxide, considering that the EDX technique is a semi-quantitative elemental analysis method (Nasrazadani and Hassani, 2016).

Element Number	Element Symbol	Element Name	Atomic Conc.	Weight Conc.
8	O	Oxygen	68.09	54.42
14	Si	Silicon	26.67	37.42
12	Mg	Magnesium	4.88	5.93

(a) 8MgO-30SiO$_2$

Element Number	Element Symbol	Element Name	Atomic Conc.	Weight Conc.
8	O	Oxygen	66.62	53.73
14	Si	Silicon	28.18	39.89
12	Mg	Magnesium	5.20	6.37

(b) 8MgO-60SiO$_2$
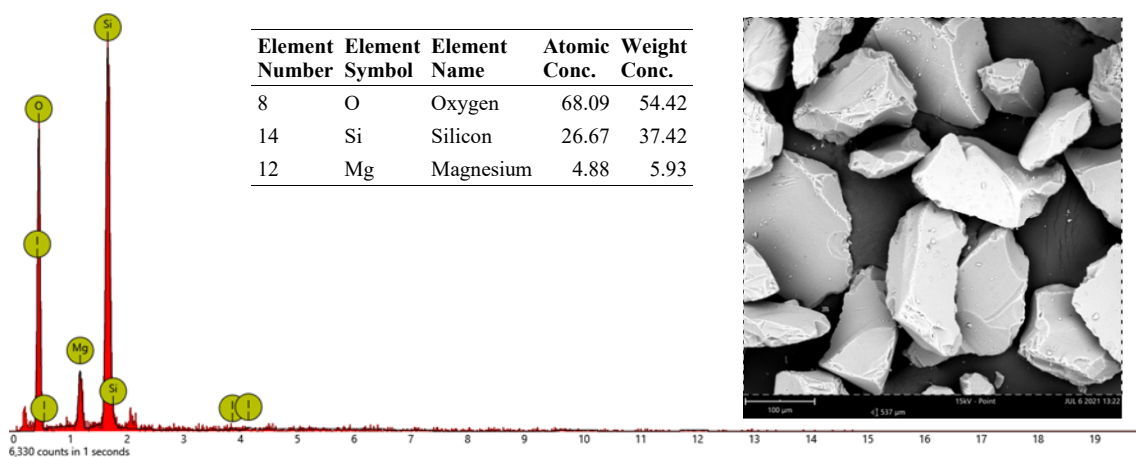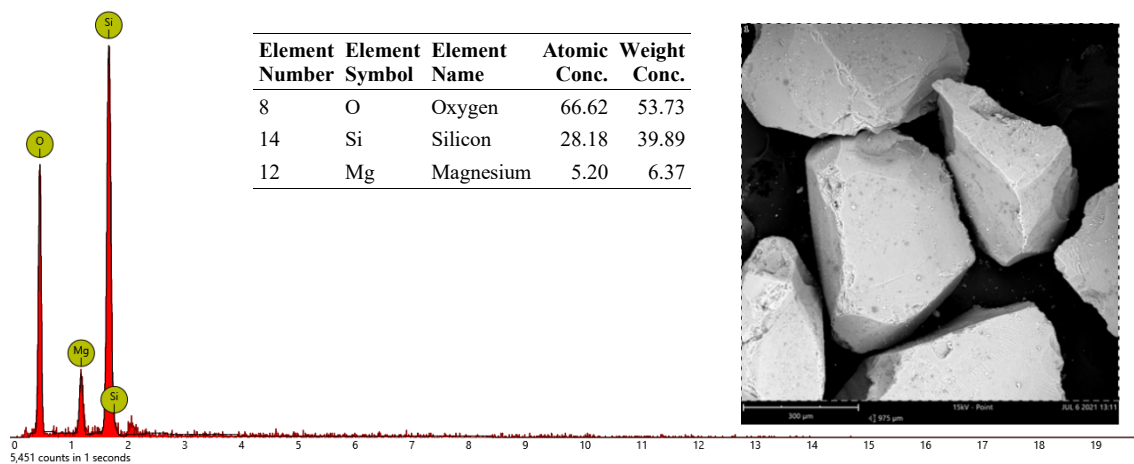
Element Number	Element Symbol	Element Name	Atomic Conc.	Weight Conc.
8	O	Oxygen	70.11	57.78
14	Si	Silicon	24.68	35.70
12	Mg	Magnesium	5.21	6.52
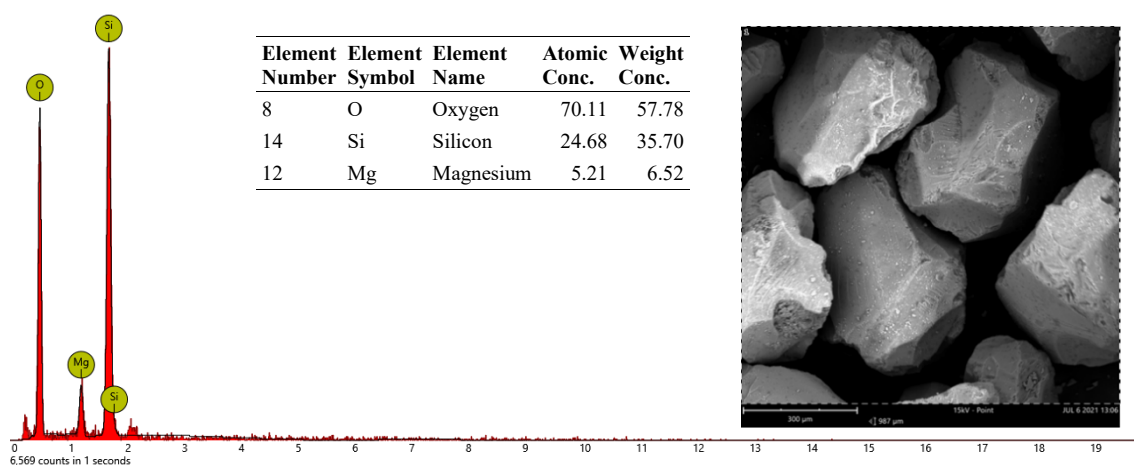
(c) 8Mgo-150SiO$_2$

Figure 4.7. SEM-EDX analysis of silica-supported magnesium oxide.

The SEM-EDX analysis of the silica-supported calcium oxides are shown in Figure 4.8 (a-c). The SEM micrographs of the supported calcium oxides show a rougher surface area than the samples of the raw silica gel, Figure 4.6 (a-c). The EDX analysis shows the presence of oxygen, silicon and calcium, which confirmed the calcination of calcium nitrate to calcium oxide as visualized. The experimentally determined loading of calcium oxide on silica gel with pore sizes of 30, 60 and 150 Å was 9.58, 9.67 and 9.18 wt.%, respectively. The experimentally determined weight percentage loading of calcium oxide on silica gel was calculated (Appendix C-2) using the composition of calcium. The experimental loading was in good agreement with the theoretical loading of 8 wt. % calcium oxide, considering that the EDX technique is a semi-quantitative elemental analysis method (Nasrazadani and Hassani, 2016).

Element Number	Element Symbol	Element Name	Atomic Conc.	Weight Conc.
8	O	Oxygen	69.31	52.43
14	Si	Silicon	27.07	40.72
20	Ca	Calcium	3.62	6.85

(c) 8CaO-30SiO$_2$

Element Number	Element Symbol	Element Name	Atomic Conc.	Weight Conc.
8	O	Oxygen	68.51	54.20
14	Si	Silicon	27.99	38.87
20	Ca	Calcium	3.49	6.93

(b) 8CaO-60SiO$_2$

Element Number	Element Symbol	Element Name	Atomic Conc.	Weight Conc.
8	O	Oxygen	69.12	54.00
14	Si	Silicon	27.17	37.26
20	Ca	Calcium	3.35	6.56
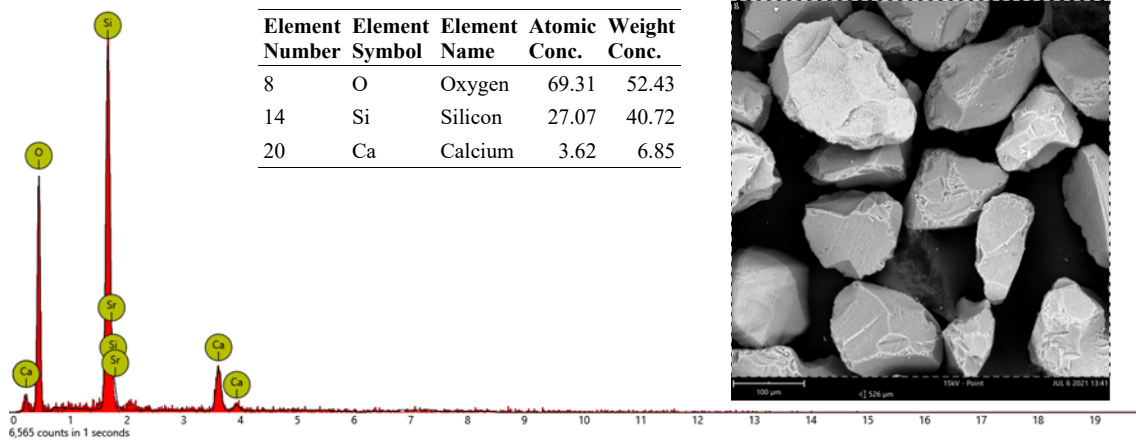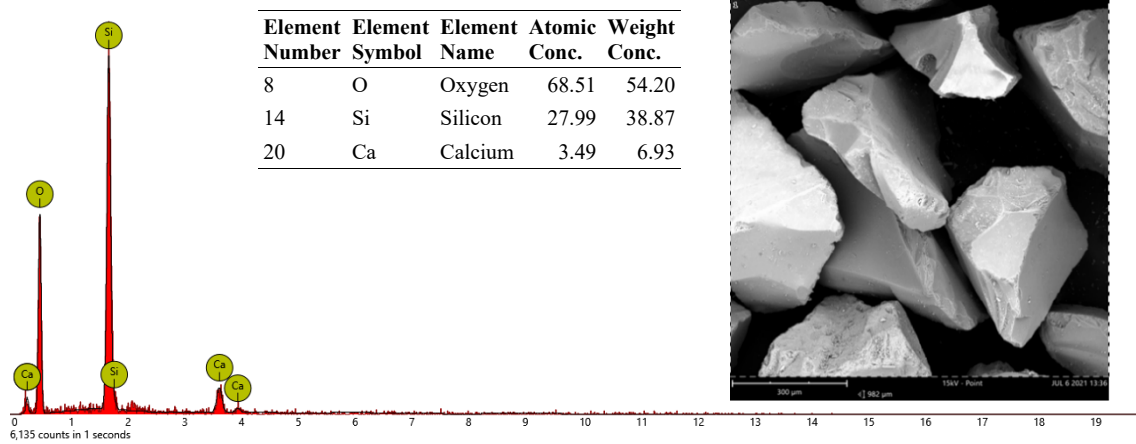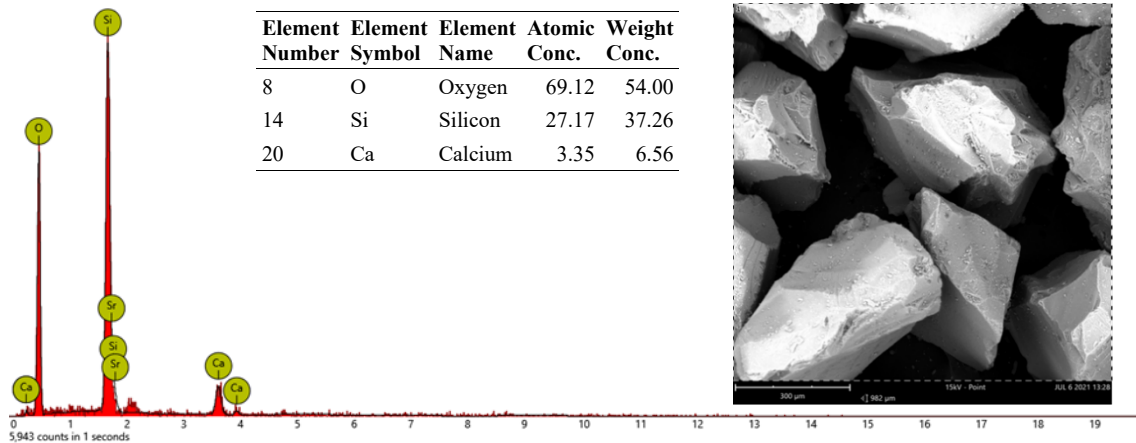
(a) 8CaO-150SiO$_2$

Figure 4.8. SEM-EDX analysis of silica-supported calcium oxide.

Figure 4.9 (a-c) shows the SEM-EDX analysis of the silica-supported barium oxides. The silica gel with pore sizes of 30, 60, 150 Å were well coated with reactive material, as seen in the SEM micrographs of Figure 4.9 (a-c). However, the SEM micrograph of 8BaO-30SiO$_2$ shows conglomerated bits attached to the surface of the silica gel. As a result, the energy peaks of barium and chlorine were not well defined. The automatic peak identification software could not identify those energy peaks, so a semi-

quantitative analysis was not performed for 8BaO-30SiO$_2$. The EDX analysis shows the presence of oxygen, silicon, chlorine and barium. The presence of chlorine suggested that the barium chloride was not fully calcined to form barium oxide. The experimental loading of barium oxide on silica gel with a pore size of 60 and 150 Å was 9.95 and 15.47 wt.%, respectively. The experimentally determined weight percentage loading of barium oxide on silica gel was calculated (Appendix C-3) using the compositions of barium and chlorine.

(a) 8BaO-30SiO$_2$

Element Number	Element Symbol	Element Name	Atomic Conc.	Weight Conc.
8	O	Oxygen	65.01	41.40
14	Si	Silicon	29.85	39.46
56	Ba	Barium	2.73	14.90
17	Cl	Chlorine	2.19	3.09

(b) 8BaO-60SiO$_2$

Element Number	Element Symbol	Element Name	Atomic Conc.	Weight Conc.
8	O	Oxygen	76.44	37.18
14	Si	Silicon	10.98	28.53
56	Ba	Barium	6.25	26.10
17	Cl	Chlorine	5.86	6.32

Thick coat of reactive material
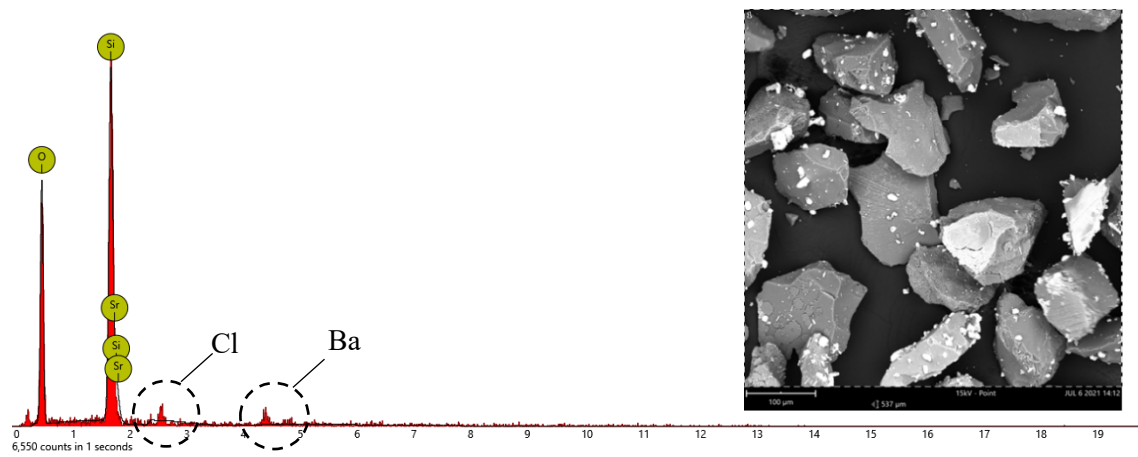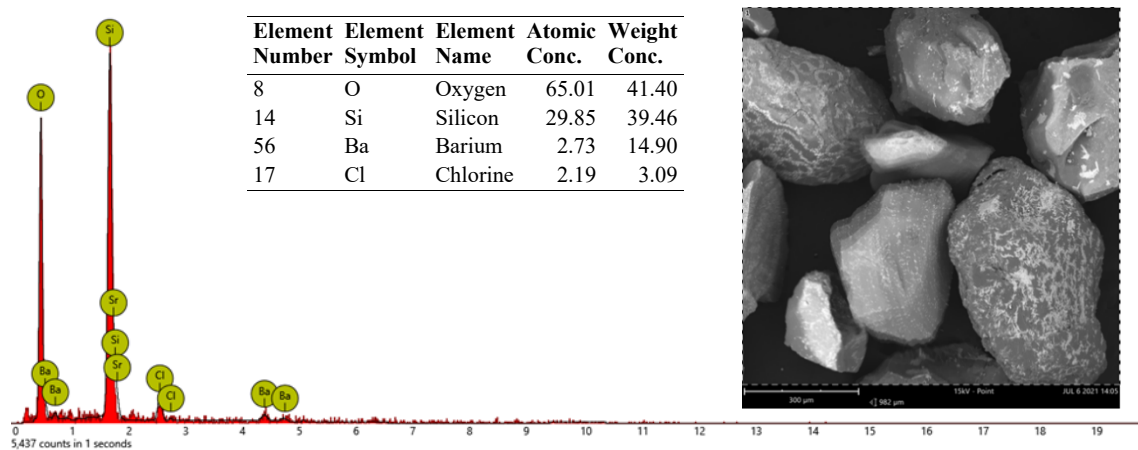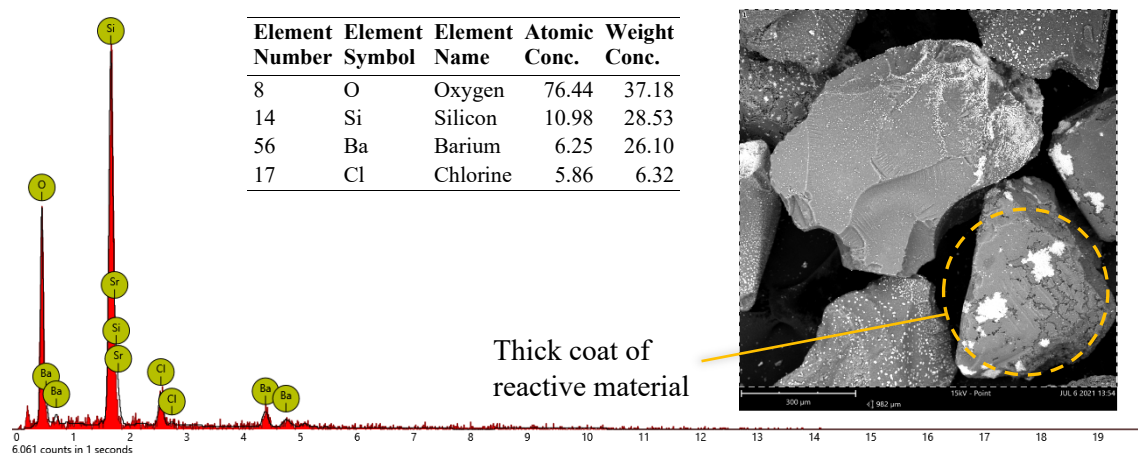
(c) 8BaO-150SiO$_2$

Figure 4.9. SEM-EDX analysis of silica-supported barium oxide.

The experimental loading of barium oxide, 15.47 wt.%, on silica gel with a pore size of 150 Å was considerably higher when compared to the experimental loading of magnesium oxide and calcium oxide on silica gel as summarized in Figure 4.10. This is possibly due to stronger adhesive forces between the salt solution and the surface of the silica particles relative to the resistance provided by the pore walls. The SEM micrograph, Figure 4.9 (c), provides visual evidence for the experimental loading of 15.47 wt.% barium oxide on the silica gel. Figure 4.10 shows that the experimental loading was higher than the theoretical loading of 8 wt.% for all silica-supported alkaline earth metal oxides, which suggested that the dispersion of the metal oxides were non-uniform, i.e. the pores of the silica particles are less rich in metal oxides.
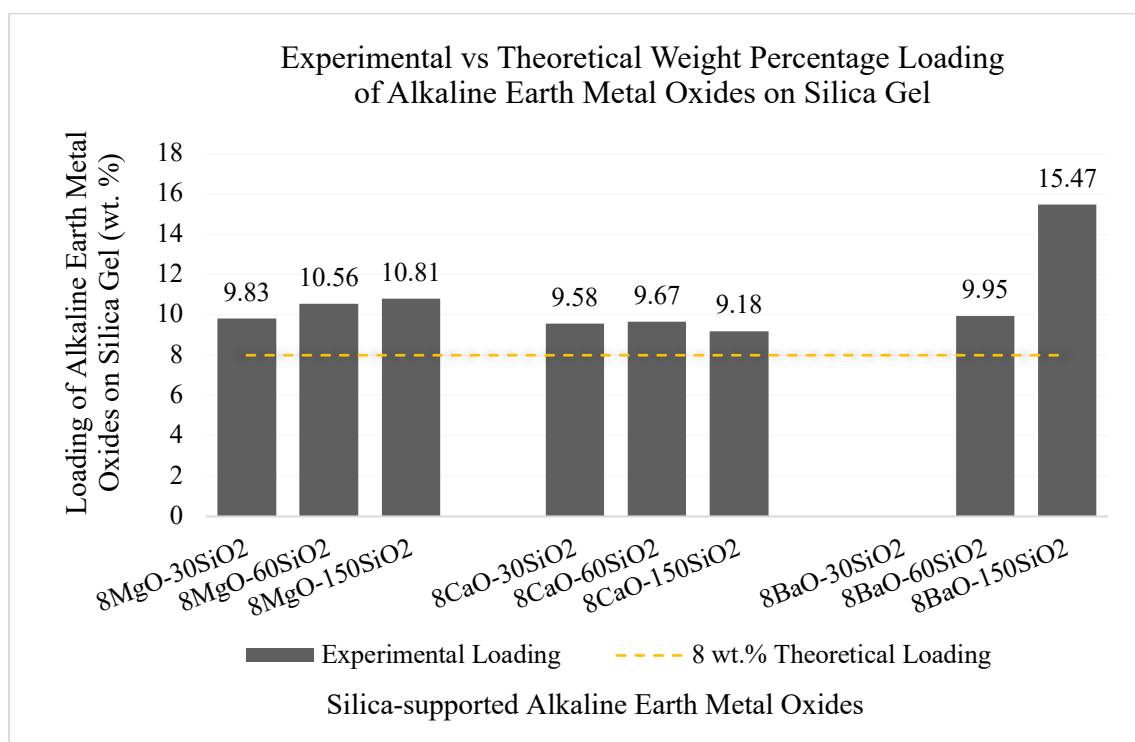
Figure 4.10. Experimental vs theoretical weight percentage of alkaline earth metal oxides on silica gel.

4.2.2. Calibration Curve for Determining Sulphur Content

Table 4.6 contains the average total peak area for each calibration standard. A low relative standard deviation (<1.41 %) indicated a small spread for the total peak areas. A sample calculation to determine the total peak area can be found in Appendix B-1.

Table 4.6. Average total peak area for the calibration standards.

Calibration Standards	Sulphur Content (wt.%)	Total Sulphur Peak Area				Relative Standard Dev. (%)
		Run 1	Run 2	Run 3	Average	
1	0.1819	591667310.8	592359763.6	584618924.1	589548666.2	0.59
2	0.3363	812329437.7	793089102.9	800524728.0	801981089.5	0.99
3	0.0778	458744117.0	462102546.7	451340424.3	457395696.0	0.98
4	0.2743	715666015.1	720201286.8	713517611.5	716461637.8	0.39
5	0.2395	685526564.1	662895130.0	669890578.9	672770757.7	1.41
6	0.1174	505797669.1	512423939.0	514224071.7	510815226.6	0.71
7	0.0619	436237533.2	437040512.9	430589662.5	434622569.5	0.66
8	0.0251	382545464.5	391514896.0	378547258.8	384202539.8	1.41
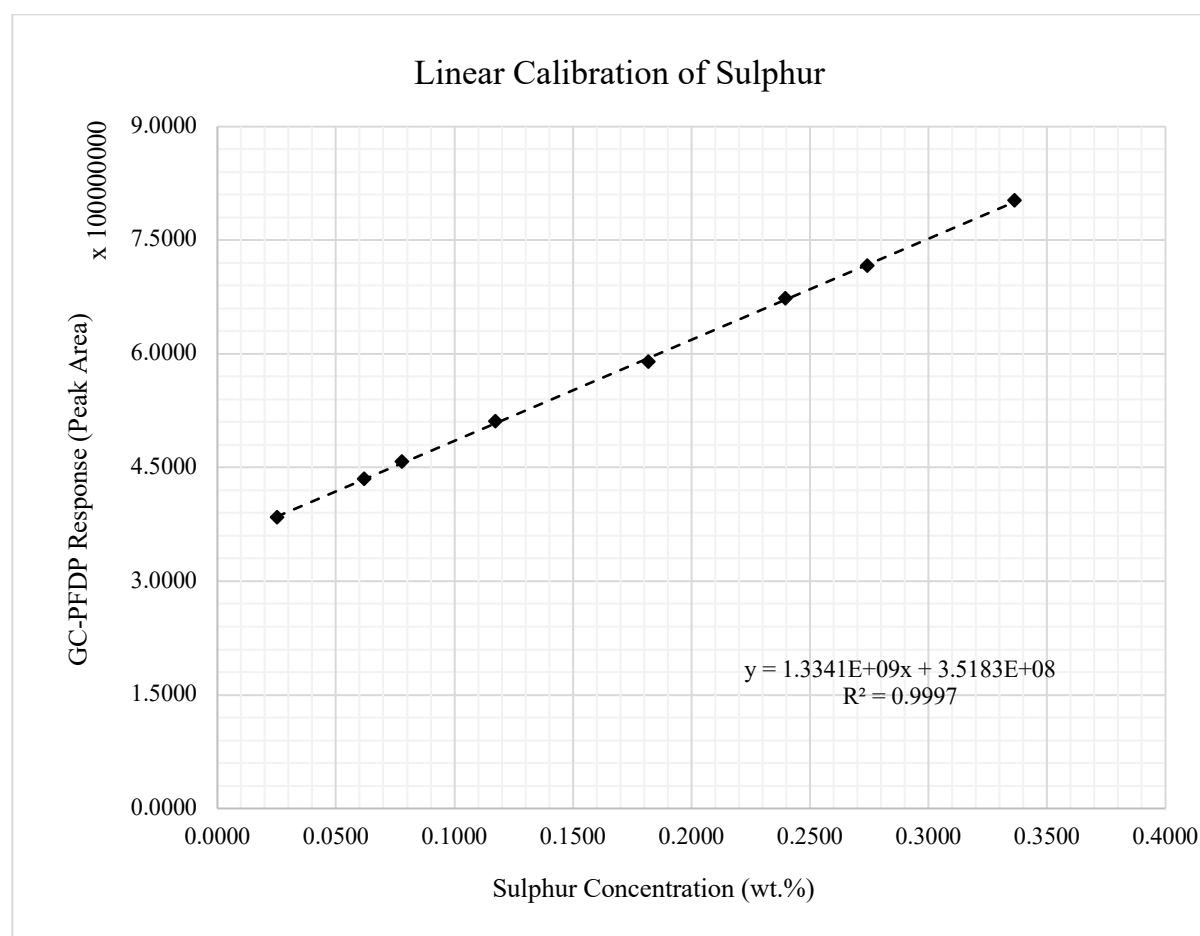
Figure 4.11. Calibration curve: plotting peak area as a function of sulphur concentration.

The calibration curve in Figure 4.11 was created to establish a relationship between the total peak area and the sulphur content. A linear regression was performed of y on x. The procedures used in the linear regression assumed that all the errors were in the y values and that the errors in the x values were insignificant. The relationship was described by the equation, $y = 1.3341 \times 10^9 x + 3.5183 \times 10^8$. The calibration equation is valid for the range between 0.0251 to 0.3363 wt.% sulphur. The calibration equation was not forced through the origin because that would imply that the detector causes neither interference nor noise for the analytical method.

Regression Statistics					
Multiple R	0.9999				
R Square	0.9997				
Adjusted R Square	0.9997				
Standard Error	2622773.4				
Observations	8				
ANOVA					
	df	SS	MS	F	Significance F
Regression	1	1.5519E+17	1.5519E+17	22560.4015	5.8744E-12
Residual	6	4.1274E+13	6.8789E+12		
Total	7	1.5523E+17			
	Coefficients	Standard Error	t Stat	P-value	Lower 95.0%	Upper 95.0%
Intercept (b)	351830090.0	1728748.2	203.5	9.4958E-13	347599995.4	356060184.5
X Variable 1 (a)	1334072752.0	8881904.5	150.2	5.8744E-12	1312339514.5	1355805989.4
$* y = ax + b$						

Figure 4.12. Data output from regression analysis using Excel.

Figure 4.12 shows the regression statistics, analysis of variance (ANOVA) and the variable coefficients. A Multiple R of 0.9999 suggested a strong linear relationship between total peak area and sulphur content. The Multiple R is the absolute value of the correlation coefficient so the correlation coefficient can fall between -1 and 1, where a value of 1 indicates a strong positive relationship, -1 indicates a strong negative relationship and 0 means there is no relationship.

An R^2 coefficient of determination of 0.9997 indicated that 99.97 % of the values fitted the regression model. A similar calibration was performed by Chambers and Duffy (2003), using thiophene (C_4H_4S) in benzene (C_6H_6). Chambers and Duffy (2003) obtained an R^2 value of 0.9992 from the linear regression between the GC-PFDP response and the sulphur content.

The precision and the average error of the regression model was evaluated using the Standard Error from the regression output. The Standard Error, 2622773.4, was relatively small compared to the total peak areas, from Table 4.6, which ranged from 378547258.8 to 812329437.7. Therefore, the relative

standard deviation ranged from +/-0.33 % to +/-0.69 % at the highest and lowest studied total peak areas, respectively.

The commonly used significance levels are 1 %, 2% or 5 % (Stigler, 2008; Ross, 2017). In the regression output, the Significance F was smaller than the commonly used significance levels. Therefore, the probability of the model regression being incorrect can be discarded because the Significance F was 5.8744×10^{-12}. The Significance F and the P-values share a similar interpretation because the Significance F applies to the entire model, whereas the P-values apply to each corresponding coefficient. A P-value of 5.8744×10^{-12} and 9.4958×10^{-13} was obtained for the a and b coefficients, respectively. The P-values were smaller than the commonly used significance levels; therefore, the probability of the a and b coefficients being unreliable can be discarded.

4.2.3. Sulphur Content of Untreated and Treated Tyre Derived Oil

Table 4.7. Average total peak area of the untreated tyre derived oil.

	Run 1	Run 2	Run 3	Average	Relative Standard Deviation (%)
Total Sulphur Peak Area	580862324.1	575346424.5	582811128.3	579673292.3	0.55

A relative standard deviation of 0.30 % indicated a small spread for the total peak areas of the untreated TDO. The sulphur content of the untreated TDO, 0.1708 wt.%, was determined using the calibration equation in Figure 4.11. Figure 4.13 shows the chromatogram of the sulphur peaks in the untreated TDO for Run 1.
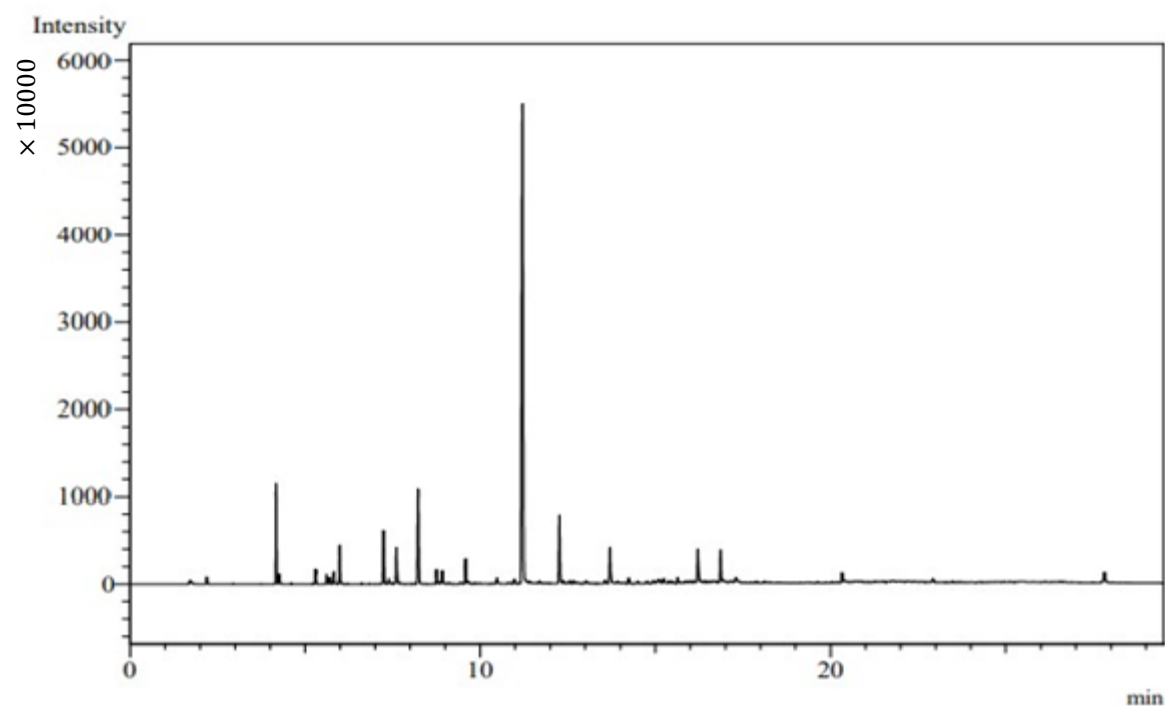
Figure 4.13. Chromatogram of the sulphur peaks in the untreated TDO for Run 1.

The treated TDO was tested 3 times on GC-PFDP to obtain an average total sulphur peak area (Appendix B-2). A low relative standard deviation (<1.10 %) indicated a small spread for the total peak areas. Table 4.8 shows the desulphurization capability of the unsupported and supported alkaline earth metal oxides for the operating conditions as obtained using the 2^3 factorial design. The sulphur removal was in the range of 6.38 to 57.59 wt.% for the various parametric interactions.

Table 4.8. Desulphurization of TDO using unsupported and supported alkaline earth metal oxides.

Run	T (ºC)	RT (min)	SO (g/ml)	MgO Ds (%)	8MgO-60SiO$_2$ Ds (%)	CaO Ds (%)	8CaO-60SiO$_2$ Ds (%)	8BaO-60SiO$_2$ Ds (%)
1	240	30	0.0125	35.11	37.16	22.34	17.72	17.57
2	240	30	0.0375	20.93	28.50	45.69	56.76	28.41
3	320	30	0.0125	28.77	31.77	31.80	21.46	6.38
4	320	30	0.0375	11.31	11.36	43.74	57.59	18.50
5	240	90	0.0125	25.92	36.48	33.49	25.26	11.96
6	240	90	0.0375	16.06	23.45	53.11	27.90	10.59
7	320	90	0.0125	24.77	31.34	15.43	15.07	7.52
8	320	90	0.0375	9.66	23.80	26.27	22.97	6.85
9	280	60	0.0250	34.25	32.62	12.99	33.39	26.14
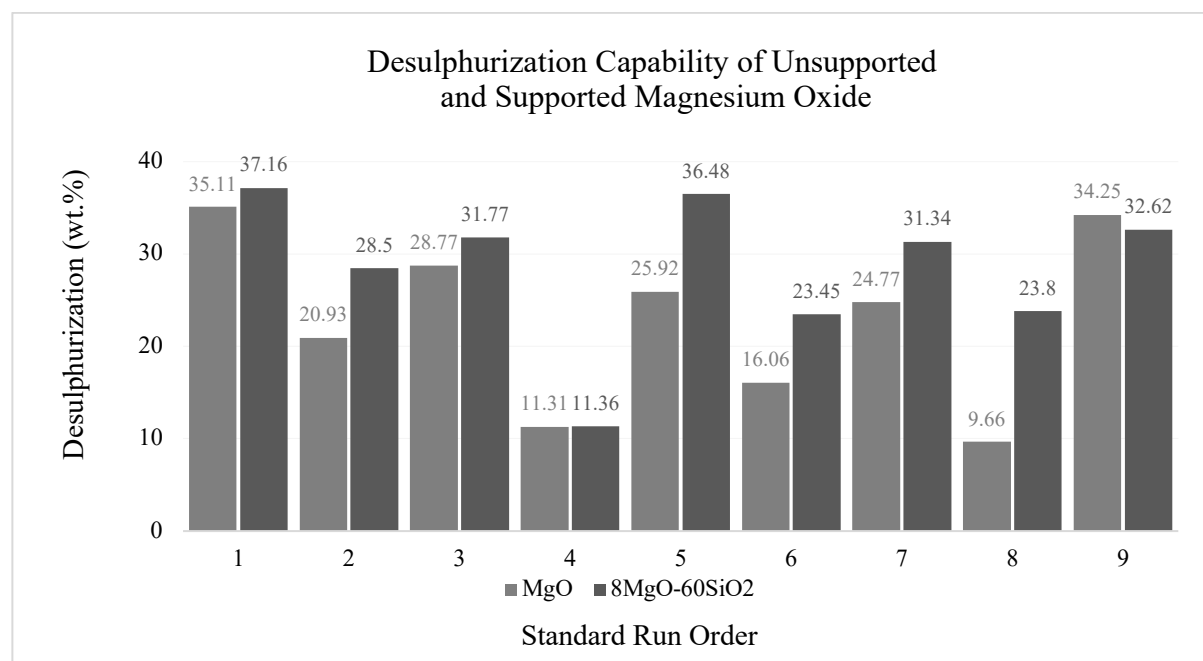
Figure 4.14. Comparison of the desulphurization capability of unsupported and supported magnesium oxide.

Figure 4.14 shows that the supported magnesium oxide provided better desulphurization than the unsupported magnesium oxide, except for the operating conditions of Run 9 ($T = 280$ ºC, $RT = 60$ min, $SO = 0.0250$ g/ml). The smaller crystallite sizes of magnesium oxide on the silica particles may have induced a better interaction with the sulphur compounds, resulting in a higher desulphurization. The

highest sulphur removal using unsupported and supported magnesium oxide was 35.11 and 37.16 wt.%, respectively. This was achieved using the operating conditions of Run 1 ($T = 240 \, ^{\circ}C$, $RT = 30$ min, $SO = 0.0125$ g/ml). The operating conditions of Run 1 can be considered optimal because Run 1 has the lowest energy and sorbent requirements compared to Run 2 – 9.

Design-Expert 12 was used to find suitable regression models for the desulphurization data presented in Table 4.8. The linear and two-factor interaction (2FI) models were not a good fit for the desulphurization data of unsupported magnesium oxide as inferred by the low R^2 and adjusted R^2 values, presented in Table 4.9. A higher-order model, such as the quadratic model, was not used because a minimum of three levels were required (Carr, 2010). For the analysis of variance (ANOVA), the linear model was preferred over the two-factor model because of a higher adjusted R^2 value, which expresses how well the model predicts various outcomes within the range of study. The fit of the linear model to the experimental data can be seen in Figure 4.15. The ANOVA and linear equation were used to identify the terms that significantly affect desulphurization. The following linear equation was used to understand the significant terms within the range of study:

$$Ds = 22.98 - 2.94X_T - 2.46X_{RT} - 7.08X_{SO}$$

The equation is in terms of coded factors. The high levels of the factors were coded as +1, and the low levels were coded as -1. The coded equation was useful for identifying the relative impact of the factors by comparing the factor coefficients. Table 4.10 provides an insight into the significant and non-significant factors for the 2^3 factorial design. A significance level of 0.05 was chosen to assess the P-values. A model P-value of 0.0543 suggested that the linear model was not significant, which means that there is a weak statistical relationship between the independent and dependant variables for the linear model. The coefficients for temperature (X_T) and reaction time (X_{RT}) were not significant, which indicated that the coefficients for X_T and X_{RT} do not impact desulphurization as significantly as the coefficient for sorbent-to-oil ratio (X_{SO}).

The linear and two-factor interaction models were not a good fit for the desulphurization data of supported magnesium oxide due to the low R^2 and adjusted R^2 values, presented in Table 4.11. For the analysis of variance (ANOVA), the linear model was preferred over the two-factor model because of a higher adjusted R^2 value. The fit of the linear model to the experimental data can be seen in Figure 4.16. The ANOVA and linear equation were used to identify the terms that significantly affect desulphurization. The following linear equation was used to understand the significant terms within the range of study:

$$Ds = 28.50 - 3.41X_T + 0.79X_{RT} - 6.20X_{SO}$$

The equation is in terms of coded factors. The high levels of the factors were coded as +1, and the low levels were coded as -1. The coded equation was useful for identifying the relative impact of the factors by comparing the factor coefficients. Table 4.12 provides an insight into the significant and non-

significant factors for the 2^3 factorial design. A model P-value of 0.0390 suggested that the linear model was significant, which means there is a statistical relationship between the independent and dependant variables for the linear model. The coefficients for temperature (X_T) and reaction time (X_{RT}) were not significant, which indicate that the coefficients for X_T and X_{RT} do not impact desulphurization as significantly as the coefficient for sorbent-to-oil ratio (X_{SO}).
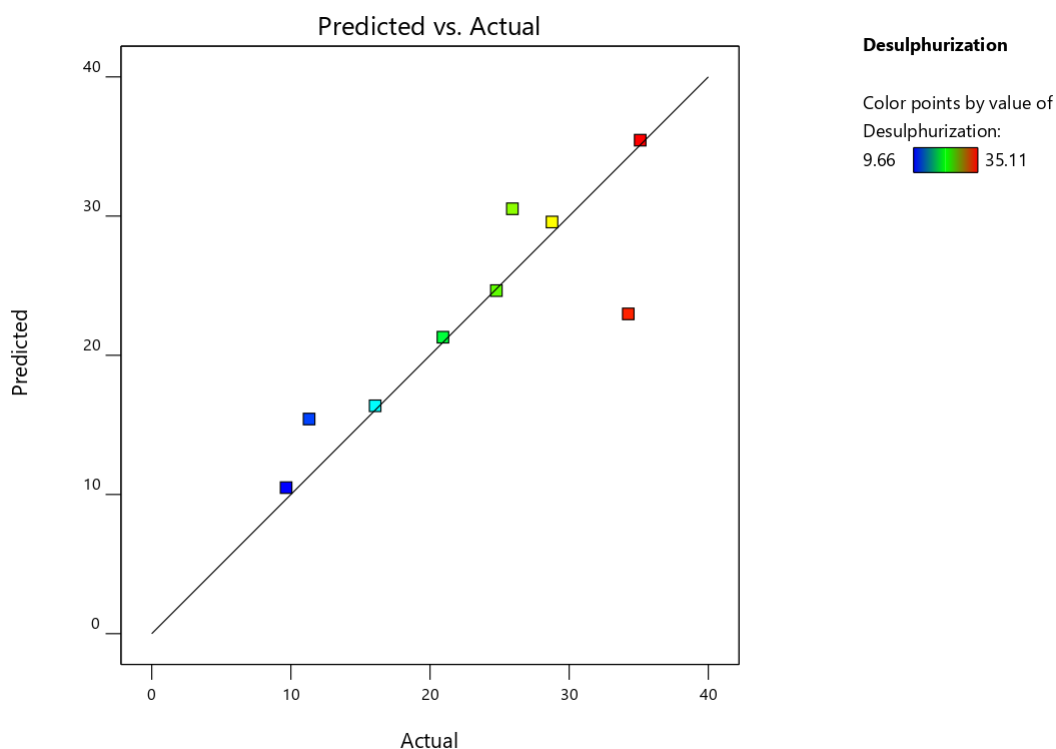
Figure 4.15. Predicted vs actual desulphurization using unsupported magnesium oxide.

Table 4.9. Model summary for unsupported magnesium oxide.

Source	Sequential P-value	R²	Adjusted R²	Predicted R²	
Linear	0.0543	0.7563	0.6101	0.5449	Suggested
2FI	0.9472	0.7906	0.1624	-0.4736	
Quadratic	0.0370	0.9993	0.9943		Aliased

Table 4.10. ANOVA for linear model (desulphurization of TDO using unsupported magnesium oxide)

Source	Sum of Squares	df	Mean Square	F-value	P-value	
Model	518.24	3	172.75	5.17	0.0543	Not significant
X_T - Temperature	69.09	1	69.09	2.07	0.2099	Not significant
X_{RT} - Residence Time	48.56	1	48.56	1.45	0.2818	Not significant
X_{SO} - Sorbent-to-Oil Ratio	400.59	1	400.59	11.99	0.0180	Significant
Residual	166.98	5	33.40			
Cor Total	685.22	8				
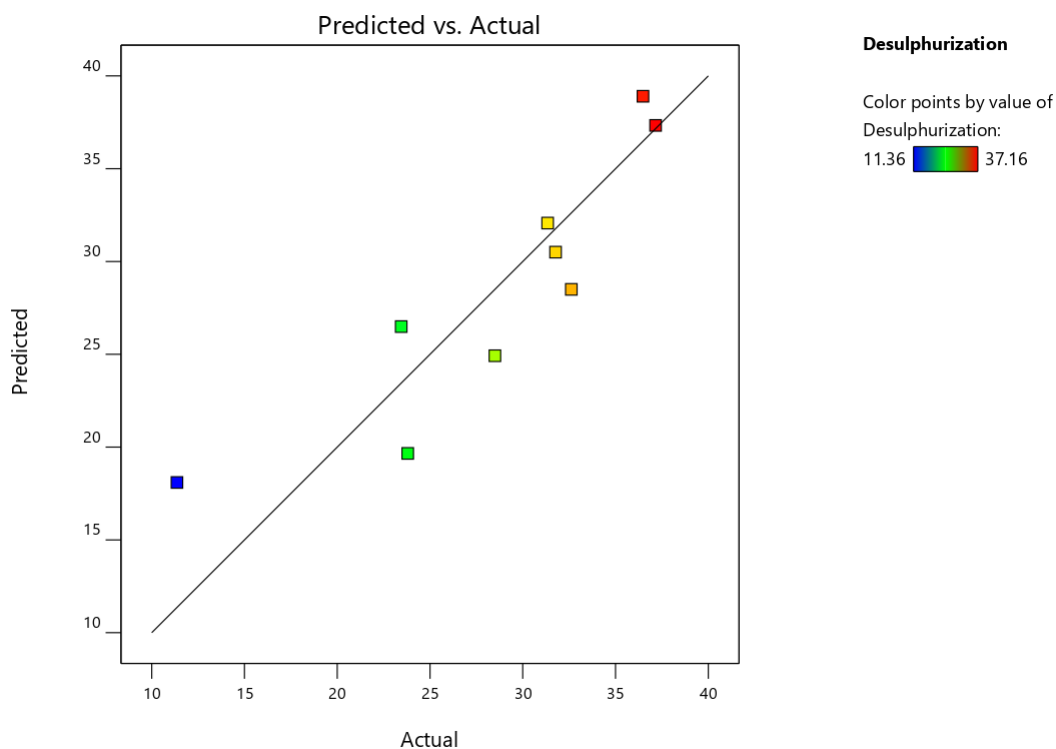
Figure 4.16. Predicted vs actual desulphurization using supported magnesium oxide.

Table 4.11. Model summary for supported magnesium oxide.

Source	Sequential P-value	R^2	Adjusted R^2	Predicted R^2	
Linear	0.0390	0.7876	0.6602	0.2789	Suggested
2FI	0.6609	0.8909	0.5636	-2.9893	
Quadratic	0.6039	0.9280	0.4238		Aliased

Table 4.12. ANOVA for linear model (desulphurization of TDO using supported magnesium oxide).

Source	Sum of Squares	df	Mean Square	F-value	P-value	
Model	406.24	3	135.41	6.18	0.0390	Significant
X_T - Temperature	93.30	1	93.30	4.26	0.0940	Not significant
X_{RT} - Residence Time	4.93	1	4.93	0.23	0.6552	Not significant
X_{SO} - Sorbent-to-Oil Ratio	308.02	1	308.02	14.06	0.0133	Significant
Residual	109.54	5	21.91			
Cor Total	515.78	8				

Figure 4.17 graphically compares the desulphurization data of unsupported and supported calcium oxide. The highest sulphur removal, 57.59 wt.%, was achieved using silica-supported calcium oxide at a reaction temperature of 320 ºC, a reaction time of 30 min and a sorbent-to-oil ratio of 0.0375 g/ml. The operating conditions used to achieve 57.59 wt.% desulphurization was not optimal because a 56.76

wt.% desulphurization was achieved using a reaction time of 30 min, a sorbent-to-oil ratio of 0.0375 g/ml and a lower reaction temperature of 240 °C. The analysis of variance, Table 4.16, shows that the coefficient for temperature was not significant, which indicated that the coefficient for temperature does not impact desulphurization as significantly as the coefficients for reaction time and sorbent-to-oil ratio. The non-significant temperature coefficient alludes to the probability that supported calcium oxide is similarly selective to sulphur containing compounds at low and high temperatures.
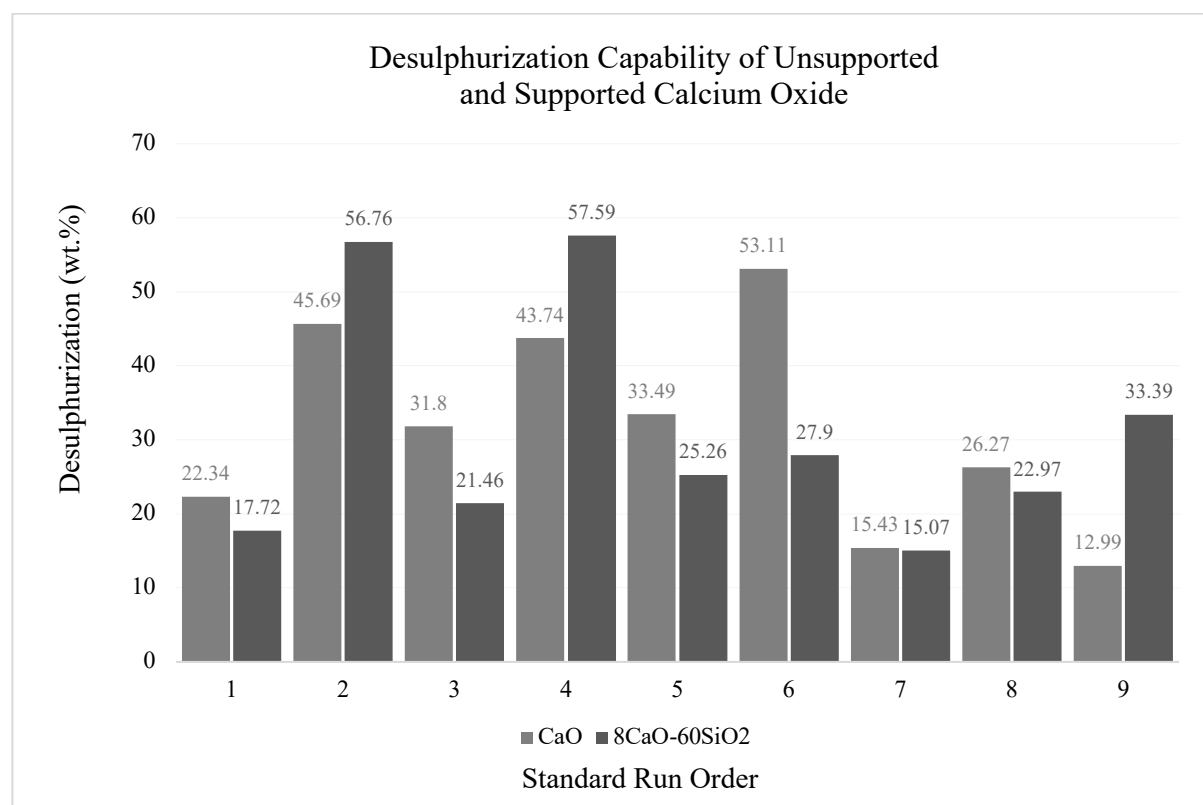
Figure 4.17. Comparison of the desulphurization capability of unsupported and supported calcium oxide.

The linear and two-factor interaction (2FI) models were not a good fit for the desulphurization data of unsupported calcium oxide as inferred by the low R^2 and adjusted R^2 values, presented in Table 4.13. A higher-order model, such as the quadratic model, was not used because a minimum of three levels were required (Carr, 2010). For the analysis of variance (ANOVA), the linear model was preferred over the two-factor model because of a higher adjusted R^2 value, which expresses how well the model predicts various outcomes within the range of study. The fit of the linear model to the experimental data can be seen in Figure 4.18. The following linear equation was obtained:

$$Ds = 31.65 - 4.67X_T - 1.91X_{RT} + 8.22X_{SO}$$

The equation is in terms of coded factors. The high levels of the factors were coded as +1, and the low levels were coded as -1. A significance level of 0.05 was chosen to assess the P-values. Table 4.14 shows that the linear model and its terms were not significant, which means there is a weak statistical

relationship between the independent and dependant variables. Therefore, the linear equation was not suitable to describe the factors affecting desulphurization.
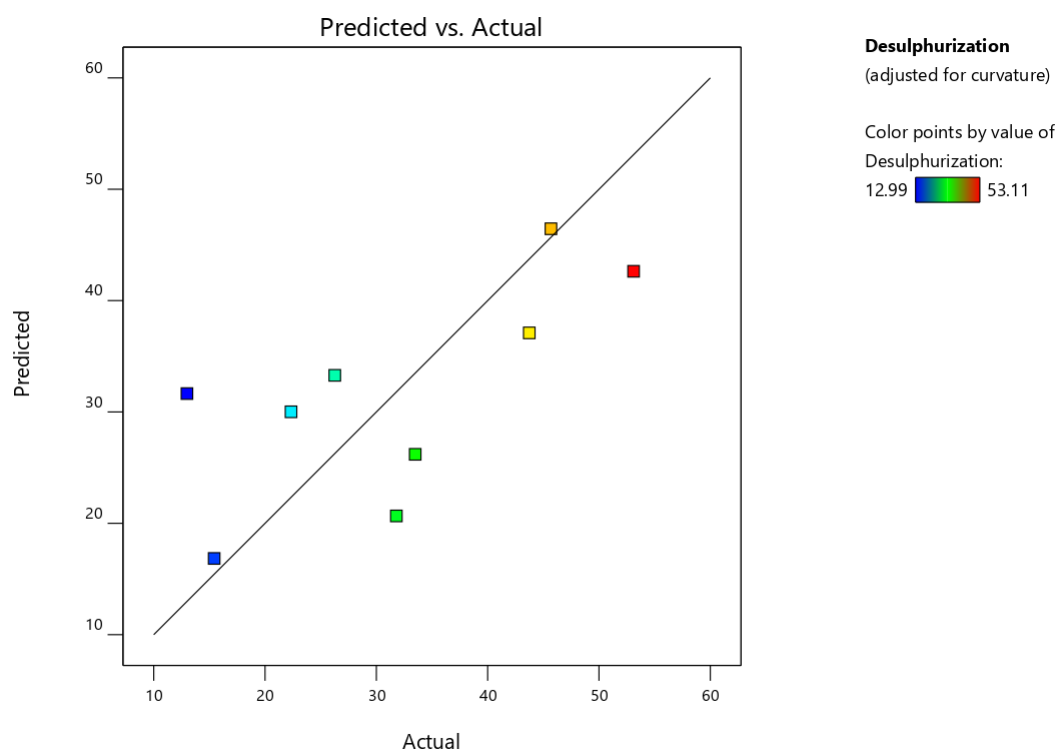
Figure 4.18. Predicted vs actual desulphurization using unsupported calcium oxide.

Table 4.13. Model summary for unsupported calcium oxide.

Source	Sequential P-value	R²	Adjusted R²	Predicted R²	
Linear	0.3070	0.4851	0.1762	-0.3773	Suggested
2FI	0.6434	0.7441	-0.0237	-0.7874	
Quadratic	0.0299	0.9994	0.9955		Aliased

Table 4.14. ANOVA for linear model (desulphurization of TDO using unsupported calcium oxide).

Source	Sum of Squares	df	Mean Square	F-value	P-value	
Model	744.28	3	248.09	1.57	0.3070	Not significant
X_T - Temperature	174.75	1	174.75	1.11	0.3411	Not significant
X_{RT} - Residence Time	29.15	1	29.15	0.18	0.6854	Not significant
X_{SO} - Sorbent-to-Oil Ratio	540.38	1	540.38	3.42	0.1236	Not significant
Residual	789.85	5	157.97			
Cor Total	1534.13	8				

Table 4.15 shows the model summary for the desulphurization data of supported calcium oxide. The two-factor model fitted the desulphurization data of supported calcium oxide as inferred by an R^2 and an adjusted R^2 value of 0.9924 and 0.9695, respectively. The predicted R^2 value of 0.7603 indicated that the model is 76.03 % accurate in predicting the percentage desulphurization outside the range of study. Therefore, the model can only be used to accurately predict the percentage desulphurization within the range of study. The fit of the two-factor model to the data can be seen visually in Figure 4.19. The following equation was found to be valid within the range of study:

$$Ds = 30.90 - 1.32X_T - 7.79X_{RT} + 10.71X_{SO} - 2.46X_T X_{RT} + 0.2937X_T X_{SO} - 8.08X_{RT} X_{SO}$$

The equation, in terms of coded factors, was used to make predictions about the response. The high levels of the factors were coded as +1, and the low levels were coded as -1. The coded equation was useful for identifying the relative impact of the factors by comparing the factor coefficients. The analysis of variance (ANOVA), Table 4.16, provides an insight into the parametric interactions of the 2^3 factorial design. A significance level of 0.05 was chosen to assess the P-values. The coefficient for temperature (X_T) was not significant, which indicated that the coefficient for X_T does not impact desulphurization as significantly as the coefficients for reaction time (X_{RT}) and sorbent-to-oil ratio (X_{SO}). Furthermore, the interaction between reaction time (X_{RT}) and sorbent-to-oil ratio (X_{SO}) had a P-value of 0.0143, which indicated that the interaction between X_{RT} and X_{SO} was significant. In contrast, the interactions between X_T and X_{RT}, and X_T and X_{SO} were not significant. A contour plot and a 3-dimensional surface response plot is shown in Figure 4.20.
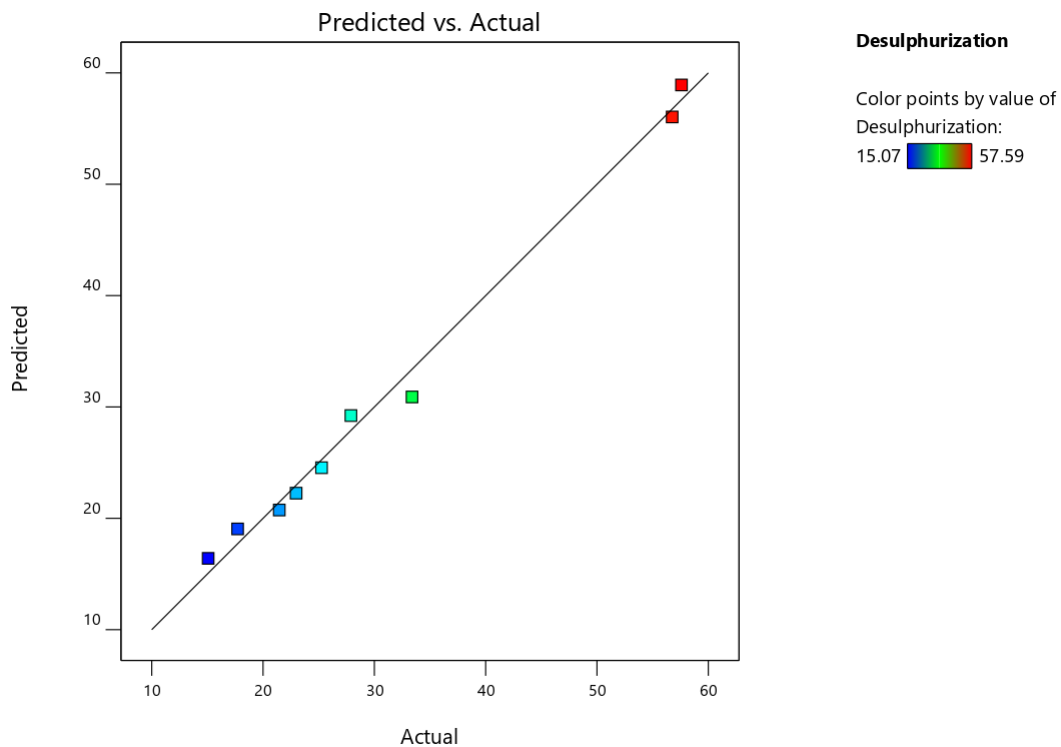
Figure 4.19. Predicted vs actual desulphurization using supported calcium oxide.

Table 4.15. Model summary for supported calcium oxide.

Source	Sequential p-value	R²	Adjusted R²	Predicted R²	
Linear	0.0839	0.7074	0.5318	-0.1004	
2FI	0.0389	0.9924	0.9695	0.7603	Suggested
Quadratic	0.5288	0.9958	0.9667		Aliased

Table 4.16. ANOVA for 2FI model (desulphurization of TDO using supported calcium oxide).

Source	Sum of Squares	df	Mean Square	F-value	P-value	
Model	1989.10	6	331.52	43.32	0.0227	Significant
X_T - Temperature	13.91	1	13.91	1.82	0.3100	Not Significant
X_{RT} - Residence Time	485.63	1	485.63	63.45	0.0154	Significant
X_{SO} - Sorbent-to-Oil Ratio	918.28	1	918.28	119.99	0.0082	Significant
$X_T X_{RT}$	48.46	1	48.46	6.33	0.1282	Not Significant
$X_T X_{SO}$	0.6903	1	0.6903	0.09	0.7923	Not Significant
$X_{RT} X_{SO}$	522.13	1	522.13	68.22	0.0143	Significant
Residual	15.31	2	7.65			
Cor Total	2004.41	8				
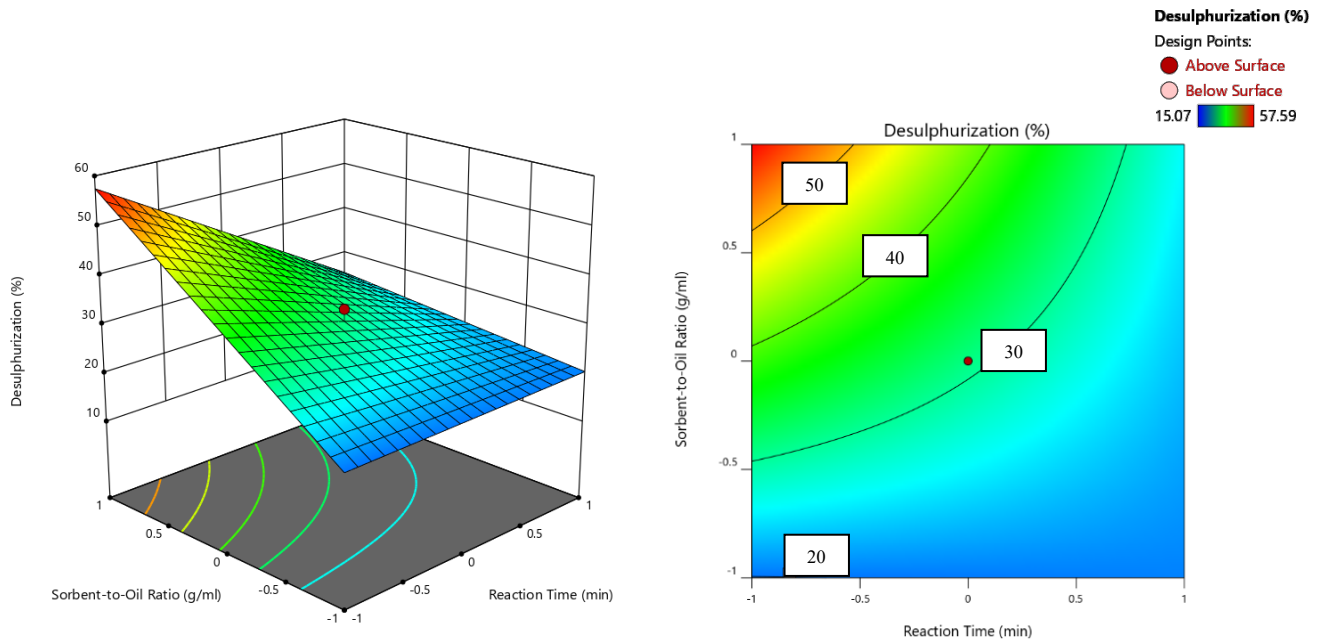
(a) $X_T = 0$
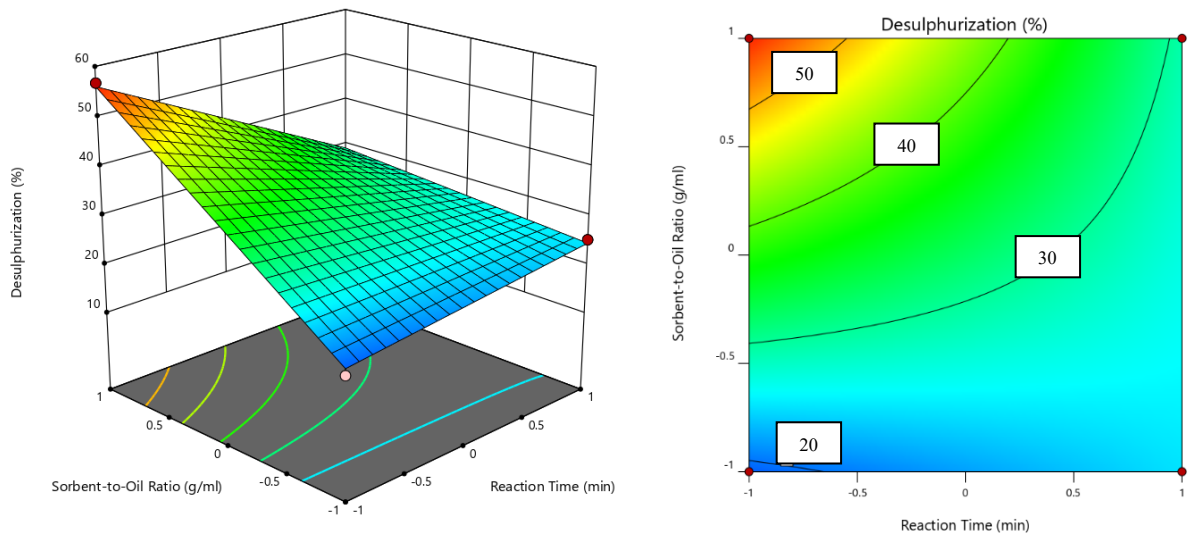
(b) $X_T = -1$
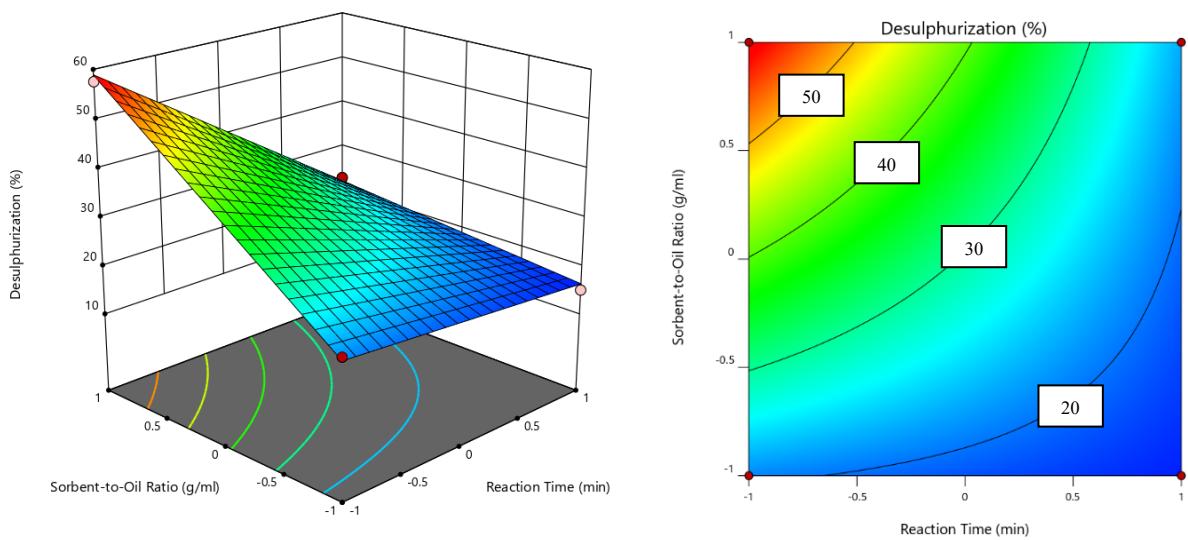
(c) $X_T = +1$

Figure 4.20. 3-Dimensional surface response and contour plot showing the effect of reaction time and sorbent-to-oil ratio on the percentage desulphurization of TDO at various temperatures using supported calcium oxide.

The highest desulphurization using supported barium oxide was 28.41 wt.% at a reaction temperature of 240 °C, a reaction time of 30 min and a sorbent-to-oil ratio of 0.0375 g/ml. The use of unsupported barium oxide for desulphurization was problematic because the barium oxide and TDO formed a thick slurry. The thick slurry could not filter through the Grade 1 Whatman® filter paper nor the 0.45 μm PTFE syringe filter for GC-PFDP analysis. Therefore, desulphurization data for unsupported barium oxide was absent from Table 4.8.

The linear and two-factor interaction (2FI) models were not a good fit for the desulphurization data of supported barium oxide as inferred by the low R^2 and adjusted R^2 values, presented in Table 4.17. A higher-order model, such as the quadratic model, was not used because a minimum of three levels were required (Carr, 2010). For the analysis of variance (ANOVA), the linear model was preferred over the two-factor model because of a higher adjusted R^2 value, which expresses how well the model predicts various outcomes within the range of study. The fit of the linear model to the experimental data can be seen in Figure 4.21. The following linear equation was obtained:

$$Ds = 14.88 - 3.66X_T - 4.24X_{RT} + 2.62X_{SO}$$

The equation is in terms of coded factors. The high levels of the factors were coded as +1, and the low levels were coded as -1. A significance level of 0.05 was chosen to assess the P-values from the analysis of variance. The analysis of variance, Table 4.18, shows that the linear model and its terms were not significant, which means that there is a weak statistical relationship between the independent and dependant variables. Therefore, the linear equation was not suitable to describe the factors affecting desulphurization.
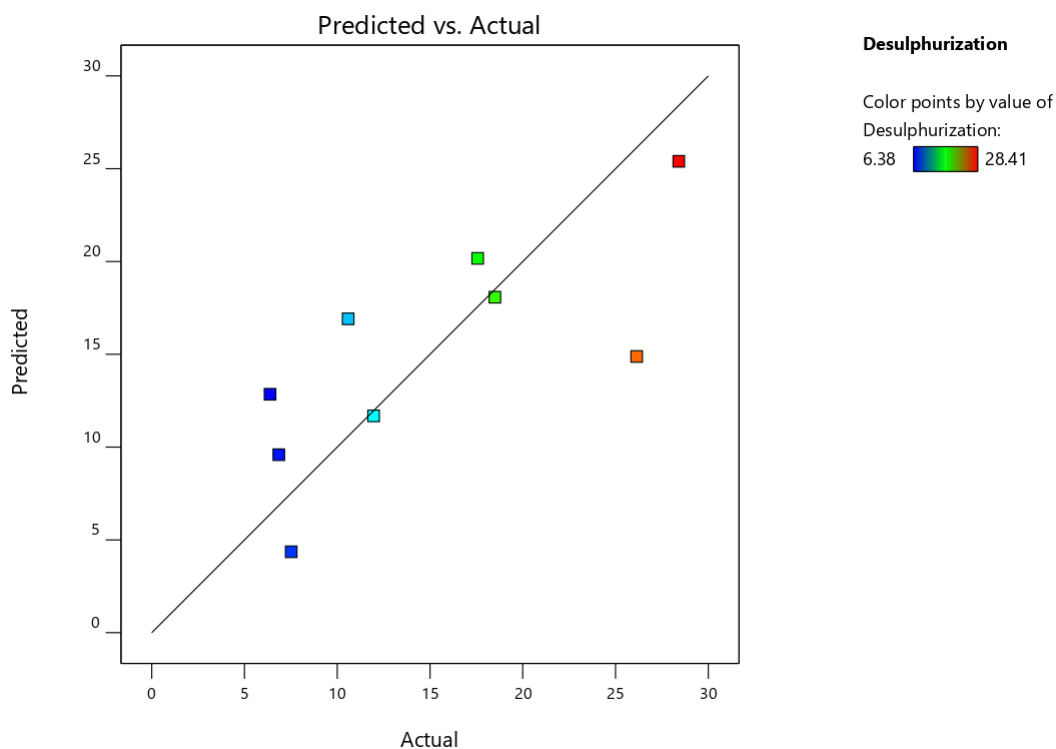
Figure 4.21. Predicted vs actual desulphurization using supported barium oxide.

Table 4.17. Model summary for supported barium oxide.

Source	Sequential p-value	R²	Adjusted R²	Predicted R²	
Linear	0.2182	0.5581	0.2930	-0.0900	Suggested
2FI	0.7367	0.7396	-0.0414	-0.7960	
Quadratic	0.0109	0.9999	0.9994		Aliased

Table 4.18. ANOVA for linear model (desulphurization of TDO using supported barium oxide).

Source	Sum of Squares	df	Mean Square	F-value	P-value	
Model	305.86	3	101.95	2.11	0.2182	Not significant
X_T - Temperature	107.16	1	107.16	2.21	0.1970	Not significant
X_{RT} - Residence Time	143.99	1	143.99	2.97	0.1453	Not significant
X_{SO} - Sorbent-to-Oil Ratio	54.71	1	54.71	1.13	0.3365	Not significant
Residual	242.16	5	48.43			
Cor Total	548.02	8				

Table 4.19 presents the optimal operating conditions for the desulphurization of TDO using alkaline earth metal oxides supported on silica gel with a 60 Å pore size and a 35-60 mesh particle size. The size of the silica gel was varied in an attempt to improve the desulphurization of TDO. The following sizes of silica gel were used for the invention: (1) silica gel with a 30 Å pore size and a 100-200 mesh particle size, and (2) silica gel with a 150 Å pore size and a 35-60 mesh particle size. The desulphurization results, using the supported metal oxides, suggested that pore diameter and mesh particle size do not significantly impact desulphurization for the operating conditions used in Table 4.19. The observation may be a result of sufficient contact between the sulphur-containing compounds and the surface and pores of the supported metal oxides. For the experimental method, Chapter 4.1, a stirring rate of 400 rpm was used for all experiments, which may have contributed to sufficient mixing between the tyre derived oil and the supported metal oxides.

Table 4.19. Desulphurization of TDO using various silica-supported alkaline earth metal oxides.

Operating Conditions			Desulphurization (wt.%)			Standard Deviation
T (°C)	RT (min)	SO (g/ml)				
240	30	0.0125	$8MgO-30SiO_2$ 39.45	$8MgO-60SiO_2$ 37.16	$8MgO-150SiO_2$ 37.98	0.95
240	30	0.0375	$8CaO-30SiO_2$ 54.97	$8CaO-60SiO_2$ 56.76	$8CaO-150SiO_2$ 56.40	0.77
240	30	0.0375	$8BaO-30SiO_2$ 31.36	$8BaO-60SiO_2$ 28.41	$8BaO-150SiO_2$ 29.99	1.21
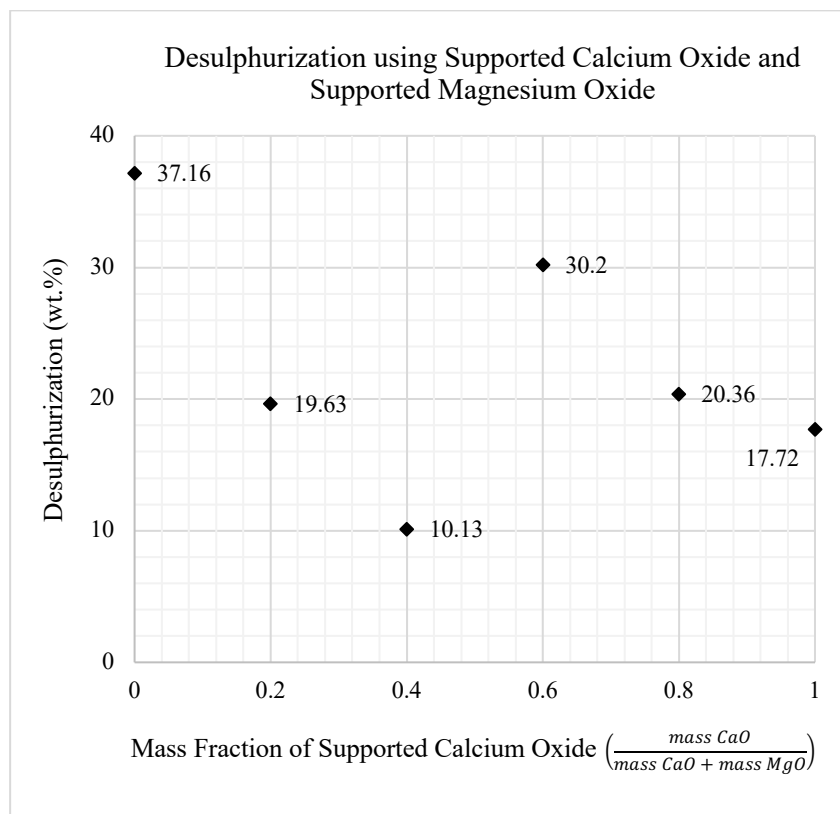
Figure 4.22. Desulphurization of TDO using a combination of supported calcium oxide and supported magnesium oxide ($T = 240$ °C, $RT = 30$ min, $SO = 0.0125$ g/ml).

Figure 4.22 shows the percentage desulphurization of TDO using a combination of supported calcium oxide and supported magnesium oxide at a temperature of 240 °C, a reaction time of 30 min and a sorbent-to-oil ratio of 0.0125 g/ml. A combination of supported calcium oxide and supported magnesium oxide was used in an attempt to improve desulphurization. The operating conditions were chosen based on the lowest material and energy requirements. Supported calcium oxide and supported magnesium oxide with a 60 Å pore size were chosen for the invention because of the complete calcination of the metal precursors to metal oxides. The desulphurization of TDO using only supported calcium oxide and supported magnesium oxide was 37.16 and 17.72 wt.%, respectively. Combining the supported alkaline earth metal oxides did not improve desulphurization. According to James (2006), hydrogen sulphide in the reactor can react with olefins to form recombinant mercaptans, high molecular weight straight chain thiols and branched-chain thiols. The formation of higher molecular weight sulphur compounds causes sulphur to be retained in the product, limiting the effectiveness of the adsorptive desulphurization process (Knudsen et al., 1999).

4.3. Conclusion

In this chapter, the purpose was to compare the performance of the various reactive adsorbents in terms of total sulphur adsorbed. Furthermore, to characterize the supported alkaline earth metal oxides that were synthesized via the wet impregnation technique. The SEM-EDX analysis confirmed the presence of alkaline earth metal oxides on the surface of the silica particles. The optimum conditions, which resulted in a 56.76 wt.% desulphurization, was at a temperature of 240 $^{\circ}$C for 30 min with a 0.0375 g/ml sorbent-to-oil ratio, using supported calcium oxide.

From the statistical analysis, the sorbent-to oil ratio impacted desulphurization more than reaction temperature and reaction time when using unsupported or supported magnesium oxide. The reaction time and sorbent-to-oil ratio were found to impact desulphurization more than reaction temperature when using supported calcium oxide. There was no statistical significance for the linear model and two-factor model for the desulphurization data, using unsupported calcium oxide or supported barium oxide for desulphurization.

The results for the supported alkaline earth metal oxides (with varied pore diameter and mesh particle size) suggested that pore diameter and mesh particle size do not significantly impact desulphurization for the operating conditions studied. A combination of supported calcium oxide and supported magnesium oxide was used in an attempt to improve desulphurization; however, there was no improvement for the operating conditions investigated, i.e., a temperature of 240 $^{\circ}$C, a reaction time of 30 min and a sorbent-to-oil ratio of 0.0125 g/ml. The balance between temperature, reaction time and sorbent-to-oil ratio provides the impetus for continued research into the combined effect of alkaline earth metal oxides for desulphurization.

4.4. References

- Carr, B. (2010). Statistical design of experiments in the 21st century and implications for consumer product testing. *Consumer-Driven Innovation in Food and Personal Care Products*, pp.427-469.

- Chambers, L. and Duffy, M. (2003). Determination of Total and Speciated Sulfur Content in Petrochemical Samples Using a Pulsed Flame Photometric Detector. *Journal of Chromatographic Science*, 41(10), pp.528-534.

- Das, A. and Dewanjee, S. (2018). Optimization of Extraction Using Mathematical Models and Computation. *Computational Phytochemistry*, pp.75-106.

- Goodge, J. (2017). *Energy-Dispersive X-Ray Spectroscopy (EDS)*. [online] SERC. Available at: <https://serc.carleton.edu/research_education/geochemsheets/eds.html> [Accessed 5 October 2021].

- James, P.N. (2006). Developing clean fuels: Novel techniques for desulfurization. *Princeton University*.

- Knudsen, K., Cooper, B. and Topsøe, H. (1999). Catalyst and process technologies for ultra low sulfur diesel. *Applied Catalysis A: General*, 189(2), pp.205-215.

- Nasrazadani, S. and Hassani, S. (2016). Modern analytical techniques in failure analysis of aerospace, chemical, and oil and gas industries. *Handbook of Materials Failure Analysis with Case Studies from the Oil and Gas Industry*, pp.39-54.

- Parr Instrument Company (2014). 5500 Compact Mini Bench Top Reactors Operating Instruction Manual. (443M R07).

- Ross, S. (2017). Testing Statistical Hypotheses. *Introductory Statistics*, pp.381-432.

- Stigler, S. (2008). Fisher and the 5% level. *CHANCE*, 21(4), pp.12-12.

Chapter 5

5. Conclusion

The following studies and experiments have been carried out and reported, based on the objectives mentioned in Chapter 1:

- Characterization of untreated tyre derived oil by gas chromatography mass spectrometry (GC-MS) and Fourier Transform Infrared Spectroscopy (FTIR) for determining the composition and functional groups of tyre derived oil, respectively.
- Development of supported alkaline earth metal oxides for the desulphurization of tyre derived oil.
- Characterization of the synthesized supported alkaline earth metal oxides using a Scanning Electron Microscope (SEM) equipped with an Energy Dispersive X-Ray (EDX) probe for semi-quantitative elemental analysis.
- Desulphurization of tyre derived oil using unsupported and supported alkaline earth metal oxides.
- Application of the 2^3 factorial design and response surface methodology to understand the interactions between reaction temperature, reaction time and sorbent-to-oil ratio on desulphurization performance.
- Desulphurization of tyre derived oil using silica-supported alkaline earth metal oxides with varying particle size and mesh particle size.
- Desulphurization of tyre derived oil using a combination of supported calcium oxide and supported magnesium oxide in an attempt to improve desulphurization.

The results obtained from the studies mentioned above have produced the following contributions to the field of desulphurization and alternative fuels:

- The high percentage of identified aromatics and naphthenic components makes tyre derived oil suitable as an alternative to conventional liquid fuels. The FTIR analysis revealed that the tyre derived oil was composed of aliphatics and aromatics as well as oxygen, nitrogen and sulphur-containing compounds. The main aromatic compounds found in the tyre derived oil were identified, i.e, toluene (0.71 %), styrene (0.15 %), xylene (1.39 %), limonene (6.55 %), cymene (2.56 %) and benzothiazole (0.80 %).
- The SEM-EDX analysis confirmed the presence of alkaline earth metal oxides on the surface of the silica particles. Therefore, the silica-supported alkaline earth metal oxides were successfully synthesized using the wet impregnation technique.
- The sulphur removal was in the range of 6.38 to 57.59 wt.% for the various parametric interactions. The optimum desulphurization using magnesium oxide was 37.16 wt.%. This was achieved at a temperature of 240 ºC for 30 min with a sorbent-to-oil ratio of 0.0125 g/ml, using supported

magnesium oxide. The optimum desulphurization using calcium oxide was 56.76 wt.%. This was achieved at a temperature of 240 ^{o}C for 30 min with a 0.0375 g/ml sorbent-to-oil ratio, using supported calcium oxide. The highest desulphurization using supported barium oxide was 28.41 wt.% at a temperature of 240 ^{o}C for 30 min with a 0.0375 g/ml sorbent-to-oil ratio. The use of unsupported barium oxide for desulphurization was problematic because the barium oxide and TDO formed a thick slurry. The thick slurry could not filter through the Grade 1 Whatman® filter paper nor the 0.45 μm PTFE syringe filter for GC-PFDP analysis. Therefore, desulphurization data for unsupported barium oxide was absent.

- From the statistical analysis, the sorbent-to oil ratio impacted desulphurization more than reaction temperature and reaction time when using unsupported or supported magnesium oxide. The reaction time and sorbent-to-oil ratio were found to impact desulphurization more than reaction temperature when using supported calcium oxide. There was no statistical significance for the linear model and two-factor model for the desulphurization data, using unsupported calcium oxide or supported barium oxide for desulphurization.

- The desulphurization results using supported alkaline earth metal oxides (with varied pore diameter and mesh particle size) suggested that pore diameter and mesh particle size do not significantly impact desulphurization for the operating conditions studied.

- There was no improvement in desulphurization (using a combination of supported magnesium oxide and supported calcium oxide) for the operating conditions investigated, i.e., a reaction temperature of 240 ^{o}C, a reaction time of 30 min and a sorbent-to-oil ratio of 0.0125 g/ml.

In summary, the promising results supplements existing literature for the use of tyre derived oil as an alternative to fossil fuels. The desulphurization data initiates an interest in using alkaline earth metal oxides for desulphurization and determining the balance between reaction temperature, reaction time, and sorbent-to-oil ratio for desulphurization.

APPENDICES

Appendix A: Equipment
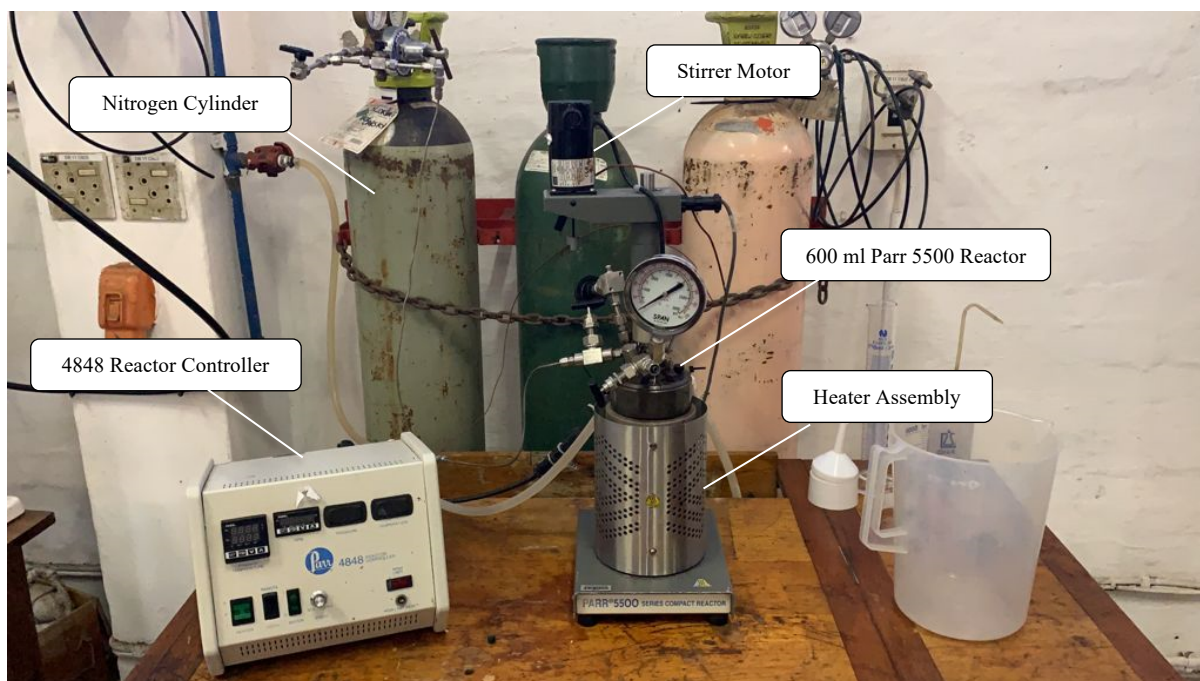
Figure A-1. Image of reactor system
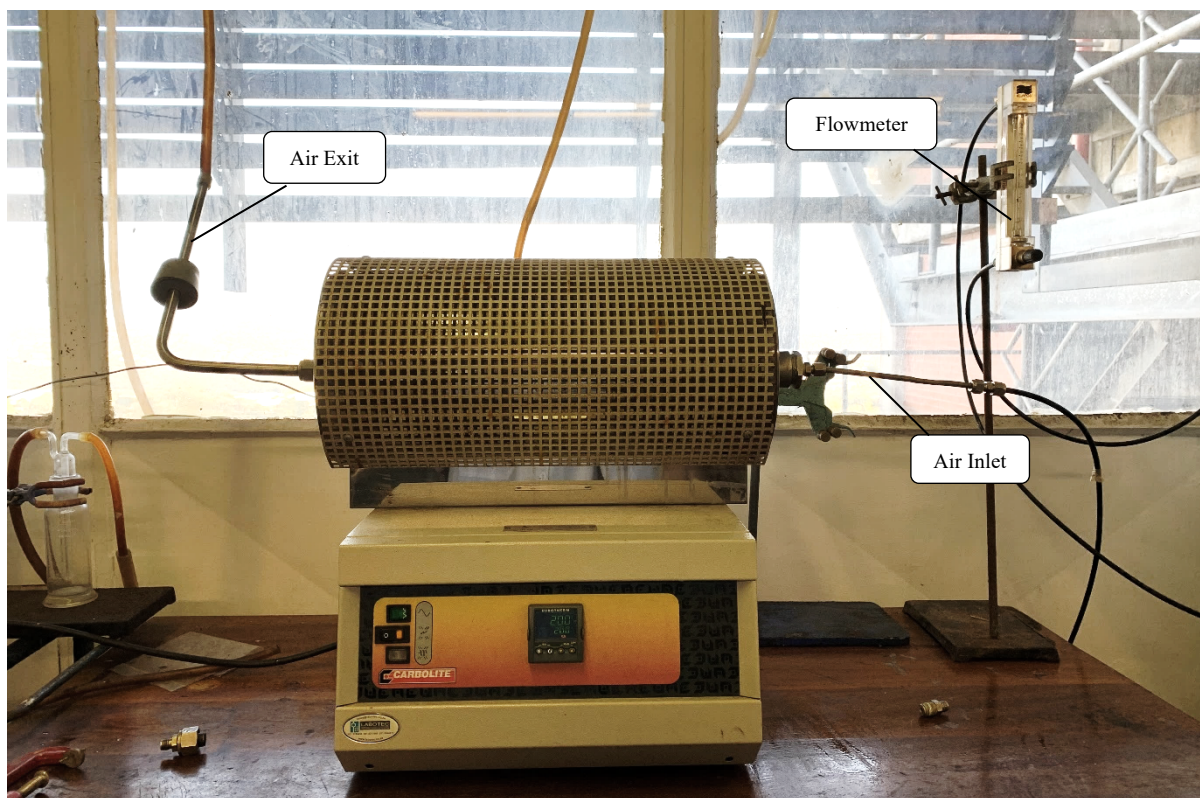
Figure A-2. Image of the Carbolite MTF 12/38/400 tube furnace.

Figure A-3. Image of GC-MS – QP2010 SE Equipped with an AOC-20i auto injector.

Figure A-4. Image of Shimadzu GC-2014 with PFDP and FID.

Figure A-5. Image of filtration system with an Edwards RV3 vacuum pump.

Appendix B: GC-PFDP Results

B-1. Determining Total Sulphur Peak Area
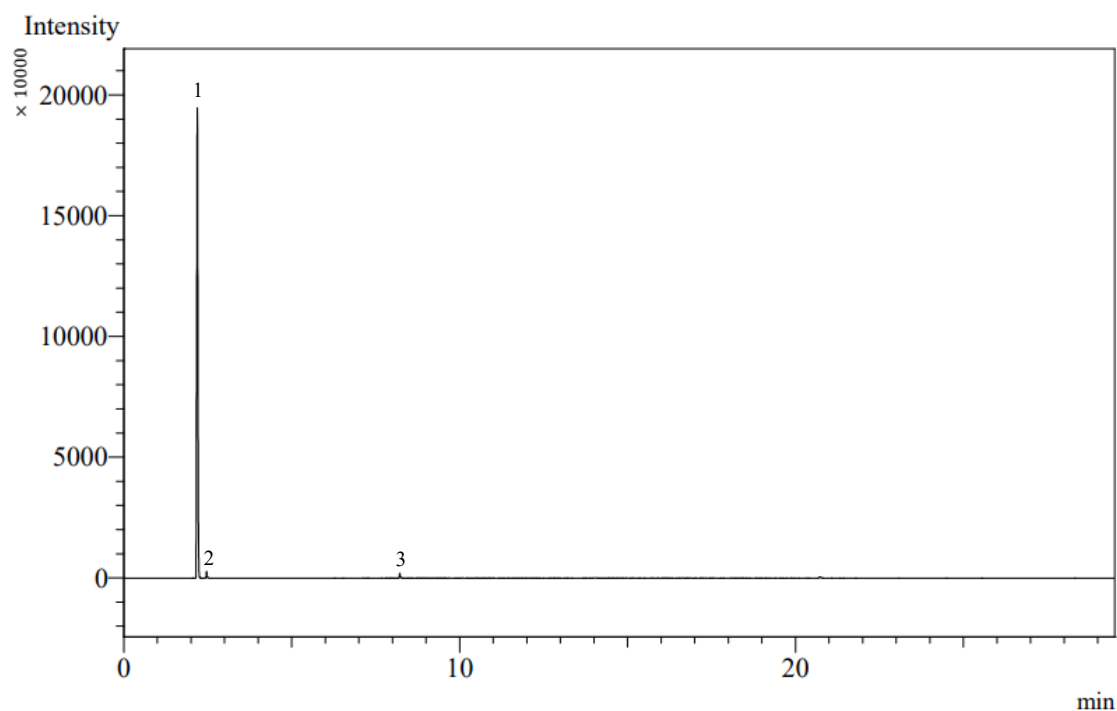
Figure B-1. Chromatogram for the sulphur peaks of Calibration Standard 1, Run 1.

The area of the sulphur peaks from the chromatogram are presented in Table B-1.

Table B-1. Details of sulphur peaks for Calibration Standard 1, Run 1.

Retention Time	Area	Height
2.191	582747010.4	193332511.7
2.469	4702086.2	2549814.0
8.219	4218214.3	2023650.3

$$\text{Total Area} = 582747010.4 + 4702086.2 + 4218214.3 = 591667310.9$$

The procedure was repeated for all calibration standards.

B-2. GC-PFDP Results for Treated Tyre Derived Oil

Table B-2 through B-6 contains the desulphurization data of TDO using alkaline earth metal oxides supported on silica gel with a 60 Å pore size and a 35-60 mesh particle size. The treated TDO was tested 3 times on GC-PFDP to obtain an average total sulphur peak area.

Table B-2. Desulphurization using unsupported magnesium oxide.

Exp.	Total Sulphur Peak Area				Relative Std. Deviation (%)	Sulphur Content (wt.%)	Ds %
	Run 1	Run 2	Run 3	Average			
1	497767554.2	508345725.7	498995972.0	501703084.0	0.94	0.1108	35.11
2	537707398.1	536118753.7	528556495.7	534127549.2	0.75	0.1350	20.93
3	511211944.4	520388107.1	517000580.8	516200210.8	0.73	0.1217	28.77
4	550626890.3	553031509.4	564657423.3	556105274.3	1.10	0.1515	11.31
5	518246476.9	526581172.2	523283977.4	522703875.5	0.66	0.1265	25.92
6	551966560.9	541747913.8	542052480.3	545255651.7	0.87	0.1434	16.06
7	525727346.4	528629578.5	521660913.8	525339279.6	0.54	0.1285	24.77
8	554295381.2	560253036.8	565131933.7	559893450.6	0.79	0.1543	9.66
9	500512783.1	503996486.3	506508600.7	503672623.4	0.49	0.1123	34.25

Table B-3. Desulphurization using supported magnesium oxide.

Exp.	Total Sulphur Peak Area				Relative Std. Deviation (%)	Sulphur Content (wt.%)	Ds %
	Run 1	Run 2	Run 3	Average			
1	502417089.8	495330245.5	493309643.7	497018993.0	0.79	0.1073	37.16
2	515062093.1	519598586.8	515822070.3	516827583.4	0.38	0.1221	28.50
3	513095499.0	503935495.9	510991658.7	509340884.5	0.77	0.1165	31.77
4	558650513.0	548691795.7	560682318.2	556008209.0	0.94	0.1514	11.36
5	497914538.8	498499798.4	499286647.3	498566994.8	0.11	0.1085	36.48
6	524732283.3	528951478.2	531433255.0	528372338.8	0.52	0.1307	23.45
7	512467362.8	506429797.8	512077723.2	510324961.3	0.54	0.1173	31.34
8	531435436.7	520491130.7	530759038.4	527561868.6	0.95	0.1301	23.80
9	511349238.2	506207370.5	504620172.1	507392260.3	0.57	0.1151	32.62

Table B-4. Desulphurization using unsupported calcium oxide.

Exp.	Total Sulphur Peak Area				Relative Std. Deviation (%)	Sulphur Content (wt.%)	Ds %
	Run 1	Run 2	Run 3	Average			
1	535466762.0	532420654.9	524790981.2	530892799.4	0.85	0.1326	22.34
2	477417712.2	477310654.1	477841850.0	477523405.4	0.05	0.0928	45.69
3	508028322.8	509026457.4	510769533.1	509274771.1	0.22	0.1165	31.80
4	486355828.9	483975168.8	475607388.1	481979461.9	0.96	0.0961	43.74
5	500889644.8	508525877.1	506833455.3	505416325.7	0.65	0.1136	33.49
6	461402403.5	456158096.2	464124728.7	460561742.8	0.72	0.0801	53.11
7	546249368.9	544349811.5	549475752.2	546691644.2	0.39	0.1444	15.43
8	528855119.7	520437925.1	516443275.4	521912106.7	0.99	0.1259	26.27
9	558955838.0	547426600.7	550436308.5	552272915.7	0.88	0.1486	12.99

Table B-5. Desulphurization using supported calcium oxide.

Exp.	Total Sulphur Peak Area				Relative Std. Deviation (%)	Sulphur Content (wt.%)	Ds %
	Run 1	Run 2	Run 3	Average			
1	540025126.6	538165246.4	546201707.7	541464026.9	0.63	0.1405	17.72
2	455246691.6	449663831.4	451719020.6	452209847.9	0.51	0.0738	56.76
3	526918606.7	538053791.5	533754698.5	532909032.2	0.86	0.1341	21.46
4	452775366.3	448615924.1	449534258.8	450308516.4	0.40	0.0724	57.59
5	520781418.3	524988501.0	526874028.6	524214649.3	0.49	0.1276	25.26
6	514186158.0	523648488.5	516701172.2	518178606.2	0.77	0.1231	27.90
7	541573245.0	549445765.8	551555026.9	547524679.2	0.78	0.1451	15.07
8	530182405.0	532768260.2	525404135.2	529451600.1	0.58	0.1316	22.97
9	499190788.1	511786958.1	505948537.5	505642094.6	1.02	0.1138	33.39

Table B-6. Desulphurization using supported barium oxide

Exp.	Total Sulphur Peak Area				Relative Std. Deviation (%)	Sulphur Content (wt.%)	Ds %
	Run 1	Run 2	Run 3	Average			
1	543681067.8	539456462.2	542284069.1	541807199.7	0.32	0.1408	17.57
2	513278680.7	520536391.8	517269179.2	517028083.9	0.57	0.1223	28.41
3	569091025.7	567218782.7	565828736.8	567379515.1	0.24	0.1599	6.38
4	544263697.9	532269665.9	542490548.7	539674637.5	0.98	0.1392	18.50
5	551198968.4	555600318	557105046.6	554634777.7	0.45	0.1504	11.96
6	558537448.3	550759690.2	563981093.9	557759410.8	0.97	0.1527	10.59
7	564525800.7	560522012.8	569293564.2	564780459.2	0.63	0.1579	7.52
8	561698451.6	570688012.3	566561578.2	566316014	0.65	0.1591	6.85
9	519065736.8	523781851.7	523815381.6	522220990.0	0.43	0.1262	26.14

Appendix C: Sample Calculations for the Silica-supported Alkaline Earth Metal Oxides

C-1. Silica-supported Magnesium Oxide

A sample calculation to obtain the experimental weight percentage of magnesium oxide on silica gel with a pore size of 30 Å is shown below:

Table C-1. Elemental composition of $8MgO-30SiO_2$ from EDX analysis.

Element Number	Element Symbol	Element Name	Atomic Conc.	Weight Conc.
8	O	Oxygen	68.09	54.42
14	Si	Silicon	26.67	37.42
12	Mg	Magnesium	4.88	5.93

A mass of 100 g $8MgO-30SiO_2$ was used for the sample calculations.

$$m_{Mg} = 5.93\ g$$

$$M_{Mg} = 24.31\ g/mol$$

$$n_{Mg} = \frac{m_{Mg}}{M_{Mg}} = \frac{5.93\ g}{24.31\ g/mol} = 0.2439\ mol$$

Where,

m_{Mg} = Mass of Magnesium

M_{Mg} = Molar Mass of Magnesium

n_{Mg} = Moles of Magnesium

The magnesium and magnesium oxide are equimolar because the molar balance is elemental. Therefore,

$$n_{Mg} = n_{MgO}$$

$$n_{MgO} = 0.2439\ mol$$

$$M_{MgO} = 40.31\ g/mol$$

$$m_{MgO} = n_{MgO} \times M_{MgO} = 0.2439\ mol \times 40.31\ g/mol = 9.83\ g$$

$$Weight\ \%\ MgO = \frac{Mass\ of\ MgO}{Total\ Mass} \times 100 = \frac{9.83\ g}{100\ g} \times 100 = 9.83\ wt.\%$$

Where,

m_{MgO} = Mass of Magnesium Oxide

M_{MgO} = Molar Mass of Magnesium Oxide

n_{MgO} = Moles of Magnesium Oxide

The calculations were repeated to obtain the experimental weight percentage of magnesium oxide on silica gel with pore sizes of 60 and 150 Å.

C-2. Silica-supported Calcium Oxide

A sample calculation to obtain the experimental weight percentage of calcium oxide on silica gel with a pore size of 30 Å is shown below:

Table C-2. Elemental composition of $8CaO\text{-}30SiO_2$ from EDX analysis.

Element Number	Element Symbol	Element Name	Atomic Conc.	Weight Conc.
8	O	Oxygen	69.31	52.43
14	Si	Silicon	27.07	40.72
20	Ca	Calcium	3.62	6.85

A mass of 100 g $8CaO\text{-}30SiO_2$ was used for the sample calculations.

$m_{Ca} = 6.85\ g$

$M_{Ca} = 40.08\ g/mol$

$n_{Ca} = \dfrac{m_{Ca}}{M_{Ca}} = \dfrac{6.85\ g}{40.08\ g/mol} = 0.1709\ mol$

Where,

m_{Ca} = Mass of Calcium

M_{Ca} = Molar Mass of Calcium

n_{Ca} = Moles of Calcium

The calcium and calcium oxide are equimolar because the molar balance is elemental. Therefore,

$n_{Ca} = n_{CaO}$

$n_{CaO} = 0.1709\ mol$

$M_{CaO} = 56.08\ g/mol$

$m_{CaO} = n_{CaO} \times M_{CaO} = 0.1709\ mol \times 56.08\ g/mol = 9.58\ g$

$Weight\ \%\ CaO = \dfrac{Mass\ of\ CaO}{Total\ Mass} \times 100 = \dfrac{9.58\ g}{100\ g} \times 100 = 9.58\ wt.\%$

Where,

m_{CaO} = Mass of Calcium Oxide

M_{CaO} = Molar Mass of Calcium Oxide

n_{CaO} = Moles of Calcium Oxide

The calculations were repeated to obtain the experimental weight percentage of calcium oxide on silica gel with pore sizes of 60 and 150 Å.

C-3. Silica-supported Barium Oxide

A sample calculation to obtain the experimental weight percentage of barium oxide on silica gel with a pore size of 150 Å is shown below:

Table C-3. Elemental composition of $8BaO\text{-}150SiO_2$ from EDX analysis.

Element Number	Element Symbol	Element Name	Atomic Conc.	Weight Conc.
8	O	Oxygen	76.44	37.18
14	Si	Silicon	10.98	28.53
56	Ba	Barium	6.25	26.10
17	Cl	Chlorine	5.86	6.32

The presence of elemental chlorine (Table C-3) suggests an incomplete conversion of barium chloride to barium oxide. A mass of 100 g $8BaO\text{-}150SiO_2$ was used for the sample calculations.

The moles of elemental chlorine was calculated to determine the moles of barium within the barium chloride, $BaCl_2$, molecule.

$$m_{Cl} = 6.32\ g$$

$$M_{Cl} = 35.45\ g/mol$$

$$n_{Cl} = \frac{m_{Cl}}{M_{Cl}} = \frac{6.32\ g}{35.45\ g/mol} = 0.1783\ mol$$

$$n_{Ba,1} = \frac{1}{2}n_{Cl}$$

$$n_{Ba,1} = 0.0892\ mol$$

Where,

m_{Cl} = Mass of Chlorine

M_{Cl} = Molar Mass of Chlorine

n_{Cl} = Moles of Chlorine

$n_{Ba,1}$ = Moles of Barium for $BaCl_2$

The mass of barium for $BaCl_2$ was subtracted from the total mass of barium to obtain the mass of barium for BaO.

$$M_{Ba} = 137.33\ g/mol$$

$$m_{Ba,1} = n_{Ba,1} \times M_{Ba} = 0.0892\ mol \times 137.33\ g/mol = 12.24\ g$$

$$m_{Ba,2} = m_{Ba} - m_{Ba,1} = 26.10 \, g - 12.24 \, g = 13.86 \, g$$

Where,

m_{Ba} = Total Mass of Barium

$m_{Ba,1}$ = Mass of Barium for $BaCl_2$

$m_{Ba,2}$ = Mass of Barium for BaO

M_{Ba} = Molar Mass of Barium

$$n_{Ba,2} = \frac{m_{Ba,2}}{M_{Ba}} = \frac{13.86 \, g}{137.33 \, g/mol} = 0.1009 \, mol$$

The barium and barium oxide are equimolar because the molar balance is elemental. Therefore,

$$n_{Ba,2} = n_{BaO}$$

$$n_{BaO} = 0.1009 \, mol$$

$$M_{BaO} = 153.33 \, g/mol$$

$$m_{BaO} = n_{BaO} \times M_{BaO} = 0.1009 \, mol \times 153.33 \, g/mol = 15.47 \, g$$

$$Weight \, \% \, BaO = \frac{Mass \, of \, BaO}{Total \, Mass} \times 100 = \frac{15.47 \, g}{100 \, g} \times 100 = 15.47 \, wt.\%$$

Where,

m_{BaO} = Mass of Barium Oxide

M_{BaO} = Molar Mass of Barium Oxide

$n_{Ba,2}$ = Moles of Barium for BaO

n_{BaO} = Moles of Barium Oxide

The calculations were repeated to obtain the experimental weight percentage of barium oxide on silica gel with a pore size of 60 Å.